

**Consequence of high-calorie diet and role of sex in a mouse
model of Marfan syndrome**

By

CORI LAU

Department of Anatomy and Cell Biology

Faculty of Medicine and Health Sciences

McGill University, Montreal, Canada

August 2022



A thesis submitted to McGill University in partial fulfillment of the

requirements of the degree of

MASTER OF SCIENCE

© Cori Lau, 2022

TABLE OF CONTENTS

ABSTRACT.....	iii
RÉSUMÉ	v
ACKNOWLEDGEMENTS.....	vii
CONTRIBUTION OF AUTHORS.....	ix
LIST OF FIGURES	x
LIST OF TABLES.....	xiii
LIST OF ABBREVIATIONS.....	xiv
CHAPTER 1: REVIEW OF LITERATURE.....	1
1.1 Overview of aorta.....	1
1.1.1 Anatomy of aorta.....	1
1.1.2 Structure of aorta	2
1.2 Elastogenesis and aorta	4
1.2.1 Role of elastin in aorta.....	4
1.2.2 Fibronectin.....	4
1.2.3 Fibrillin-1	5
1.2.4 Fibulin-4	7
1.2.5 Fibulin-5	7
1.2.6 Latent TGF- β binding protein-4	8
1.2.7 Elastin	9
1.3 Fibrillinopathies and TAA	12
1.4 Dysregulated signaling related to TAA.....	13
1.4.1 Embryonic origins of SMCs.....	13
1.4.2 Hypoxia-inducible factor 1 alpha	14
1.4.3 Matrix metalloproteinases	14
1.4.4 Proteoglycan.....	16
1.4.5 Collagen.....	18
1.5 Marfan syndrome and sexual dimorphism.....	20
1.5.1 Metabolism in Marfan syndrome	20
1.5.2 Thoracic aortic aneurysms and aortic dissection in Marfan syndrome	21
1.5.3 High-calorie-induced metabolism and aneurysm	22
1.6 Rationale, hypotheses and objectives.....	23
1.6.1 Rationale.....	23
1.6.2 Hypotheses	23
1.6.3 Objectives	23
CHAPTER 2: MATERIALS AND METHODS	24
2.1 Mouse model and diets.....	24
2.2 Genotyping.....	27
2.3 Measurement of in situ aortic diameters and preparations for histological and RNA analyses	28
2.4 Quantification of aortic lumen area and wall thickness	29

2.5 Indirect immunofluorescence.....	29
2.6 Histological staining.....	30
2.7 RNA extraction and real-time quantitative PCR (qPCR)	31
2.8 Statistics	32
CHAPTER 3: METABOLIC ANALYSIS OF MALE AND FEMALE MGR MICE FED WITH HIGH-CALORIE DIETS.....	34
3.1 HFD- and WD-induced weight gain in male and female mgR mice	34
3.2 HFD- and WD-induced final body parameters in male and female mgR mice	36
3.3 HFD- and WD-induced insulin intolerance in male and female mgR mice	38
3.4 HFD- and WD-induced glucose intolerance in male and female mgR mice	40
CHAPTER 4: SURVIVAL ANALYSIS AND CHARACTERIZATION OF AORTAE IN MALE AND FEMALE MGR MICE FED WITH HIGH-CALORIE DIETS	43
4.1 Overall survival and aortic-rupture-specific survival in male and female mgR mice fed with CD, HFD or WD.....	43
4.2 Analysis of aortae of male and female mgR mice fed with CD, HFD or WD (gross view)	46
4.3 Analysis of aortae of male and female mgR mice fed with CD or HFD (cross section).....	49
4.4 HFD-induced changes in FBN1 deposition, assembly and gene expression levels of male and female mgR mice.....	51
4.5 HFD-induced changes in HIF-1 α protein and gene expression levels of male and female mgR mice	53
4.6 HFD-induced changes in elastic fiber fragmentations, <i>Mmp2</i> and <i>Mmp9</i> gene expression levels of male and female mgR mice	55
4.7 HFD-induced changes in MMP-12 protein and gene expression of male and female mgR mice.....	57
4.8 HFD-induced changes in proteoglycan deposition and <i>Acan</i> and <i>Vcan</i> gene expression levels of male and female mgR mice	59
4.9 HFD-induced changes in collagen deposition and <i>Coll1a1</i> and <i>Col3a1</i> gene expression levels of male and female mgR mice	61
CHAPTER 5: DISCUSSION.....	63
5.1 Sexual dimorphism of mgR mice in metabolism	63
5.2 Sexual dimorphism of mgR mice in aortic aneurysm.....	65
CHAPTER 6: CONCLUSION AND KEY FINDINGS.....	74
REFERENCES	76

ABSTRACT

Introduction: Marfan syndrome (MFS) is a multi-system connective tissue disorder caused by mutations in the *FBNI* gene encoding fibrillin-1 (FBN1). MFS is clinically characterized by ascending aortic aneurysms, among many other clinical symptoms. With previous data revealing a sexual dimorphism in MFS metabolism and ascending aortic aneurysm formation, this thesis project addresses the consequence of both high-calorie diet and biological sex in these aspects.

Methods: *Fbn1^{mgR/mgR}* (mgR) mice represent an established MFS mouse model with significantly reduced production of normal fibrillin-1 (~20-25%), leading to the typical MFS clinical symptoms in the thoracic aorta and in other tissues. Both male and female mgR as well as wild type (WT) littermate mice were fed with control diet (CD, 10% fat), high-fat diet (HFD, 60% fat) or western diet (WD, 45% fat; 30% sucrose) starting from 4 weeks until 12 weeks of age. We determined metabolism complications through body mass measurements, insulin tolerance test (ITT) and glucose tolerance test (GTT). Aortic complications were determined through Kaplan-Meier analyses, as well as by assessment of key parameters including the aortic diameter and thickness of the aortic wall, HIF-1 α level, elastic fiber fragmentation, *Mmp12* gene expression, proteoglycan and collagen levels.

Results: Female mgR mice were resistant to weight gain from HFD or WD but not male mgR mice. However, ITT and GTT did not reveal metabolic abnormalities between WT and mgR mice, neither in males nor females. Surprisingly, male mgR mice showed a lower aortic-rupture-specific survival rate compared to WT mice when fed with CD but not HFD or WD. The aortic-rupture-specific survival rate was not different between female WT and mgR mice. Interestingly, HFD reduced the aortic vessel diameter in female but not male mgR mice. Therefore, our subsequent studies focused on the consequences of HFD compared to CD. Importantly, elastic fiber

fragmentation and proteoglycan deposition correlated with the aortic diameter. Aortic wall thickness increased in male mgR compared to male WT mice but not in females fed with either CD or HFD. The HIF-1 α level was higher in male mgR mice than in male WT mice fed with CD or HFD, and in female mgR compared to female WT mice fed with HFD. These data correlated well with the analysis of collagen deposition. The *Mmp12* gene expression was higher in male mgR than in WT mice when fed with CD but not HFD, whereas no difference was detectable in females. These results revealed specific sexual dimorphisms in MFS mice responding to HFD. Surprisingly, a HFD diet rescued some of the aneurysm phenotypes, especially in females.

Conclusion: Male and female mice with MFS responded differently to HFD in metabolism and ascending aortic aneurysm development. The findings provide a basis to start developing nutritional recommendations for patients with MFS.

RÉSUMÉ

Introduction: Le syndrome de Marfan (MFS) est un trouble multisystémique du tissu conjonctif causé par des mutations du gène *FBN1* codant pour la protéine fibrilline-1 (FBN1). Parmi d'autres symptômes cliniques, le MFS est principalement caractérisé cliniquement par des anévrismes de l'aorte ascendante. En s'appuyant sur des données antérieures révélant un dimorphisme sexuel dans le métabolisme du MFS et le développement d'un anévrisme de l'aorte ascendante, ce projet de thèse porte sur les conséquences d'un régime hypercalorique et du sexe biologique dans ces aspects.

Méthodes: Les souris *Fbn1^{mgR/mgR}* (mgR) représentent un modèle animale MFS bien établi avec une production de la fibrilline-1 considérablement réduite par rapport à celle normale (~ 20-25%), conduisant aux symptômes cliniques typiques de la MFS dans l'aorte thoracique et dans d'autres tissus. Les souris mâles et femelles mgR ainsi que les souris de type sauvage (WT) ont été nourries avec un régime témoin (CD, 10% de matières grasses), un régime riche en graisses (HFD, 60% de matières grasses) ou un régime occidental (WD, 45% de matières grasses ; 30% de saccharose) et cela à partir de 4 semaines jusqu'à l'âge de 12 semaines. Nous avons déterminé les complications du métabolisme dans les souris par des mesures de masse corporelle, un test de tolérance à l'insuline (ITT) et un test de tolérance au glucose (GTT). Les complications aortiques ont été déterminées par des analyses de Kaplan-Meier, ainsi que par l'évaluation de paramètres clés, notamment le diamètre de l'aorte et l'épaisseur de la paroi aortique, le niveau de HIF-1 α , la fragmentation des fibres élastiques, l'expression du gène *Mmp12* et les niveaux de protéoglycane et de collagène.

Résultats: Les souris mgR femelles étaient résistantes à la prise de poids due au HFD ou au WD, mais pas les souris mgR mâles. Cependant, ITT et GTT n'ont pas révélé d'anomalies métaboliques

entre les souris WT et mgR, ni chez les mâles ni chez les femelles. Étonnamment, les souris mgR mâles ont montré un taux de survie spécifique à la rupture aortique inférieur à celui des souris WT lorsqu'elles étaient nourries dans le régime CD, mais pas avec du HFD ou du WD. Le taux de survie spécifique à la rupture aortique n'était pas différent entre les souris femelles WT et mgR. Fait intéressant, HFD a conduit à la réduction du diamètre du vaisseau aortique chez les souris mgR femelles mais pas les souris mgR mâles. Par conséquent, nos études ultérieures se sont concentrées sur les conséquences du HFD par rapport au CD. Il est important de noter qu'il avait une corrélation entre la fragmentation des fibres élastiques et le dépôt de protéoglycanes et le diamètre aortique. L'épaisseur de la paroi aortique a augmenté chez les mâles mgR par rapport aux souris mâles WT, mais pas chez les femelles nourries sous le régime ou HFD. Le niveau de HIF-1 α était plus élevé chez les souris mâles mgR que chez les souris mâles WT nourries avec le régime CD ou HFD, et chez les femelles mgR par rapport aux souris femelles WT nourries avec HFD. Ces données étaient bien corrélées avec l'analyse du dépôt de collagène. L'expression du gène *Mmp12* était plus élevée chez les souris mâles mgR que chez les souris WT lorsqu'elles étaient nourries avec du CD mais pas avec du HFD, alors qu'aucune différence n'était détectable chez les femelles. Ces résultats ont révélé des dimorphismes sexuels spécifiques chez les souris MFS répondant au HFD. Étonnamment, un régime HFD a sauvé certains des phénotypes d'anévrisme, notamment chez les femmes.

Conclusion: Les souris mâles et femelles atteintes de MFS ont répondu différemment au régime HFD dans le métabolisme et le développement de l'anévrisme de l'aorte ascendante. Ces résultats fournissent une base consistante pour commencer à développer des recommandations nutritionnelles pour les patients atteints de MFS.

ACKNOWLEDGEMENTS

My graduate school experience is a fruitful and meaningful experience in my life. I would not be able to achieve my current success without all these amazing people who supported me throughout my journey at graduate school. I would want to use this opportunity to thank all of them sincerely.

First of all, I would like to give my deepest gratitude to my supervisor, Dr. Dieter Reinhardt. He provided me an amazing project involving both metabolic and cardiovascular aspects. He did not only provide the opportunity for me to study and work in his laboratory but also provided his expertise in extracellular matrix. With countless hours of weekly or biweekly meetings, I was able to think critically as a scientist. I also appreciate his dedication to science and his open-door policy. These provided me the flexibility to ask questions about the project or make important project-related decisions. Moreover, I appreciate the solid setup he provided in the lab for research data security and backup strategies which was essential for my project. I am also very grateful for his huge commitment in applying and receiving multiple grants to consistently provide the laboratory with plentiful supplies and my stipend.

I am very thankful to have Dr. Muthu Lakshmi Muthu as my colleague and mentor. With her help and guidance in many aspects of the project, I was able to start and conduct a large animal study to analyze various aspects in Marfan syndrome. Throughout my MSc project years in weekly or biweekly meetings, she provided her critical thinking and extended knowledge in metabolism and the extracellular matrix. There were numerous times that the project did not go what we expected, but with her motivation and encouragement, I was able to troubleshoot the problems and push through all these barriers. Her clear voice and confidence in her presentations have set up a role model how to be a good presenter and scientist. She taught me the foundation of multiple

laboratory skills and the meaning of being a scientist to always have an open and innovative mindset, so I can think critically as a researcher.

I would want to use this opportunity to extend my thanks to Dr. Ling Li, the lab manager. Her positivity helps me to release my burden and drives me to be strong when I struggle. She also seeks for new knowledge and takes initiative to self-learn all the time as a researcher. This attitude in science taught me to always accept new knowledge and approaches, especially when I was new to the field. In addition, she has a lot of knowledge in aorta preparation and sectioning. The time she spent for sectioning was countless in order to provide the best aorta cross sections as possible.

I would want to give my thanks to Neha Dinesh for helping me to adjust the lifestyle when I just arrived as a newcomer to Montreal. Therefore, I was able to quickly adapt to the new environment. I would want to express my thanks to a previous lab member, Dr. Rongmo Zhang. He helped me to understand how to maintain a good life balance between the lab and private aspects. I gained a lot from multiple discussions or even lessons from him about exercising and time management. I also extend my thanks to Dr. Valentin Nelea who is a great and supportive colleague and who helped revising the French thesis abstract. I was very fortunate to have Elahe Mirzarazi and Iram Siddiqui as my colleagues providing support on various levels.

I would want to thank my committee members Dr. Chantal Autexier, Dr. Svetlana Komarova and Dr. Elaine Davis. I could not have asked for better committee members who provided different great feedbacks during my committee meetings and the MSc seminar.

Last but not least, I would like to give my sincerely thanks to my friends, bible study mentor and family. Calling my family gave me strength each day and allowed me to know that I am not alone. Their unconditional love, support and patience made me stronger each day.

CONTRIBUTION OF AUTHORS

Chapter 1:

This chapter was written by me and reviewed and edited by Dr. Dieter Reinhardt.

Chapter 2 to 6:

The experiments were designed by me, Dr. Muthu Lakshmi Muthu and Dr. Dieter Reinhardt (Chapter 2). The insulin tolerance test and glucose intolerance test were conducted by Dr. Muthu Lakshmi Muthu and me together. The quantitative real-time polymerase chain reaction was conducted by Dr. Muthu Lakshmi Muthu. All mouse colonies were managed by me. The rest of the experiments (indirect immunofluorescence and histological staining) and analyses were performed by me under the supervision of Dr. Dieter Reinhardt and Dr. Muthu Lakshmi Muthu. All aortae were dissected by me and sectioned by Dr. Ling Li. These chapters were written by me and edited by Dr. Dieter Reinhardt. Chapter 3 to 6 were edited by Dr. Muthu Lakshmi Muthu as well.

LIST OF FIGURES

Chapter 1:

Figure 1.1: Diagram of a thoracic aorta.....	2
Figure 1.2: Layers of aortic wall.....	3
Figure 1.3: Schematic representation of elastogenesis.....	11
Figure 1.4: Schematic structure of MMP-2, -9 and -12.....	16
Figure 1.5: Schematic overview of known physiological drivers of elastic fiber fragmentation leading to TAA in MFS.....	20

Chapter 2:

Figure 2.1: Timeline of experiments.....	25
Figure 2.2: Genotyping of WT, mgR and mgR/+ mice.....	28
Figure 2.3: No primary antibody control of aorta from a male WT mouse.....	30

Chapter 3:

Figure 3.1: Relative body mass of 4-12-week-old male and female WT and mgR mice fed with CD, HFD or WD.....	35
Figure 3.2: Body parameters and food consumption of 12-week-old male and female WT and mgR mice fed with CD, HFD or WD.....	37
Figure 3.3: ITT of 12-week-old male and female WT and mgR mice fed with CD, HFD or WD.....	39

Figure 3.4: GTT of 12-week-old male and female WT and mgR mice fed with CD, HFD or WD.....	41
---	----

Chapter 4:

Figure 4.1: Survival of 4-12-week-old male and female WT and mgR mice fed with CD, HFD or WD.	45
---	----

Figure 4.2: Analysis of thoracic aortae from male and female WT and mgR mice fed with CD, HFD or WD at 12 weeks.	48
--	----

Figure 4.3: Ascending aortic lumen area and thickness of male and female WT and mgR mice fed with CD, HFD or WD at 12 weeks of age.....	50
--	----

Figure 4.4: FBN1 deposition, assembly and <i>Fbn1</i> gene expression levels in ascending aortae from male and female WT and mgR mice fed with CD or HFD at 12 weeks of age.....	52
---	----

Figure 4.5: HIF-1 α protein and <i>Hif1a</i> gene expression levels in ascending aortae from male and female WT and mgR mice fed with CD or HFD at 12 weeks of age.....	54
---	----

Figure 4.6: Elastic fiber fragmentation and <i>Mmp2</i> and <i>Mmp9</i> gene expression levels in ascending aortae from male and female WT and mgR mice fed with CD or HFD at 12 weeks of age.....	56
---	----

Figure 4.7: MMP-12 protein and gene expression in ascending aortae from male and female WT and mgR mice fed with CD or HFD at 12 weeks of age.....	58
---	----

Figure 4.8: Proteoglycan deposition, <i>Acan</i> and <i>Vcan</i> gene expression levels in ascending aortae from male and female WT and mgR mice fed with CD or HFD at 12 weeks of age.....	60
--	----

Figure 4.9: Collagen deposition and *Colla1* and *Col3a1* gene expression levels in ascending aortae from male and female WT and mgR mice fed with CD or HFD at 12 weeks of age. 62

Chapter 5:

Figure 5.1: Comparison between gross view and cross sections. 68

Chapter 6:

Figure 6.1: Schematic of metabolic phenotype in 12-week-old male and female WT and mgR mice fed with HFD. 74

Figure 6.2: Schematic of aortic aneurysm phenotype in 12-week-old male and female WT and mgR mice fed with CD or HFD. 75

LIST OF TABLES

Chapter 2:

Table 2.1: Composition of diets used in this study.....	25
Table 2.2: Overview of number of mice in each sex, genotypes and diets.....	26
Table 2.3: Mouse-specific primers used for qPCR.....	32

Chapter 4:

Table 4.1: Survival of mice fed with CD, HFD or WD at the experimental endpoint of 12 weeks.....	46
--	----

LIST OF ABBREVIATIONS

AUC	Area under the curve
AWT	Aortic wall thickness
cbEGF	Calcium-binding and epidermal growth factor-like
CD	Control diet
cFN.....	Cellular fibronectin
CNC	Cardiac neural crest cells
CS.....	Chondroitin sulfate
DAPI	4', 6-diamidino-2-phenylindole
ELN.....	Elastin
FBLN4	Fibulin-4
FBLN5	Fibulin-5
FBN1	Fibrillin-1
FN	Fibronectin
GTT.....	Glucose tolerance test
HFD.....	High fat diet
HIF-1 α	Hypoxia-inducible factor 1-alpha
ITT	Insulin tolerance test
LA	Lumen area
LAP	Latency-associated peptide
LOX	Lysyl oxidase
LOXL.....	Lysyl oxidase like enzymes
LTBP4.....	Latent TGF- β binding protein-4
LTBP4L	Latent TGF- β binding protein-4 long form
LTBP4S.....	Latent TGF- β binding protein-4 short form
MFS.....	Marfan syndrome
mgR/+	<i>Fbn1</i> ^{mgR/+}

mgR.....	<i>Fbn1</i> ^{mgR/mgR}
MMP-12.....	Matrix metalloproteinase 12
PBS.....	Phosphate-buffered saline
pFN.....	Plasma fibronectin
Pi.....	Perimeter of inner elastic laminae
Po.....	Perimeter of outer elastic laminae
qPCR.....	Real-time polymerase chain reaction
Sca-1.....	Stem cells antigen-1
SEM.....	Standard error of mean
SMC.....	Smooth muscle cell
SNF.....	Second heart field
TAA.....	Thoracic aortic aneurysm
TAAD.....	Thoracic aortic aneurysm dissection
TB.....	Transforming growth factor beta binding-like
TBST.....	Tris-buffered saline with 0.05% Tween
TGF- β	Transforming growth factor beta
WD.....	Western diet
VSMC.....	Vascular smooth muscle cell

CHAPTER 1: REVIEW OF LITERATURE

1.1 Overview of aorta

1.1.1 Anatomy of aorta

Among the arteries, aorta is the largest where all systemic arteries branch from. The aorta consists of 5 anatomical segments: aortic root, ascending aorta, aortic arch, descending aorta and subdiaphragmatic abdominal aorta [Dagenais, 2011; Murillo et al., 2012; White et al., 2022]. The aortic root extends from the aortic valve in the left ventricle of the heart to the sinotubular junction [Murillo et al., 2012]. This region is where coronary arteries are extended from to supply oxygenated blood for the myocardium of the heart [Paiocchi et al., 2021; Ogobuiro et al., 2022]. Following the aortic root, the ascending aorta extends upwards to the left until it reaches the aortic arch, the next aortic segment [Dagenais, 2011; Murillo et al., 2012]. The aortic arch branches to the brachiocephalic trunk, left common carotid artery and left subclavian artery for supplying blood to the head, neck, left and right upper limb [Cakirer et al., 2002; Szpinda, 2005; Hanneman et al., 2017; Kandemirli, 2020; Alhuzaimi et al., 2021]. As the aorta descends from the arch above the diaphragm, oxygenated blood is supplied to the pericardium, bronchi of lungs, esophagus, intercostal and chest muscles, superior and posterior surfaces of diaphragm [Duckworth, 1869; Dagenais, 2011; McKenzie et al., 2016; Riambau et al., 2017]. The aorta that branches into these arteries is known as descending thoracic aorta (**Figure 1.1**). Abdominal aorta locates below the diaphragm and supplies blood to any organs or body parts in abdominal cavity including renal, digestive and reproductive organs [Lin & Chaikof, 2000; Lech & Swaminathan, 2017].

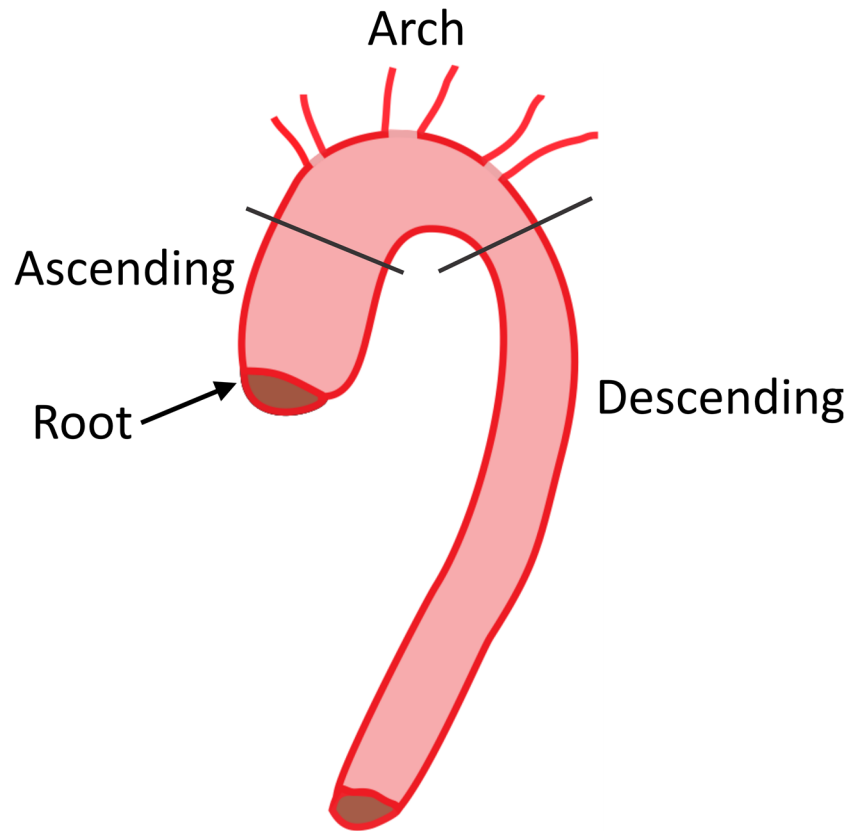


Figure 1.1: Diagram of a thoracic aorta. The thoracic aorta can be conceptually divided into 4 major segments: the aortic root, the ascending aorta, the aortic arch and the descending aorta.

1.1.2 Structure of aorta

Aorta contains 3 layers: tunica intima, tunica media and tunica adventitia (**Figure 1.2**). The innermost layer, tunica intima, consists of a layer of simple squamous epithelium known as endothelium. The endothelial lining composes of endothelial cells not only contributes to the formation of the internal elastic lamina that separates the tunica media from the tunica intima but also provides frictionless pathway for the movement of blood [Tucker *et al.*, 2022]. The endothelium is continuous throughout the entire cardiovascular system and the closest layer to the lumen where the blood flows. The next layer away from the lumen is tunica media which is the thickest layer in the aorta. This layer consists of vascular smooth muscle cells (VSMCs) and

multiple elastic lamellae alternating proteoglycans or collagen over 50 layers in humans or 7 layers in mice [Karimi & Milewicz, 2016; Cocciolone et al., 2018]. As the arteries branch out, the number of lamellar units decreases [Wolinsky, 1970]. The external elastic lamina separates the tunica media and tunica adventitia layer which is the outermost layer. The tunica adventitia consists of fibroblasts, fibrocytes and collagen-rich matrix. Since the cells in the tunica adventitia are too far away from the arterial lumen for oxygen and nutrients, the vasa vasorum exists in the tunica adventitia to supply blood to the cells in the tunica adventitia [Cocciolone et al., 2018].

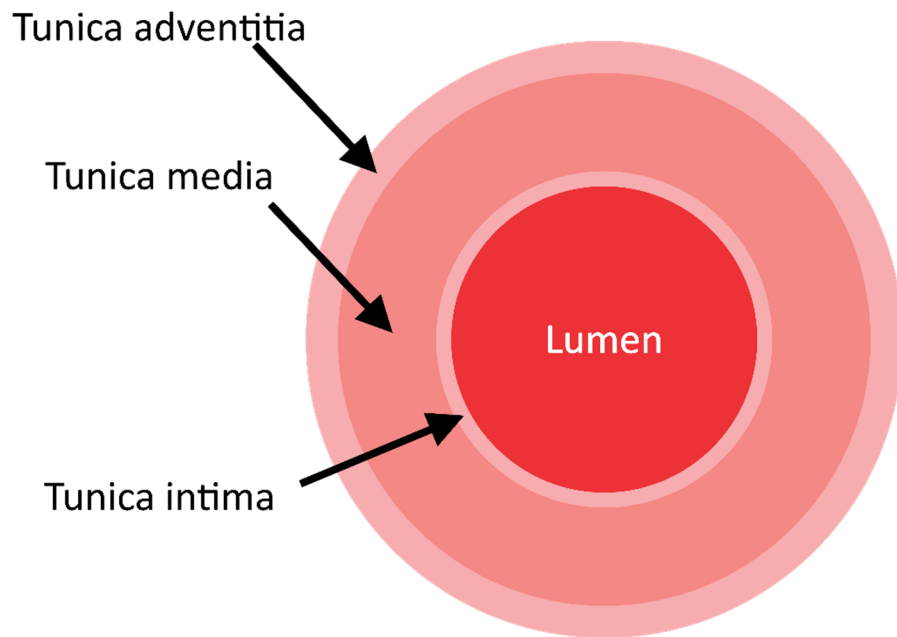


Figure 1.2: Layers of aortic wall. The figure schematically shows the 3 typical tissue layers surrounding the lumen of the aortic wall. Note that the dimensions are not drawn to scale.

1.2 Elastogenesis and aorta

1.2.1 Role of elastin in aorta

Aorta is the first segment of arterial tree branched from the left ventricle of the heart to receive blood, so a constantly pulsating supply of blood is required to be distributed ultimately to each organ. The primary function of the elastic lamellae allows aortae to store blood during the systole and recoil to its original structure during the diastole to send the blood to entire body [Safar *et al.*, 2003; Shin & Yanagisawa, 2019]. This physiological process is known as the “Windkessel” effect to reduce the fluctuation of blood pressure, minimize the systolic flow and maximize the diastolic flow in arterioles [Dobrin, 1978].

Elastic laminae are essential in aortae. Elastogenesis is the process from mid-embryogenesis to early postnatal life to form elastic fibers and laminae which have a half-life of 74 years [Fukuda *et al.*, 1984; Shapiro *et al.*, 1991]. This involves complex multistep events of different extracellular matrix (ECM) molecules, including fibronectin (FN), fibrillin-1 (FBN1), fibulin-4 (FBLN4), fibulin-5 (FBLN5) and latent transforming growth factor-beta binding protein 4 (LTBP4) [Reinhardt *et al.*, 1996a; Lin *et al.*, 2002; Wagenseil & Mecham, 2007; Sabatier *et al.*, 2009; Yanagisawa & Davis, 2010; Sabatier *et al.*, 2013; Hubmacher *et al.*, 2014; Kumra *et al.*, 2019]. Each of these ECM molecules has its unique domain organization and function to form a template for tropoelastin to be deposited eventually forming elastic fibers and lamellae. More details for the role of each of these components are explained in the following paragraphs.

1.2.2 Fibronectin

FN is secreted from cells as a dimer with a molecular mass around 250 kDa for each subunit. Depending on alternative splicing, FN adopts various sizes [Norton & Hynes, 1990]. It consists of

two forms: cellular FN (cFN), which is secreted by numerous types of cells in connective tissues forming an insoluble network, and plasma FN (pFN), which is soluble circulating in the bloodstream and is secreted by hepatocytes in the liver [Morrison *et al.*, 1948; Kuusela *et al.*, 1975]. pFN consists principally of three types of domains: I, II and III, whereas cFN has additional domains either EIIIA, EIIIB or both domains. Although both EIIIA and EIIIB are not required for FN assembly, both domains affect the FN level in the matrix [Singh *et al.*, 2010]. Since dimers are connected by a disulfide bond, activation of FN is required to acquire proper conformation for assembly [Mao & Schwarzbauer, 2005].

The assembly of FN begins with the arginine-glycine-aspartate (RGD) sequence in FN interacting with integrins on the cell surface [Sottile *et al.*, 2000]. Through Rho and actin-myosin pathways, cells contract and thus change the FN conformation [Zhang *et al.*, 1994; Singh *et al.*, 2010]. Integrin clustering promotes FN-FN interactions [Pankov *et al.*, 2000; Mao & Schwarzbauer, 2005; Tomasini-Johansson *et al.*, 2006]. This process exposes cryptic sites in FN and further allows FN to assemble [Ugarova *et al.*, 1995; Ensenberger *et al.*, 2004]. The cryptic regions including III₂, III₄₋₅ and III₁₂ domains interact with the 70 kDa fragment (N-terminal region of FN), suggesting a role in FN assembly [Aguirre *et al.*, 1994; Bultmann *et al.*, 1998; Maqueda *et al.*, 2007]. These hierarchical multistep molecular processes form the insoluble and stable FN fibril matrix.

1.2.3 Fibrillin-1

The fibrillin family consists of fibrillin-1 (FBN1), -2 (FBN2) and -3 (FBN3) encoded by *FBN1*, *FBN2* and *FBN3* genes, respectively, which are expressed in humans and most mammals, but *FBN3* is not active in rodents [Zhang *et al.*, 1995; Corson *et al.*, 2004; Piha-Gossack *et al.*, 2012].

Both FBN2 and FBN3 are expressed during development, but the main form present in microfibrils in postnatal life is FBN1 [Zhang *et al.*, 1995; Corson *et al.*, 2004; Sabatier *et al.*, 2011]. FBN1 is a large extracellular glycoprotein ubiquitously deposited in multiple tissues in the body [Sakai *et al.*, 1986; Milewicz *et al.*, 1992; Milewicz *et al.*, 1995]. Both N- and C-terminal prodomains of profibrillin-1 (350 kDa) are cleaved by endoprotease furin forming mature FBN1 (~320 kDa) [Milewicz *et al.*, 1995; Reinhardt *et al.*, 1996b; Lönnqvist *et al.*, 1998]. Asprosin, the C-terminal propeptide of FBN1, is released and circulates in the bloodstream as a hunger hormone, ultimately leading to the insulin production [Lönnqvist *et al.*, 1998; Wallis *et al.*, 2003; Romere *et al.*, 2016; Petersen & Shulman, 2018]. The mature FBN1 is characterized by its multiple tandem arrays of calcium-binding epidermal growth factor-like (cbEGF) domains and transforming growth factor (TGF)- β binding-like (TB) domains [Handford *et al.*, 1991; Robertson *et al.*, 2015]. The structure in these domains is stabilized by interacting with calcium and by characteristic intradomain disulfide bonds. In a cell-dependent manner, the C-terminus of FBN1 forms globular beads with 8-12 peripheral arms through multimerization, which increases its affinity to the FBN1 N-terminus, heparan sulfate and fibronectin [Hubmacher *et al.*, 2008]. With the higher affinity of FBN1 to heparan sulfate than to fibronectin, the multimerized fibrillin beads are suggested to bind to heparan sulfate located on cell surface before interacting with the FN matrix. With the densely assembled C-terminus of FBN1, heparan sulfate interacts with C-terminus more likely than with the N-terminus [Yadin *et al.*, 2013]. This interaction promotes focal adhesions mediated by actin filaments to position the FBN1 beads for N-to-C terminal interactions. Elongation of the FBN1 occurs to form the characteristic bead-on-the-string structure. The N-terminal half of FN eventually interacts with C-terminal half of FBN1 to stabilize or allow further interactions with

other molecules [Reinhardt *et al.*, 1996a; Lin *et al.*, 2002; Sabatier *et al.*, 2009; Sabatier *et al.*, 2013; Hubmacher *et al.*, 2014].

1.2.4 Fibulin-4

FBLN4 (~48 kDa) is another microfibril-associated protein contributing to elastogenesis [Kumra *et al.*, 2019]. It is one of the members of the fibulin family composed of cbEGF and C-terminal fibulin domain [Papke & Yanagisawa, 2014]. Both cbEGF-like motif with insertion and the subsequent four cbEGF-like motifs interact with FBN1, whereas the C-terminal fibulin domain can interact with tropoelastin for elastin coacervation at the later stage of elastogenesis [Choudhury *et al.*, 2009; Kumra *et al.*, 2019]. FBLN4 multimerizes through the interactions of its central and C-terminal domains forming a disk-shaped particle with around 10 molecules which recruits tropoelastin and interacts with LTBP4 as explained in later paragraphs [Djokic *et al.*, 2013; Kumra *et al.*, 2019]. Furthermore, the N-terminal extended cbEGF-like motif interacts with the propeptide of lysyl oxidase (LOX) and activates it for cross-linking in elastogenesis [Horiguchi *et al.*, 2009; Noda *et al.*, 2020]. Although FBN1 interacts with FBLN4, FBN1 does not mediate FBLN4 assembly, but both pFN and cFN are necessary [El-Hallous *et al.*, 2007; Kumra *et al.*, 2018; Kumra *et al.*, 2019].

1.2.5 Fibulin-5

FBLN5 (~ 66 kDa) is another member of the fibulin family which shares a high homology with FBLN4 [El-Hallous *et al.*, 2007; Kobayashi *et al.*, 2007; Yanagisawa *et al.*, 2009]. However, FBLN5 has a higher binding affinity to tropoelastin compared to FBLN4 [Kobayashi *et al.*, 2007;

Choudhury et al., 2009]. FBLN5 also tethers and activates lysyl oxidase like 1 (LOXL1) for cross-linking in elastogenesis [*Liu et al., 2004; Choi et al., 2009*]. Furthermore, FBLN5 can interact with the N-terminal half of FBN1 and the C-terminal half of FBLN4 to potentially mediate tropoelastin deposition and coacervation although the function of these bindings is not studied extensively [*Freeman et al., 2005; Zheng et al., 2006; Choudhury et al., 2009*]. Although FBLN5 contributes to elastogenesis, FBLN5 neither interacts with FN nor contributes to the formation of fibrillin-containing microfibrils [*El-Hallous et al., 2007*].

1.2.6 Latent TGF- β binding protein-4

LTBP4 (~250 kDa), one of the members in LTBP family, has structural similarities with FBN1 [*Saharinen et al., 1998; Saharinen & Keski-Oja, 2000*]. LTBP4 binds via the latency-associated peptide (LAP) to TGF- β which is a major mediator of ECM formation and modulates vascular remodeling and potentially elastogenesis [*Saharinen & Keski-Oja, 2000; Chen et al., 2005; Randell & Daneshtalab, 2017*]. LTBP4 occurs in two isoforms identified by the number of cysteine domains at the N-terminus: the long (LTBP4L) and the short (LTBP4S) isoforms. The isoforms are determined by differential transcriptional start sites. The FBLN4 center fragment interacts the strongest with LTBP4L, whereas FBLN4 C-terminus has a weaker binding with LTBP4L [*Kumra et al., 2019*]. With the interaction between FBLN4 multimers and LTBP4L, LTBP4L undergoes a conformational change from a compact to an extended structure [*Kumra et al., 2019*]. Even when FBLN4 is removed after initiating this conformational change, the extended structure of LTBP4L persists, revealing that FBLN4 acts as a chaperone for the conformational change of LTBP4L [*Kumra et al., 2019*]. The extended LTBP4L interacts stronger with FBN1 and less with FN leading to a switch from FN fibers to microfibrils [*Kumra et al., 2019*]. FBLN4 then

escorts tropoelastin to the microfibril-bound extended LTBP4L to promote tropoelastin deposition [Noda *et al.*, 2013; Kumra *et al.*, 2019].

FBLN5 also interacts with LTBP4L and changes the conformation of LTBP4L, but the efficiency is lower than the FBLN4-induced conformational change, resulting in less amount and length of elastic fiber equivalents *in vitro* [Bultmann-Mellin *et al.*, 2015; Kumra *et al.*, 2019]. FBLN5-induced LTBP4L alone is not able to interact with FBN1 and pFN showing a weaker role of FBLN5 in LTBP4L function related to elastogenesis [Kumra *et al.*, 2019].

1.2.7 Elastin

Tropoelastin (60–70 kDa), the monomeric precursor of multimeric elastin (ELN), is produced by elastogenic cells, including in the aorta primarily smooth muscle cells, but also endothelial cells and fibroblasts. With alternations of hydrophobic and cross-linking domains, ELN can self-aggregate and form cross-links [Dyksterhuis *et al.*, 2007]. The hydrophobic domains which contain non-polar amino acid residues (glycine, valine, alanine and proline) allow tropoelastin to self-assemble to some extent [Vrhovski *et al.*, 1997; Debelle & Tamburro, 1999; Toonkool *et al.*, 2001]. The cross-linking domains consist of lysine residues not only mediating limited self-assembly but also allowing the formation of mature elastic fibers. The cross-linking process requires LOX or LOXL enzymes in a copper-dependent manner [Schmelzer *et al.*, 2019]. However, domain 36, a unique C-terminal domain in tropoelastin, is the only lysine-containing domain that does not form cross-links [Hedtke *et al.*, 2019]. The domain 36 does not only consist of positive-charged arginine residues located between the lysines but also two cysteine residues forming the only disulfide bond in tropoelastin. These components are required for tropoelastin's self-assembly and interaction with microfibril scaffold [Nonaka *et al.*, 2014; Ozsvar *et al.*, 2021] (**Figure 1.3**). Elastic fibers in

aorta are required to maintain the aortic compliance, which in turn is the ability of blood vessel wall to increase in volume in response to higher hemodynamic pressure [*Wagenseil et al., 2010; Jadidi et al., 2021*]. It is calculated as change in volume of aortic segment divided by aortic pulse pressure, determined through echocardiography and pressure transmitter. Aortic compliance correlates negatively with aortic wall stiffness and elastic fiber fragmentation [*Nettersheim et al., 2021*]. Patients with thoracic aortic aneurysm (TAA) and aortic dilation of 1.5 times or higher are known to have increased loss of elastic fibers and reduced aortic compliance [*Zhou et al., 2018; Tobey et al., 2019*].

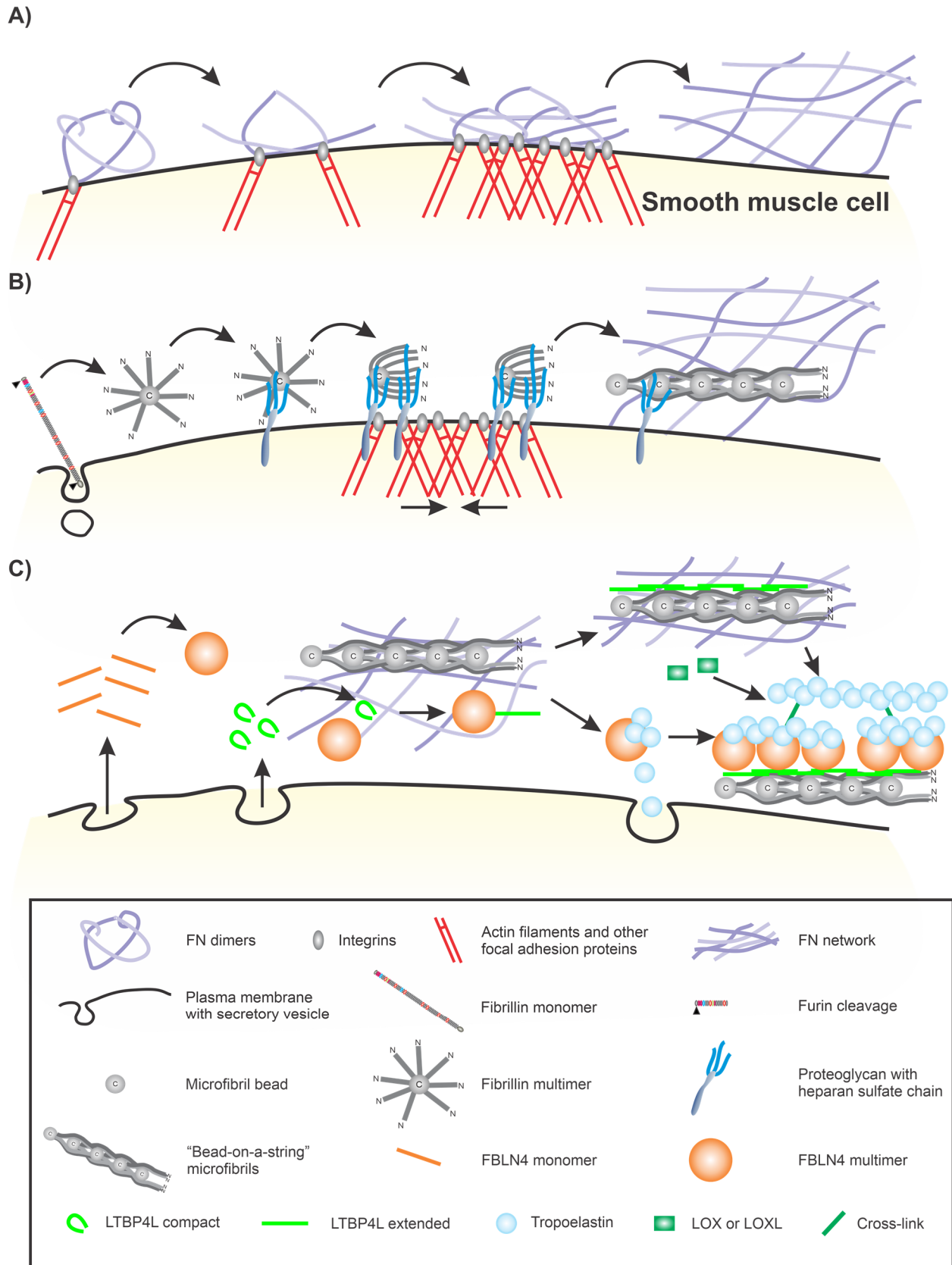


Figure 1.3: Schematic representation of elastogenesis. (Figure legend next page)

Figure 1.3: Schematic representation of elastogenesis. (Figure legend continued)

(A) FN assembly. Cells secrete FN dimers that interact with cells via cell surface receptors integrins. These interactions initiate focal adhesion formation (integrin, actin filament and other focal adhesion proteins) and cellular contraction leading to conformational change in FN, facilitating FN fiber assembly in matrix. The initial cell surface associated FN fibers gradually transition into insoluble FN fibers over time, providing a master scaffold for other matrix proteins.

(B) Fibrillin microfibril formation. Following furin mediated cleavage of propeptides, FBN1 undergoes multimerization via its C-terminus. The process of multimerization facilitates enhanced interaction with cell surface associated heparan sulfate proteoglycans and initiates a downstream cascade of focal adhesion formation and actin remodelling. This process increases cellular tension allowing better N-to-C-terminal self-interaction and formation of the “bead-on-a-string” microfibril structure. The FBN1 multimers interact with FN which is essential for stabilization and further assembly of FBN1.

(C) Role of FBLN4 and LTBP4 in elastogenesis. LTBP4 once secreted from cells is deposited onto FN fibers in compact form. FBLN4 when secreted from cells, undergoes multimerization and interacts with the compact LTBP4 to induce LTBP4 extension, unmasking the FBN1 binding sites. The extended LTBP4 then interacts with FBN1 containing microfibrils. FBLN4 then interacts with tropoelastin to linearly deposit it onto the extended LTBP4 fibers. Both LOX and LOXL enzymes initiate crosslinking of tropoelastin to form the mature elastic fibers in the matrix.

1.3 Fibrillinopathies and TAA

Fibrillin-containing microfibrils are required to form elastic fibers. Heritable connective tissue disorders occur due to mutations in fibrillin-1 known as type 1 fibrillinopathies [*Dietz et al., 1991; Collod-Beroud et al., 2003*]. Diseases associated with *FBN1* mutations are Marfan syndrome (MFS), dominant Weill-Marchesani syndrome, stiff skin syndrome, acromicric and geleophysic dysplasia, among others [*Dietz et al., 1991; Tsipouras et al., 1992; Faivre et al., 2003; Loeys et al., 2010; Le Goff et al., 2011*]. Among these, MFS is the most prevalent occurring 2-3 in every 10000 individuals [*Groth et al., 2015*]. MFS is a heritable and progressive connective tissue disorder with over 3000 known mutations leading to multiple systemic pathologies in the cardiovascular, skeletal, ocular, and adipose tissue [*Dietz et al., 1991; Pyeritz, 2000; Judge & Dietz, 2005; Kinori et al., 2017; Milewicz et al., 2021*]. Among these pathologies, aortic aneurysm

is the most detrimental. Due to mutations of fibrillin-1 in MFS patients, improper fibrillin-containing microfibril formation can lead to elastic fiber fragmentation [Canadas *et al.*, 2010; Zhang *et al.*, 2022]. Consequently, TAA in these patients occurs and eventually leads to aortic rupture which is the primary cause of death in MFS [Pyeritz, 2000].

1.4 Dysregulated signaling related to TAA

1.4.1 Embryonic origins of SMCs

Among the layers in the aorta, the focus of interest of this thesis is the media layer in TAA, which is typically heavily remodelled by SMCs during disease progression. SMC heterogeneity in the media is a hallmark of 3 distinct embryological origins. SMCs located at aortic root and outer media layer throughout anterior and posterior ascending aorta are derived by *Isl1*⁺ secondary heart field (SHF) cells; SMCs located at the aortic arch and inner media layer throughout ascending aorta are derived from *Wnt1*⁺ cardiac neural crest (CNC) cells; SMCs located at descending aorta are derived from *Meox1*⁺ somites [Cai *et al.*, 2003; Sun *et al.*, 2007; Wasteson *et al.*, 2008; Zhou & Pu, 2008; Zhang *et al.*, 2018]. This heterogeneity does not only contribute to the variation of aneurysm region but also how SMCs from different origins respond to pathological signals. With elevated TGF- β , Smad signaling is defective in SHF-derived SMCs but elevated in CNC-derived SMCs [MacFarlane *et al.*, 2019]. Furthermore, CNC-derived SMCs are prone to calcification which signifies severe aneurysm development, whereas the somite-derived SMCs are not [Leroux-Berger *et al.*, 2011].

Another origin of SMCs is adventitia-derived *Sca-1*⁺ progenitor cells. These cells are not originated in the aortic media layer. However, they migrate from the adventitia into media layer

and differentiate into SMCs during artery injuries and aneurysm leading to the elevation of collagen levels and to a stiffer ECM [*Kramann et al., 2016; Gharraee et al., 2022*].

1.4.2 Hypoxia-inducible factor 1 alpha

Hypoxia-inducible factor 1 alpha (HIF-1 α) is a transcription factor activated under hypoxic conditions [*Wang & Semenza, 1995*]. Under normoxic conditions, the proline residues of HIF-1 α undergo oxygen-dependent hydroxylation by prolyl hydroxylase (PHD). The von Hippel-Lindau-containing (VHL-containing) E3 ubiquitin ligase complex subsequently ubiquitinates HIF-1 α , and consequently, HIF-1 α is degraded by proteasomes. However, under hypoxic conditions, both PHD and VHL are phosphorylated and become inactive leading to an increased levels of HIF-1 α translocating to the nucleus [*Ampofo et al., 2010; Di Conza et al., 2017*]. Downstream signals associated with hypoxia responding element (HRE) are consequently elevated. This leads to elevation of matrix metalloproteinase-2, -9, -12, proteoglycan and collagen levels [*Xiong & Liu, 2017; Hiden et al., 2018; Oller et al., 2021; Shimomura et al., 2021*]. Although both mRNA and protein levels of HIF-1 α are elevated in MFS and non-MFS associated aortic aneurysms, the full mechanisms still require more investigations to understand the upstream and downstream pathways associated with HIF-1 α in the MFS aorta [*Liu et al., 2017; Li et al., 2018; Oller et al., 2021; Zhang et al., 2022*].

1.4.3 Matrix metalloproteinases

Matrix metalloproteinases (MMPs) cause elastin degradation in the ascending aortic wall leading to aortic aneurysm [*Kadoglou & Liapis, 2004; Nagase et al., 2006; Rabkin, 2017*]. Imbalance of

MMP enzymes and inhibitors leads to the degradation of vascular ECM and subsequently aortic aneurysm. Among these MMPs, MMP-2, -9 and -12 are the most recognized ones associated with thoracic aortic aneurysm [Xiong et al., 2012; Song et al., 2013; Rabkin, 2014; Tscheuschler et al., 2016]. Different MMPs utilize different combinations of transcription factors binding to their promoter regions of the genes [Fanjul-Fernandez et al., 2010]. The above mentioned 3 MMPs are upregulated by HIF-1 α , but only MMP-9 is regulated by nuclear factor kappa B which is a transcription factor regulated in inflammation [Robert et al., 2009; Li et al., 2013; Hiden et al., 2018]. These MMPs are classified by their structural differences (**Figure 1.4**). Although they share structural homologies in the N-terminal propeptide, catalytic zinc-binding and hemopexin-like domains, MMP-2 and -9 have three extra FN-like repeats in their catalytic domain to interact with collagens or gelatins, whereas MMP-12 does not [Allan et al., 1995; Steffensen et al., 1995; Kim & Joh, 2012]. In addition, MMP-9 has a type V collagen-like domain, but MMP-2 and -12 do not [Wilhelm et al., 1989]. Despite the structural differences, all three MMPs are capable to degrade elastin mediated by a zinc-binding catalytic domain [Klein & Bischoff, 2011; Lu & Aikawa, 2015]. Therefore, MMP-2, -9 and -12 are often analyzed in MFS [Oller et al., 2021; Zhang et al., 2022].

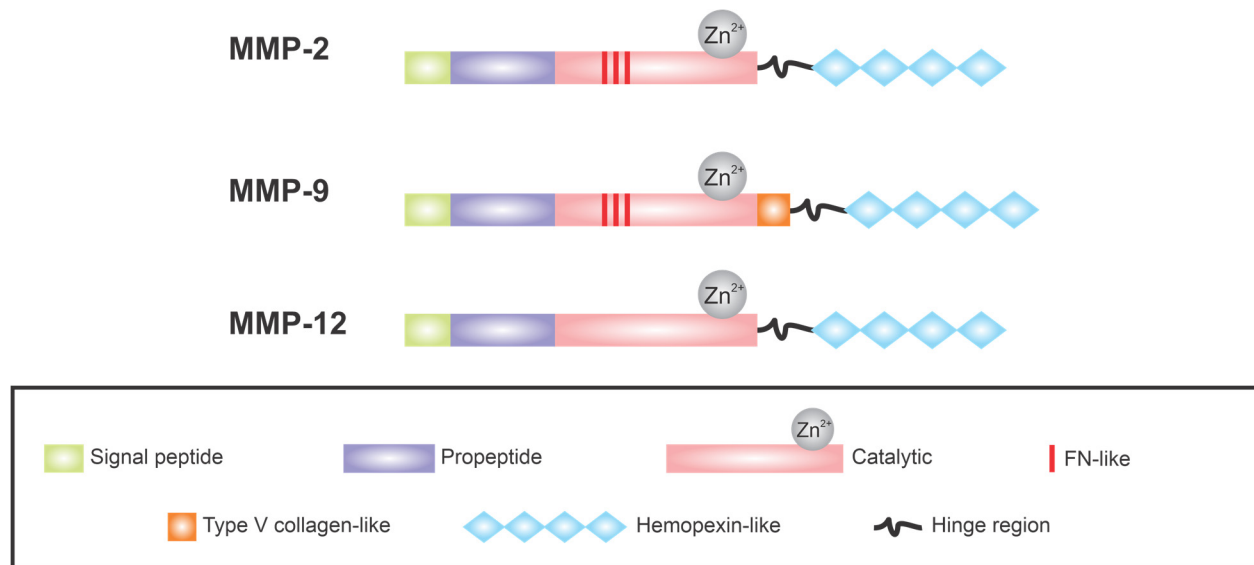


Figure 1.4: Schematic structure of MMP-2, -9 and -12. MMP-2, -9 and -12 have signal peptide, propeptide, catalytic domain, hinge region and hemopexin-like domain. Both MMP-2 and -9 have 3 FN-like domains. MMP-9 has a unique type V collagen-like domain. MMP-12 is devoid of any FN-like or type V collagen-like domains.

1.4.4 Proteoglycan

Proteoglycans are important extracellular matrix proteins to maintain aortic structure. Under normal conditions, proteoglycans with their covalently attached long unbranched sulfated (and thus negatively charged) glycosaminoglycans retain water molecules to form a stable aortic structure and allow mechanosensing of smooth muscle cells to prevent deformation of blood vessels [LeBaron *et al.*, 1992; Evanko *et al.*, 1999; Azeloglu *et al.*, 2008; Roccabianca *et al.*, 2014b]. Furthermore, proteoglycan promotes formation of elastic fibers [Merrilees *et al.*, 2002]. However, in a pathological condition, proteoglycan is over-deposited in the ECM potentially mediated by HIF-1 α [Cikach *et al.*, 2018; Shimomura *et al.*, 2021]. In this situation, smooth muscle cells can be over-pressurized leading to the loss of mechanosensing and cell integrity [Roccabianca *et al.*, 2014b]. There are two types of proteoglycans known to be elevated in MFS: aggrecan and versican [Cikach *et al.*, 2018; Yin *et al.*, 2019].

Aggrecan consists of three globular domains (G1, G2 and G3) and three extended domains (inter-globular, keratan sulfate and chondroitin sulfate domain) [Kiani et al., 2002]. The G1 domain serves as an anchor to bind to hyaluronic acid and interacts with link protein to stabilize the formation of aggrecan [Watanabe et al., 1998; Kiani et al., 2002]. The inter-globular domain locates between G1 and G2 domains. This region is where the MMP-2, -9 and -12 cleaves to modulate the retention of water molecules [Little et al., 1999; Durigova et al., 2011]. Compared to MMPs, a disintegrin and metalloproteinase with thrombospondin motifs (ADAMTS) are capable and more efficient to cleave this region of the aggrecan [Durigova et al., 2011]. Following the inter-globular domain is G2 domain [Kiani et al., 2001]. The subsequent domain is keratan sulfate domain which holds water molecules in aggrecan with the negatively charged glycosaminoglycan chains [Kiani et al., 2001]. The next domain is chondroitin sulfate domain which is the largest aggrecan domain. Compared to keratan sulfate domain, chondroitin sulfate domain holds a larger amount of water leading to tissue swelling and stiffening [Urban et al., 1979; Humphrey, 2013]. Among these domains in aggrecan, G2, keratan sulfate and chondroitin sulfate domain are required for product secretion [Kiani et al., 2001]. The C-terminal G3 domain connects to ECM molecules such as fibrillin-1 and fibulins [Aspberg et al., 1999; Olin et al., 2001; Isogai et al., 2002; Scuderi et al., 2010; Aspberg, 2012].

Versican also share similar structure as aggrecan having G1, chondroitin sulfate, and G3 domains. Although versican lacks certain domains compared to aggrecan, it retains water molecules as well [McGee & Wagner, 2003]. However, aggrecan harbors more chondroitin sulfate chains than versican, and thus the potential of swelling pressure is greater. Therefore, aggrecan is suggested to be a more prominent root cause of aortic swelling compared to versican [Kiani et al., 2002; Humphrey, 2013; Roccabianca et al., 2014a].

1.4.5 Collagen

Collagen is the most abundant protein in mammals and forms ~30% of body protein [Vuorio & de Crombrughe, 1990; Di Lullo et al., 2002; Stefanovic, 2013]. Collagen does not only provide mechanical support for tissues but also modulates cell migration and signaling [da Rocha-Azevedo & Grinnell, 2013; Li et al., 2021; Schuh et al., 2022]. It consists of three polypeptide chains (α -chains) to form a triple helix structure. The polypeptide chains are composed of Gly-X-Y repeating motifs. Glycine occupies every third residue in the polypeptide chains to form a tight configuration and resist pressure or stress. The X and Y amino acid motifs are often proline and hydroxyproline to support the helix structure of collagen [Beck et al., 2000]. Hydroxylation occurs through prolyl hydroxylase and lysyl hydroxylase to add a hydroxyl group to proline and lysine residues, respectively [Yamauchi & Shiiba, 2008; Sipila et al., 2018]. Glycosylation also occurs by adding carbohydrate to hydroxyl groups via galactosyltransferase (addition of galactose) and glycosyltransferase (addition of glucose) [Eyre et al., 1984]. Hydrogen bonds do not only stabilize the triple helix structure between hydroxylated proline and water but also hold the three polypeptide chains together connecting between the N-H group in glycine and C=O bonds in neighbouring chains [Bella & Berman, 1996; Rappu et al., 2019]. Immature procollagens are formed and secreted out of cells. To form tropocollagen, the loose ends at N- and C-terminal of procollagen molecules are cleaved by collagen peptidases [Orgel et al., 2000]. These tropocollagen molecules undergo copper-dependent crosslinking by lysyl oxidase to form mature collagen. A staggered pattern known as D-bands (~67 nm) are observed [Mallinger et al., 1992]. With its organized structure, collagen is recognized by its stability and resistance responding to stress compared to other ECM macromolecules [Sawicki et al., 2009].

Multiple types of collagens form the basis of various tissues [Gelse et al., 2003]. Among them, collagen I and III which are fibrillar-forming collagens are recognized as highly deposited ECM in fibrotic tissues [Ely et al., 2010; Perrucci et al., 2020; Nettersheim et al., 2021]. Collagen I is composed of two $\alpha 1$ and one $\alpha 2$ chains encoded by the *COL1A1* and *COL1A2* genes, respectively, whereas collagen III is composed of three $\alpha 1$ chains encoded by the *COL3A1* gene. Recent studies revealed that TAA in MFS is characterized by elevated total collagen protein levels and gene expressions of *COL1A1* and *COL3A1* [Perrucci et al., 2020; Nettersheim et al., 2021]. Dilating aorta in TAA is associated with a phenotypic switch of SMCs from healthy contractile state to synthetic state with increased production of ECM proteins including collagens. Additionally, HIF-1 α is known to upregulate collagen levels, promoting fibrosis like phenotype in the aortic tissue [Xiong & Liu, 2017; Nam et al., 2021]. Higher levels of collagen in matrix eventually results in stiffening of the aortic wall and thereby lowering the aortic compliance [Zhu et al., 2006; Steed et al., 2010; Jadidi et al., 2021]. Therefore, collagen expression and deposition are important factors investigated in MFS. Based on the results presented in multiple studies, the current proposed mechanism of elastic fiber fragmentation in TAA is shown in the following model (**Figure 1.5**).

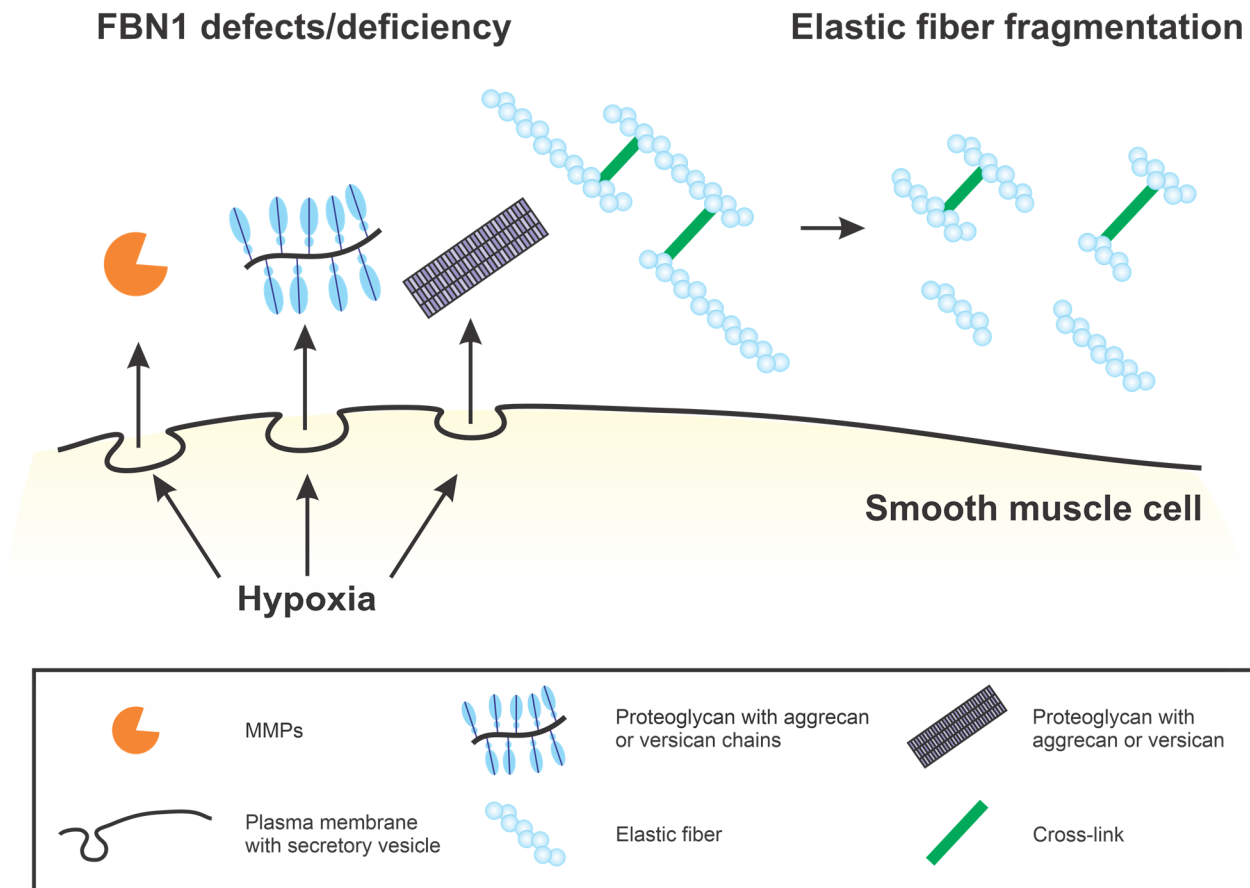


Figure 1.5: Schematic overview of known physiological drivers of elastic fiber fragmentation leading to TAA in MFS. Alterations or deficiency of FBN1 in aorta is associated with elevation in hypoxia or HIF1- α , increased MMP secretion, and extensive ECM remodelling with higher levels of proteoglycans and collagens in matrix. Increased proteoglycans and collagens contribute to aortic stiffness, loss of mechanosensing and elasticity and elastic fiber fragmentation. Additionally, MMPs further degrade the elastic fibers contributing to further loss of elastic fiber system. These processes altogether contribute to weakening of aortic wall and dilation under the physiological hemodynamic stress.

1.5 Marfan syndrome and sexual dimorphism

1.5.1 Metabolism in Marfan syndrome

Abnormal metabolism in individuals with MFS is characterized by a lipodystrophic phenotype with 36% being overweight or even obese (body mass indices of $>30 \text{ kg/m}^2$) [Erkula et al., 2002; Graul-Neumann et al., 2010; Yetman & McCrindle, 2010; Goldblatt et al., 2011; Jacquinet et al., 2014; Passarge et al., 2016; von Kodolitsch et al., 2019; Hansen et al., 2020]. Adiposity increases

with age in MFS patients [Erkula et al., 2002; von Kodolitsch et al., 2019; Hansen et al., 2020]. With abnormal adipose tissue deposition, patients experience insulin resistance and type 2 diabetes mellitus and have a higher risk of cardiovascular diseases [Erkula et al., 2002; Orio et al., 2007; Graul-Neumann et al., 2010; Yetman & McCrindle, 2010; Goldblatt et al., 2011; Bastien et al., 2012; Jacquinet et al., 2014; Passarge et al., 2016; von Kodolitsch et al., 2019; Hansen et al., 2020; Zheng et al., 2021]. To study MFS, *Fbn1*^{mgR/mgR} (mgR) mice are used in this study. This mouse model has an insertion of a “neo-cassette” in the intron between exons 18 and 19 in the *Fbn1* gene, leading to a reduction of FBN1 protein to 20-25%, long bone overgrowth and kyphosis [Pereira et al., 1999]. Male mgR mice are more susceptible to weight gain compared to female mgR mice [Muthu et al., 2022]. Surprisingly, the C-terminal half of FBN1 attenuates adipogenic differentiation, suggesting the inhibition of adipogenesis in early commitment [Muthu et al., 2022]. However, the response to high-calorie diet in MFS is not investigated extensively.

1.5.2 Thoracic aortic aneurysms and aortic dissection in Marfan syndrome

Thoracic ascending aortic aneurysms (TAA) increase the risk of dissection (TAAD), a more severe form of aortic complication with tears in the inner layer of aortic wall [Pape et al., 2007; Cheung et al., 2017; Chung et al., 2020]. Nearly 70% of patients who have no genetic etiology and experience TAAD are male individuals, showing that men are more prone to TAAD than women, but the risk of TAAD in women with TAA is three times higher than men [Juvonen et al., 1997; Davies et al., 2002; Nienaber et al., 2004]. Furthermore, women have 40% higher chance to die from TAA than men [Pape et al., 2007; Cheung et al., 2017]. This parallels with TAA or TAAD prevalence in MFS. In MFS, TAA occurs more severe and earlier in men than in women [Detaint et al., 2010; Roman et al., 2017]. However, women with MFS experienced higher TAAD rates at

later stages of their lives than men [Meijboom *et al.*, 2005]. Possibly, in women, estrogen decreasing with increasing age may lead to a higher risk of aneurysm [Wu *et al.*, 2007; Tripathi *et al.*, 2017; Qi *et al.*, 2020]. The mgR mice also experience severe TAA and die around 12 to 16 weeks of age [Pereira *et al.*, 1999]. Aortae in male mgR mice are more dilated than aortae in female mgR mice even as early as 4 weeks of age, revealing the sexual dimorphism of TAA [Zhang *et al.*, 2022].

1.5.3 High-calorie-induced metabolism and aneurysm

Although the consequence of high-calorie diet in metabolism and aneurysm have not been studied in MFS, a high-calorie diet promotes abnormal metabolism and non-thoracic aortic aneurysm. The high-calorie diets can contain high fat, high sucrose or a combination of both (western diet), and induce insulin resistance, obesity and non-alcoholic fatty liver disease with elevation of inflammation markers [Lackey *et al.*, 2016; Stanhope, 2016; Taskinen *et al.*, 2019; Liang *et al.*, 2022]. Although both fat and sucrose can contribute to abnormal metabolic phenotypes, a study emphasizes that sucrose induces non-alcoholic fatty liver phenotype stronger than fat [Ishimoto *et al.*, 2013]. Both high fat and high sucrose diets promote inflammation and collagen levels in abdominal aortic aneurysm [Miyamoto *et al.*, 2018; Takahara *et al.*, 2018; Shimizu *et al.*, 2019; Xu *et al.*, 2019]. Excess adiposity often correlates with aortic aneurysm progression in humans, but the high-calorie-induced consequence in TAA is not studied [Yetman & McCrindle, 2010].

1.6 Rationale, hypotheses and objectives

1.6.1 Rationale

Individuals with MFS are characterized by the mutations in the *FBNI* gene, leading to abnormal metabolism (obesity and lipodystrophy) and TAA. Previous studies from the Reinhardt laboratory showed the sexual dimorphism of MFS metabolism and aneurysm correlating with clinical data [Muthu *et al.*, 2022; Zhang *et al.*, 2022]. In addition, high-calorie diets contribute to abnormal metabolism and multiple cardiovascular diseases [Yetman & McCrindle, 2010; Lackey *et al.*, 2016; Takahara *et al.*, 2018; Shimizu *et al.*, 2019; Xu *et al.*, 2019; Liang *et al.*, 2022]. However, there are no studies on the consequence of these diets in MFS metabolism and TAA.

1.6.2 Hypotheses

We hypothesize that high-calorie diets will worsen body metabolism and promote aortic aneurysm development in MFS. Based on previous data in the lab, we also hypothesize that MFS females are protected from metabolic phenotypes and aneurysm development, responding to high-calorie diets compared to MFS males.

1.6.3 Objectives

This MSc project aimed to characterize and investigate the consequences of high-calorie diets in male and female MFS metabolism and TAA with these specific objectives:

1. Investigate the role of high-calorie diet and sex in metabolic phenotype of MFS mice
2. Study the consequence of high-calorie diet and sex in TAA of MFS mice

CHAPTER 2: MATERIALS AND METHODS

2.1 Mouse model and diets

The McGill University Animal Care Committee approved all experimental procedures following the guidelines of the Canadian Council on Animal Care (Protocol #2014-7561). *Fbn1*^{mgR/mgR} (mgR) mice were kindly provided by Dr. Francesco Ramirez at the Icahn School of Medicine at Mount Sinai in New York. These mice have a neomycin cassette inserted in the *Fbn1* gene between exons 18 and 19 which leads to a transcriptional interference ultimately reducing normal fibrillin-1 levels to 20-25% compared to wild-type (WT) mice. Consequently, the mgR mice experienced severe aortic aneurysm, leading to death around 12 to 16 weeks of age [Pereira et al., 1999]. WT mice from the same breeding were used as a littermate control in the study. Both mgR and WT mice were on the C57BL/6J genetic background and housed in a pathogen-free animal facility. Male *Fbn1*^{mgR/+} (mgR/+) were bred with female WT mice purchased from Jackson Laboratories as backcrossing to generate mgR/+ and WT mice and prevent genetic drift. From the backcrossing, male mgR/+ mice were bred with female mgR/+ mice to generate WT, mgR/+ and mgR mice. WT and mgR mice were used for experiments. The mgR mouse colonies were fed with chow diet (grain-based) purchased from Envigo, USA (Cat #2920X). All mice were maintained under 12 h of light-dark cycle. For the experiments, male and female WT and mgR mice were fed from 4-12 weeks of age with control (10% fat), high fat (60% fat) and western diet (45% fat; 30% sucrose) purchased from Research Diets (**Figure 2.1, Table 2.1**). Breakdown of number of mice per genotype per diet that was used in the study for both sexes in various experiments are provided in Table 2.2. The survival of each mouse was recorded daily to obtain a Kaplan-Meier survival curve. The cause of death due to aortic rupture in these mice was determined through dissection.

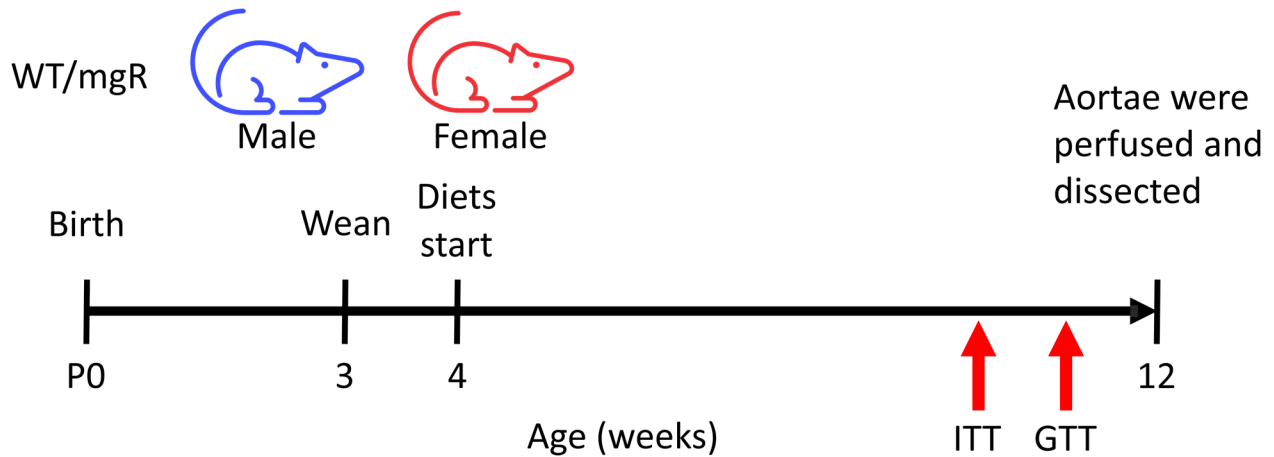


Figure 2.1: Timeline of experiments. Male and female WT and mgR mice were fed for 8 weeks starting at 4 weeks with CD, HFD or WD as outlined in Table 2.1. ITT was performed at 10 weeks and GTT at 11 weeks of age. At 12 weeks of age, the mice were euthanized and the aortae were perfused and dissected.

Table 2.1: Composition of diets used in this study.

Type of diet	Control diet (CD)		High fat diet (HFD)		western diet (WD)	
Product ID	D12450KY		D08060104B		D08112601R	
	%kcal	%gm	%kcal	%gm	%kcal	%gm
Protein	20	19	20	26	20	24
Carbohydrate	70	67	20	26	35	41
Fat	10	4	60	35	45	24
Other	0	10	0	13	0	11
Total	100	100	100	100	100	100
Selected key ingredients modified from control diet (highlighted)						
	kcal	gm	Kcal	gm	kcal	gm
Lard (fat)	180	20	2205	245	1598	178
Sucrose (sugar)	0	0	0	0	1182	296
Total kcal	4057		4057		4057	

Table 2.2: Overview of number of mice in each sex, genotypes and diets.

Sex	Genotype	Diet	Total
Male	WT	CD	20
	mgR	CD	25
	WT	HFD	15
	mgR	HFD	21
	WT	WD	15
	mgR	WD	16
Female	WT	CD	17
	mgR	CD	17
	WT	HFD	17
	mgR	HFD	19
	WT	WD	14
	mgR	WD	15

The initial body mass was measured before providing known food quantities. Body mass and left-over food mass were determined weekly until the experimental endpoint. The difference of provided food quantities and left-over food quantities was determined to capture the total food consumption. By converting grams to kilocalories based on each diet (see **Table 2.1**) and dividing by the number of days consuming the food, food consumption was analyzed for each mouse. At 10 weeks of age, insulin tolerance test (ITT) was performed in the afternoon after starving the mice for 6 h. At 11 weeks of age, glucose tolerance test (GTT) was performed in the morning after starving the mice for 12 h overnight. This experimental setup was standardized based on numerous literature evidences and the previous published work from lab, giving stable readouts during the course of study [*Lundbaek, 1962; Okita et al., 2014; Vinue & Gonzalez-Navarro, 2015; Benede-Ubieto et al., 2020*]. A drop of blood was collected by puncturing gently the tail vein with a needle and measured by dipping the blood glucose strips into the blood. The blood glucose level was measured by a blood glucometer (Verio Flex, OneTouch) immediately before (time 0) and after 15, 30, 60, 90 and 120 min of intraperitoneal insulin (0.75 U/kg) or glucose (2 g/kg) injection.

Mice were euthanized by overdosed ketamine/xylazine/acepromazine cocktail (100/10/3 mg/kg) intraperitoneal injection at 12 weeks of age. Tibiae from male and female WT and mgR mice were dissected and the length was measured. Following phosphate-buffered saline (PBS) perfusion for 3 min, thoracic aortae were micro-dissected for gross tissue image recording.

2.2 Genotyping

The genomic DNA was extracted from mouse tails, followed by polymerase chain reaction (PCR) using the protocol and materials from the Fast Lysis-PCR Genotyping Kit (ZmTech Scientific, GT-001P). WT mice generated a 690 bp product, and mgR mice generated a 480 bp product due to the neo-cassette disrupting the *Fbn1* gene (**Figure 2.2**). The forward (5'-GGGTAAAGGATGCACATATGTAAAGTGGTGC-3'), reverse (5'-AATCCAGTACTAGGAGGAGAAGGCCATG-3') and neo-cassette (5'-GCCAAGTTCTAATTCATCAGAAGCTGGTC-3') primers were used at 250 nM concentration in the PCR reaction.

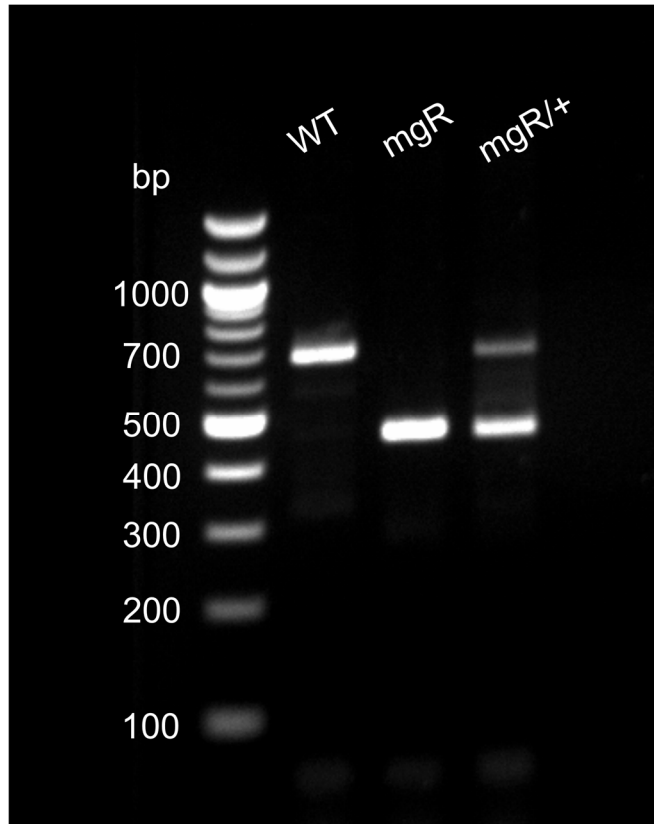


Figure 2.2: Genotyping of WT, mgR and mgR/+ mice. WT, mgR and mgR/+ mice generated a 690 bp, 480 bp and a combination of both 690 bp and 480 bp, respectively. Marker bands are shown on the left.

2.3 Measurement of in situ aortic diameters and preparations for histological and RNA analyses

After perfusion with PBS, the diameter of the most dilated region perpendicular to the aortic wall was measured on images of the dissected aortae. For histological analysis, the aortae were perfused with an additional 4% paraformaldehyde in PBS for 2 min and fixated in a different 4% paraformaldehyde in PBS at 4°C overnight. The aortae were then washed with PBS 3 times and embedded in paraffin. The tissues were sectioned at 5 µm per section followed by deparaffinization through baking slides at 65°C for 45 min and incubating the slides in CitriSolv (Decon Labs) 2 times 5 min each. Hydration was conducted by decreasing the percentage of ethanol (from 100%

to 0% ethanol) and simultaneously increasing the water content. Indirect immunofluorescence or histological staining was conducted immediately after this procedure. For RNA analysis at a later time, aortae were snap-frozen in liquid nitrogen and immediately transferred to a -80°C freezer.

2.4 Quantification of aortic lumen area and wall thickness

Autofluorescence images were captured by Axio Imager M2 microscope (Zeiss) equipped with an ORCA-flash 4.0 camera (Hamamatsu) at 50× magnification using the 517 nm filter. Both perimeter of outer elastic laminae (P_o) and inner elastic laminae (P_i) were measured by ImageJ. The lumen area was determined according to this formula: $\text{lumen area} = \pi \times (P_i/2\pi)^2$. To measure the aortic wall thickness, this formula was used: $\text{Wall thickness} = (P_o - P_i) / 2\pi$.

2.5 Indirect immunofluorescence

After deparaffinization, both antigen retrieval methods using citric acid buffer (10 mM citric acid, pH 6.0, 0.05% Tween 20: 20 min) dissolved in distilled water and consecutively protease XXIV (10 μ M, Sigma-Aldrich, Cat #P8038: 5 min) dissolved in 50 mM Tris-HCl, pH 7.6 were performed. The sections were washed with Tris-buffered saline with 0.05% Tween (TBST) for 3 times (5 min each) followed by blocking with 2% bovine serum albumin for 1 h. The sections were incubated with primary antibodies using α -rF6H polyclonal anti-fibrillin-1 antiserum [Tiedemann *et al.*, 2001], anti-HIF-1 α (Novus Biologicals, Cat #NB100-479) and anti-MMP12 (Abcam, Cat #ab52897) at 1:1000, 1:200 and 1:500 dilution, respectively, overnight at 4°C. The sections were later incubated with secondary antibodies using goat anti-rabbit Cy5-conjugated antibody (ThermoFisher, Cat #A10523) for 1 h at room temperature at 1:200 dilution. Nuclei were stained

with Vectashield containing 4', 6-diamidino-2-phenylindole (DAPI) (Vector labs, Cat #VECTH1200). No primary antibody control was used as the non-specific binding control (**Figure 2.3**). Immunofluorescence images were taken using an Axio Imager M2 microscope (Zeiss) equipped with an ORCA-flash 4.0 camera (Hamamatsu). The fluorescence signal was detected at 517 nm (green: autofluorescence), 673 nm (red: target protein), and 465 nm (blue: DAPI). Mean intensity of fibrillin-1, HIF-1 α and MMP-12 were quantified with original images in the tiff format using ImageJ [Schneider *et al.*, 2012; Zhang *et al.*, 2020]. Multiple images were taken to cover 70-80% of the entire aorta.

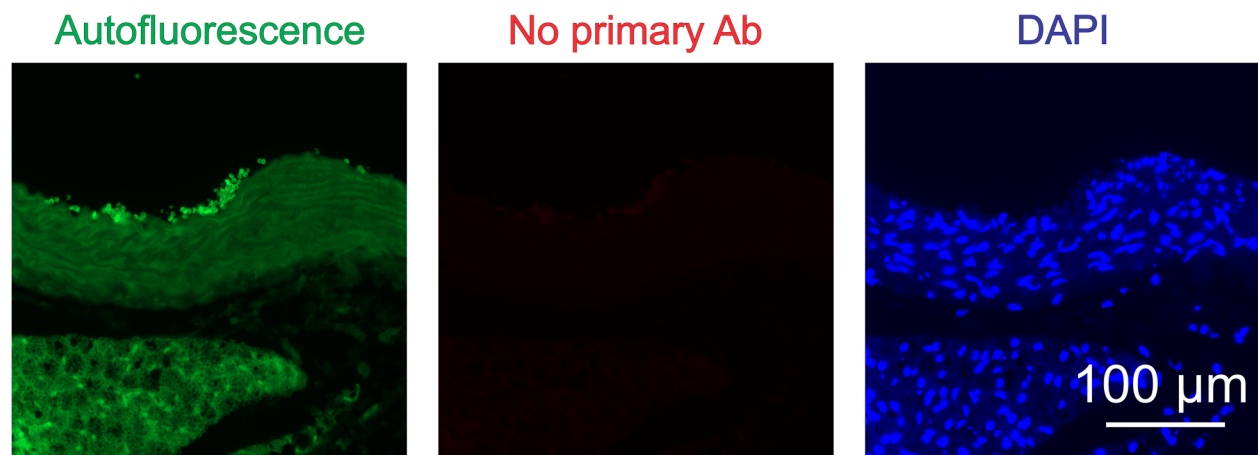


Figure 2.3: No primary antibody control of aorta from a male WT mouse. Autofluorescence, primary antibody and DAPI fluorescence signals were detected at 517 nm, 673 nm, and 465 nm, respectively.

2.6 Histological staining

To quantify elastic fiber fragmentation, proteoglycan and collagen deposition levels, the aorta sections were stained using Hart's, alcian blue and picrosirius red staining procedures, respectively. For Hart's staining, the aorta sections were incubated in resorcin fuchsin solution (PolyScientific

R&D, Cat #s265s) for 6 h and counter-stained by metanil yellow (Sigma, Cat #M7276) solution for 5 min. These solutions were produced as previously described [Davis & Li, 2017]. To stain proteoglycan, alcian blue powder (Sigma, A5268-10G) was solubilized in 3% acetic acid at a 1g:100mL ratio. The pH was adjusted to 2.5 with acetic acid before usage. The aorta sections were incubated in the alcian blue solution for 30 min. To stain collagen, aorta sections were stained by picrosirius red (Abcam, ab150681) for 1 h and rinsed by 0.5% acetic acid solution based on the recommended protocol. The sections were then dehydrated to absolute alcohol and incubated in CitriSolv (Decon Labs) for 5 min. Lastly, the sections were mounted with Permount (Fisher, SP15-100). Images were captured with an Axio Imager M2 bright field microscope (Zeiss) equipped with an AxioCam ICc5 colour camera. Elastic fiber fragmentation of the entire aorta section was quantified by two independent researchers blinded to the sample groups and normalized to the total area of aortic wall. For quantification of alcian blue and picrosirius red staining, immunohistochemistry toolbox in ImageJ was used for quantifying the intensity of histological staining [Shu *et al.*, 2016]. Multiple images were taken covering 70-80% of the entire aorta section for alcian blue and picrosirius red staining.

2.7 RNA extraction and real-time quantitative PCR (qPCR)

Total RNA was extracted from the aortae through sonification (Branson sonifier 150) and the RNeasy Kit (Qiagen, Cat #217004), following the manufacturer's instructions. The mRNAs isolated from the aortae were reverse transcribed into cDNAs using the ProtoScript II First-Strand Synthesis System (New England Biolabs, Ipswich, MA, USA, Cat #E6560S). To quantify mRNAs, qPCR was conducted on the cDNA products using SYBR Green SelectMaster Mix (Applied Biosystems, Cat #4472908). The qPCR began by running at 50°C for 2 min and at 95°C

for 2 min to initiate. Afterwards, the qPCR was followed by 40 cycles of 3-step cycling program: denaturation at 95°C for 15 s, annealing at 58°C for 15 s and extension at 72°C for 1 min. Postamplification melting curve analysis was performed and target mRNA expression level was measured through delta-delta Ct method. Mouse-specific forward and reverse primers of the target genes at 5µM were used for qPCR (Table 2.2). *Gapdh* was used as the reference gene.

Table 2.3: Mouse-specific primers used for qPCR.

Gene	Forward (5'-3')	Reverse (5'-3')
<i>Fbn1</i>	GGTAGTGGATTCTCTGAGAC	GGCGTATTGCACATGCTGTG
<i>Hif1a</i>	ACTTCTGGATGCCGGTGGTC	CGCCGTCATCTGTTAGCACC
<i>Mmp2</i>	TCGCAGTGATGGCTTCCTC	AAACAAGGCTTCATGGGGGC
<i>Mmp9</i>	CACCACAGCCAACTATGACC	AGGAAGACGAAGGGGAAGAC
<i>Mmp12</i>	GGCCATTCCTTGGGGCTGCA	GGGGGTTTCACTGGGGCTCC
<i>Acan</i>	TCAGAAGGGTCAGGGGAGAC	AGTGTCCAAGGCATCCACGC
<i>Vcan</i>	ACTACAAGGGGCGAGTGTCC	ATCACATCGGTAGACGCCTG
<i>Coll1a1</i>	TGCTCCTCTTAGGGGCCACT	TTTCCACGTCTCACCATTGGG
<i>Col3a1</i>	AGGTGAACCCGGCAAGAACG	CCATCTTCGCCCTTAGGTCC
<i>Gapdh</i>	CACTCTTCCACCTTCGATGC	CACCACCCTGTTGCTGTAGC

2.8 Statistics

For the Kaplan-Meier analyses, the survival rate comparisons were analyzed by the log-rank test. All other data are shown as means ± standard error of the mean (SEM). For growth curves, ITT and GTT, the means comparisons were analyzed by 2-way ANOVA with repeated measures Tukey's test, whereas for other analyses, the means comparisons were analyzed by 3-way ANOVA Tukey's test. All statistical analyses were performed using OriginPro version 2021 software

(OriginLab). Outliers were detected by Grubb's test with confidence levels of 95%. In all relative analyses, the value of the male WT mice fed with CD was set to 1.

CHAPTER 3: METABOLIC ANALYSIS OF MALE AND FEMALE MGR MICE FED WITH HIGH-CALORIE DIETS

3.1 HFD- and WD-induced weight gain in male and female mgR mice

Male and female WT and mgR littermates were fed with CD, HFD or WD starting from 4 to 12 weeks of age. The body mass was recorded weekly to determine weight gain throughout the duration of the HFD and WD period (**Figure 3.1**). There was no difference in body mass between male WT and mgR mice when fed with CD, HFD or WD. However, female mgR mice were significantly heavier than female WT mice when fed with CD starting from 8 weeks of age but not with HFD or WD (**Figure 3.1A**). Both male WT and mgR mice increased weight starting from 5 weeks of age when fed with HFD or WD, confirming the expected consequences of these high-calorie diets. This was similar in female WT mice, whereas female mgR mice were protected from weight gain fed with HFD or WD (**Figure 3.1B**). Therefore, male mgR were heavier than female mgR mice when fed with HFD starting from 5 weeks of age or fed with WD starting from 8 weeks of age (**Figure 3.1C**). Comparing male and female mice fed with the high-calorie diets, the female mgR mice resisted weight gain when fed with HFD or WD, but not the male mgR mice.

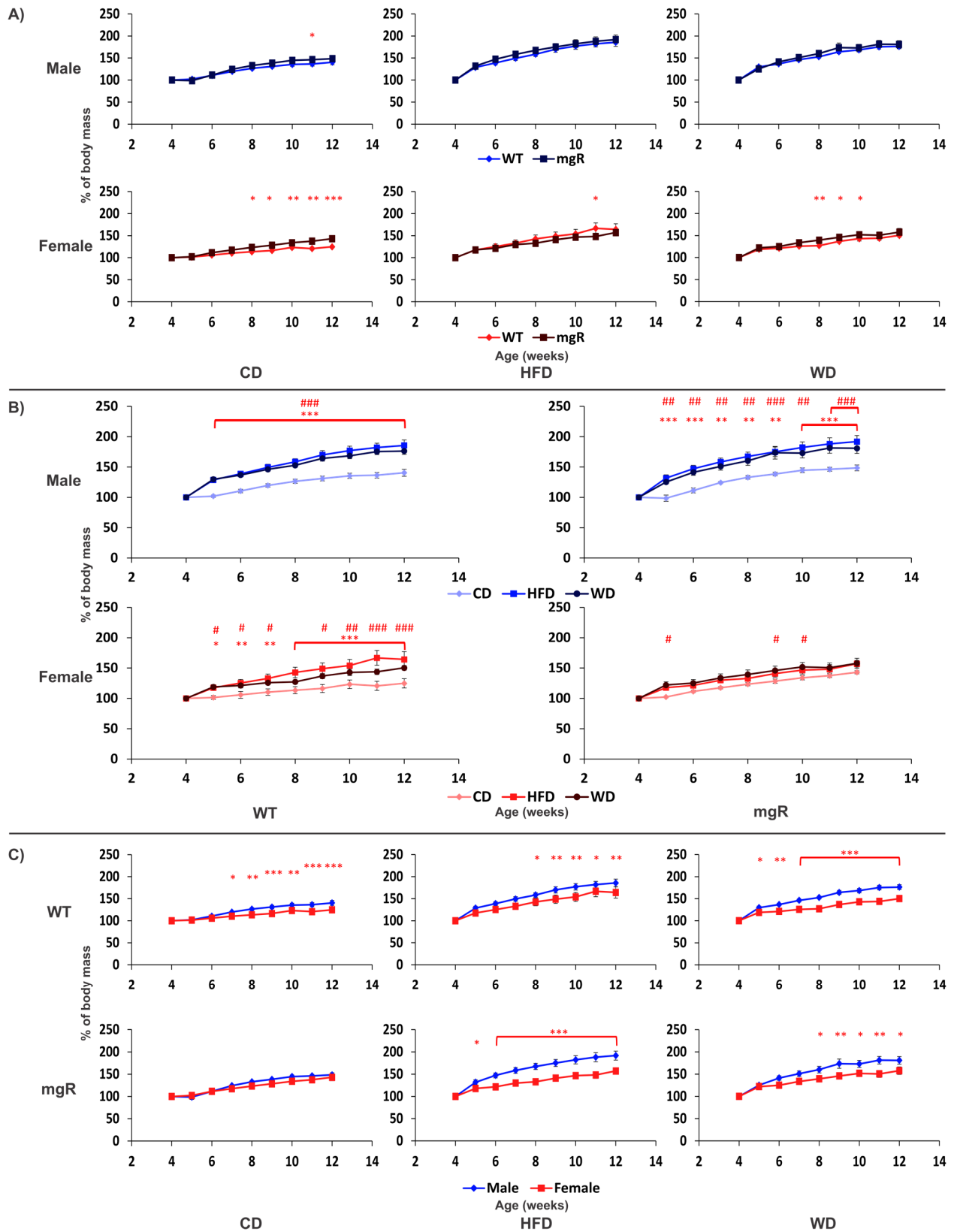


Figure 3.1: Relative body mass of 4-12-week-old male and female WT and mgR mice fed with CD, HFD or WD. (Figure legend next page)

Figure 3.1: Relative body mass of 4-12-week-old male and female WT and mgR mice fed with CD, HFD or WD. (Figure legend continued)

The weight of each mouse at 4 weeks of age was set to 100%. **(A)** Genotype-dependent differences of male (top panel) and female (bottom panel) mice fed with CD (left column), HFD (middle column) or WD (right column). **(B)** Diet-dependent differences of male (top panel) and female (bottom panel) WT (left column) and mgR mice (right column). * compared HFD to CD; # compared WD to CD. **(C)** Sex-dependent differences of WT (top panel) and mgR (bottom panel) mice fed with CD (left column), HFD (middle column) or WD (right column). Data are represented as means \pm SEM, n = 6–9 mice per group. Significance was assessed by 2-way ANOVA repeated measures and indicated as *p<0.05, **p<0.01, ***p<0.001, #p<0.05, ##p<0.01, and ###p<0.001.

3.2 HFD- and WD-induced final body parameters in male and female mgR mice

The final body mass and tibia length of male and female WT and mgR mice were determined at the experimental endpoint (12 weeks of age) (**Figure 3.2A and B**). To examine the overweight phenotype, body mass was normalized to the tibia length. The results correlate with the previous data in that male mgR mice were susceptible to weight gain but not the female mgR mice when fed with HFD. However, WD had no consequence in weight gain for both male and female mgR mice. Overall, male mgR mice were heavier than female mgR mice but only when fed with HFD or WD (**Figure 3.2C**). There was no difference in mgR mice except that female mgR mice fed with HFD had an increased food consumption while having a lower body mass (**Figure 3.2D**). This data further emphasizes the protective phenotype of the female mgR mice against weight gain.

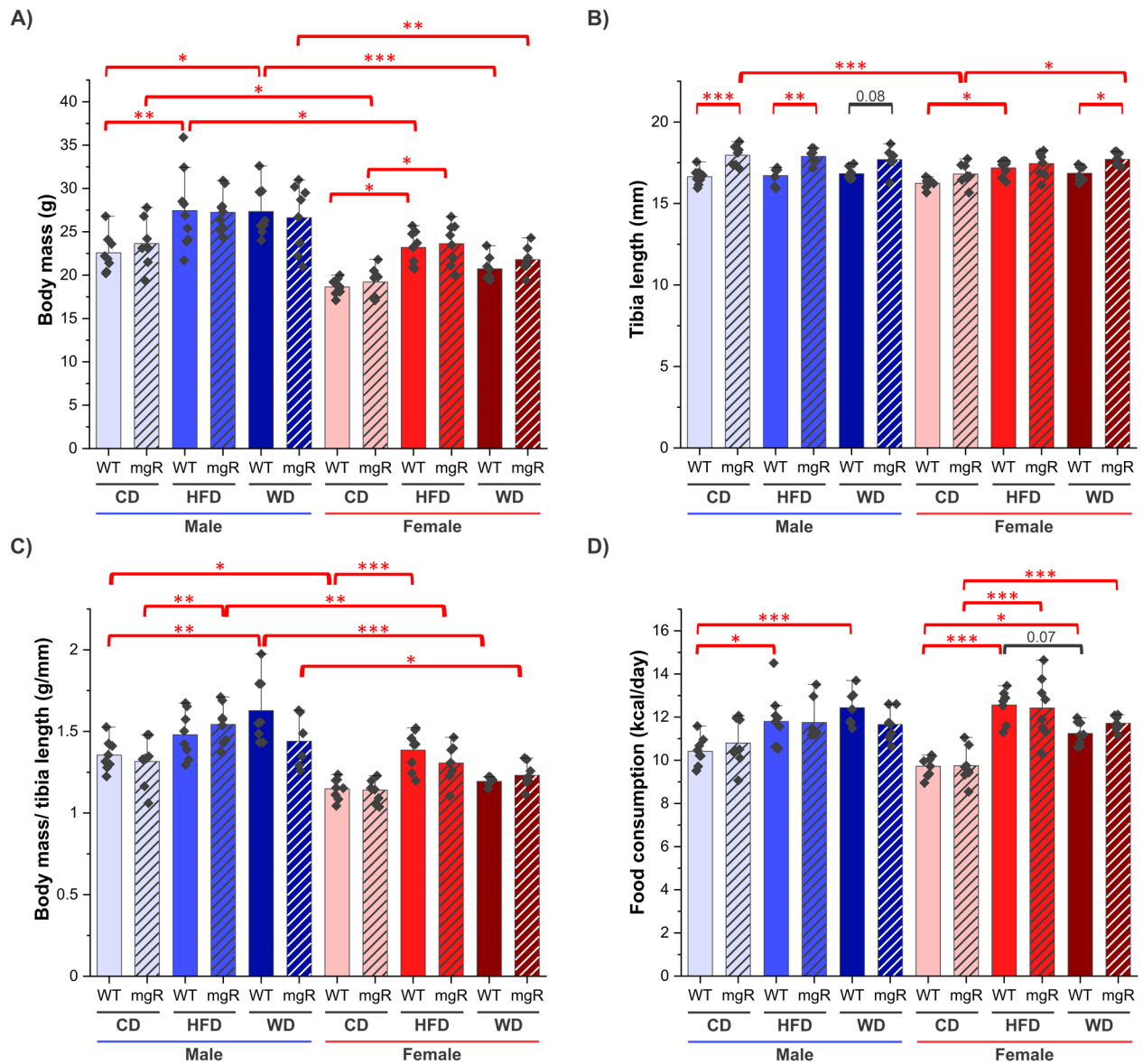


Figure 3.2: Body parameters and food consumption of 12-week-old male and female WT and mgR mice fed with CD, HFD or WD. (A) Body mass. (B) Tibia length. (C) Body mass/tibia length. (D) Food consumption. Each data point represents an individual mouse and error bars represent \pm SEM, $n = 6-9$ mice per group. Significance was assessed by 3-way ANOVA and indicated as $*p < 0.05$, $**p < 0.01$, and $***p < 0.001$.

3.3 HFD- and WD-induced insulin intolerance in male and female mgR mice

To evaluate insulin sensitivity, ITT was performed 2 weeks before the experimental endpoint of 12 weeks (**Figure 3.3**). Male WT mice fed with HFD but not with CD or WD showed a higher blood glucose level than male mgR mice from 15 to 60 min of ITT (**Figure 3.3A**). Female WT mice had a higher blood glucose level than female mgR mice that were fed with CD but not with HFD from 15 to 30 min of ITT (**Figure 3.3A**). However, there was no difference in blood glucose level when the area under the curve (AUC) was plotted comparing WT with mgR mice (**Figure 3.3D**). This revealed that genotype alone could not affect insulin sensitivity.

The role of HFD or WD alone was evaluated in insulin resistance as well. HFD did not affect the blood glucose level in male or female mice throughout the duration of ITT, whereas WD lowered it from 30 to 60 min of insulin injection in male WT mice and from 15 to 60 min in female WT mice (**Figure 3.3B**). Despite these differences, AUC only showed the reduced level of blood glucose in female WT mice fed with WD but not in male WT mice, revealing that WD had less effect in male WT than female WT mice (**Figure 3.3D**). These differences were not observed between different diets in male or female mgR mice demonstrated from the ITT curves and AUC, revealing that both male and female mgR mice had improved insulin sensitivity in response to HFD or WD compared to CD (**Figure 3.3B and D**). Although males and females responded to HFD or WD differently in insulin sensitivity, there was no difference between them when fed with HFD or WD (**Figure 3.3C and D**).

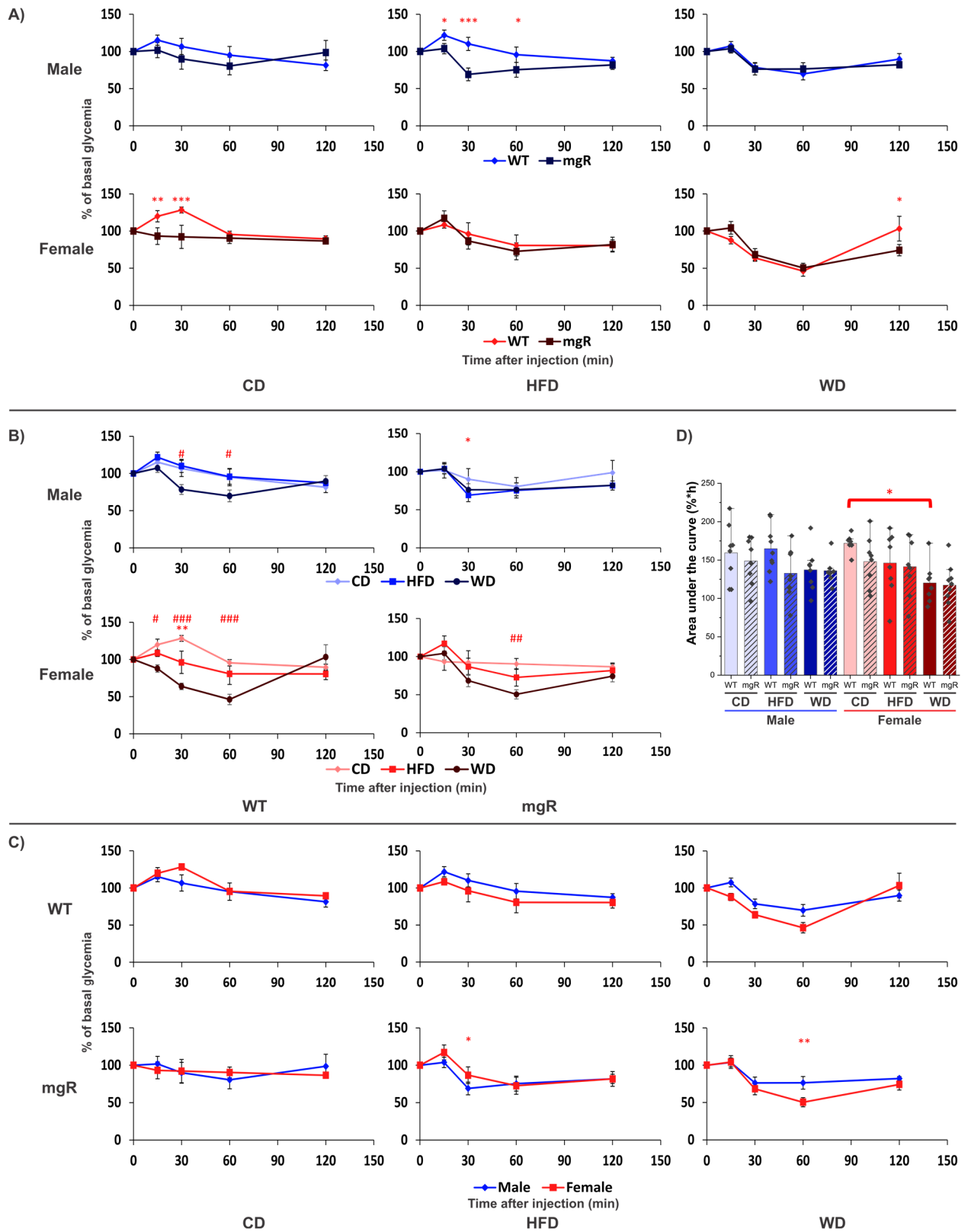


Figure 3.3: ITT of 12-week-old male and female WT and mgR mice fed with CD, HFD or WD. (Figure legend next page)

Figure 3.3: ITT of 12-week-old male and female WT and mgR mice fed with CD, HFD or WD. (Figure legend continued)

(A) Genotype-dependent differences of male (top panel) and female (bottom panel) mice fed with CD (left column), HFD (middle column) or WD (right column). (B) Diet-dependent differences of male (top panel) and female (bottom panel) WT (left column) and mgR mice (right column). * compared HFD to CD; # compared WD to CD. (C) Sex-dependent differences of WT (top panel) and mgR (bottom panel) mice fed with CD (left column), HFD (middle column) or WD (right column). (D) Quantification of area under the curve. Data are means \pm SEM, n = 6–9 mice per group. Significance was assessed by 2-way ANOVA repeated measures or 3-way ANOVA depending on the analysis mentioned in the method section. Significance was indicated as *p<0.05, **p<0.01, ***p<0.001, #p<0.05, ##p<0.01, and ###p<0.001.

3.4 HFD- and WD-induced glucose intolerance in male and female mgR mice

GTT was performed 1 week before the experimental endpoint to evaluate the glucose intolerance in male and female WT and mgR mice (**Figure 3.4**). Genotype and diet alone did not contribute to a difference in glucose intolerance among these mice demonstrated from the GTT curves and AUC (**Figure 3.4A, B and D**). Male WT mice were more glucose intolerant than female WT mice when fed with HFD but not with WD. However, HFD-fed male and female mgR mice did not have different glucose intolerance compared to CD, revealing their improved metabolic phenotype (**Figure 3.4C and D**). Therefore, both male and female mgR mice were resistant to HFD- and WD-induced glucose intolerance.

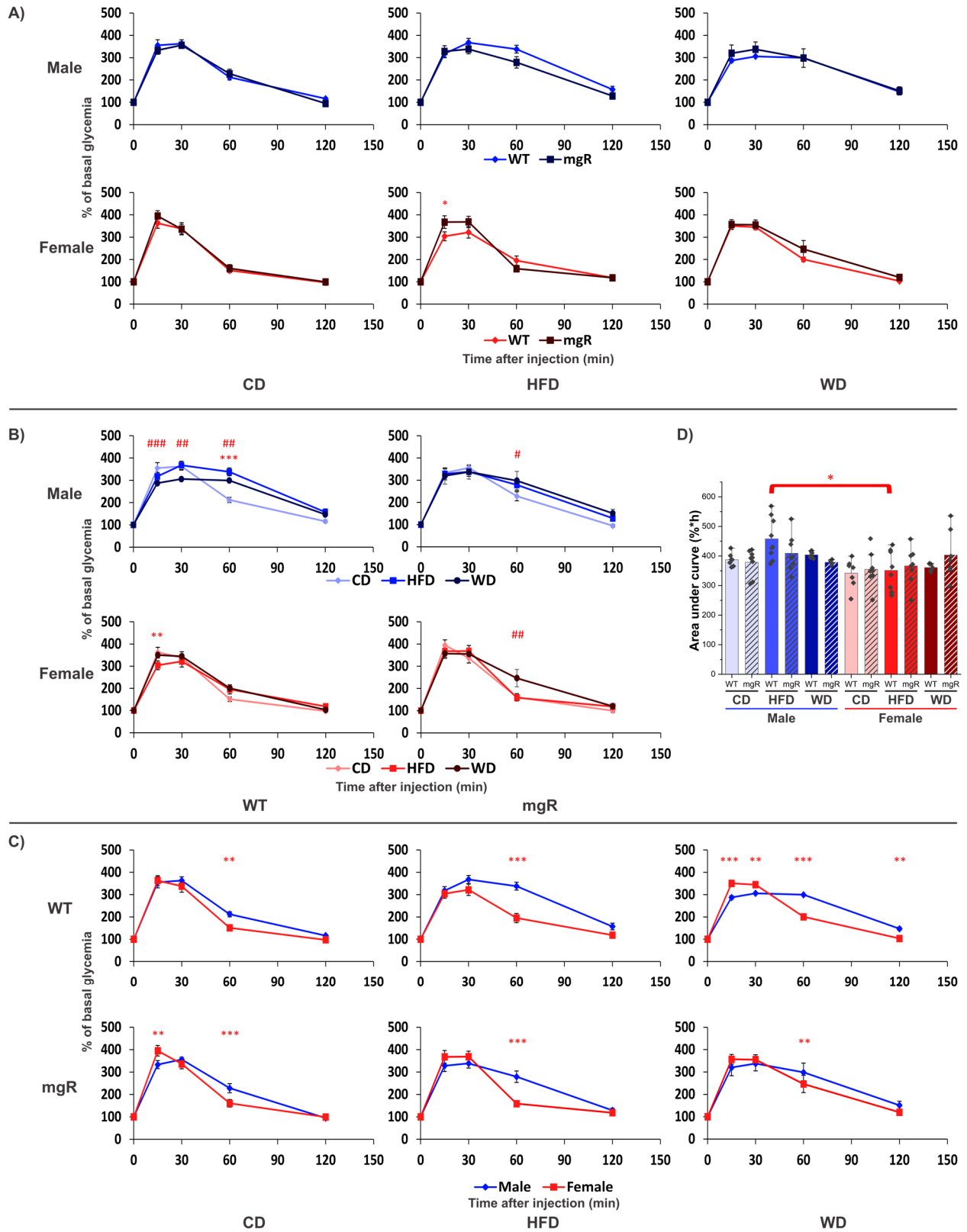


Figure 3.4: GTT of 12-week-old male and female WT and mgR mice fed with CD, HFD or WD. (Figure legend next page)

Figure 3.4: GTT of 12-week-old male and female WT and mgR mice fed with CD, HFD or WD. (Figure legend continued)

(A) Genotype-dependent differences of male (top panel) and female (bottom panel) mice fed with CD (left column), HFD (middle column) or WD (right column). **(B)** Diet-dependent differences of male (top panel) and female (bottom panel) WT (left column) and mgR mice (right column). * compared HFD to CD; # compared WD to CD. **(C)** Sex-dependent differences of WT (top panel) and mgR (bottom panel) mice fed with CD (left column), HFD (middle column) or WD (right column). **(D)** Quantification of area under the curve. Data are means \pm SEM, n = 6–9 mice per group. Significance was assessed by 2-way ANOVA repeated measures or 3-way ANOVA depending on the analysis mentioned in the Methods. Significance was indicated as *p<0.05, **p<0.01, ***p<0.001, #p<0.05, ##p<0.01, and ###p<0.001.

CHAPTER 4: SURVIVAL ANALYSIS AND CHARACTERIZATION OF AORTAE IN MALE AND FEMALE MGR MICE FED WITH HIGH-CALORIE DIETS

4.1 Overall survival and aortic-rupture-specific survival in male and female mgR mice fed with CD, HFD or WD

To evaluate the role of high calorie diet and biological sex in survival, Kaplan-Meier analysis was conducted (**Figure 4**). The overall survival rate was lower in male and female mgR mice fed with HFD (male: 76%; female: 79%) than the respective WT mice fed with HFD (male: 100%; female: 100%) but not with CD (male WT: 90%; male mgR: 64%; female WT: 88%; female mgR: 88%) or WD (male WT: 93%; male mgR: 81%; female WT: 100%; female mgR: 87%). Diet or sex alone did not affect the survival of these mice (**Figure 4.1A, B and C, Table 4.1**). To determine the role of aortic complication in survival, the cause of death due to aortic rupture was validated by dissection followed by aortic-rupture-specific survival analysis. Both male and female WT mice did not experience death caused by aortic rupture. Male mgR mice had a lower survival rate than male WT mice when they were fed with CD (WT: 100%; mgR: 76%) but not with HFD (male WT: 100%; male mgR: 80%) or WD (WT: 100%; mgR: 81%), whereas female mgR and WT mice showed the same aortic-rupture-specific survival rate when fed with CD (WT: 100%; mgR: 100%), HFD (WT: 100%; mgR: 94%) or WD (WT: 100%; mgR: 93%). Diet alone did not contribute to differences in survival caused by aortic rupture, but biological sex difference did. The male mgR mice demonstrated a lower aortic-rupture-specific survival than female mgR mice when fed with CD but not with HFD or WD, revealing the sexual dimorphism between male and female mgR mice responding to the diets (**Figure 4.1D, E and F, Table 4.1**). These results showed

unexpectedly that HFD or WD rescued premature death in male mgR mice by reducing aortic rupture incidences.

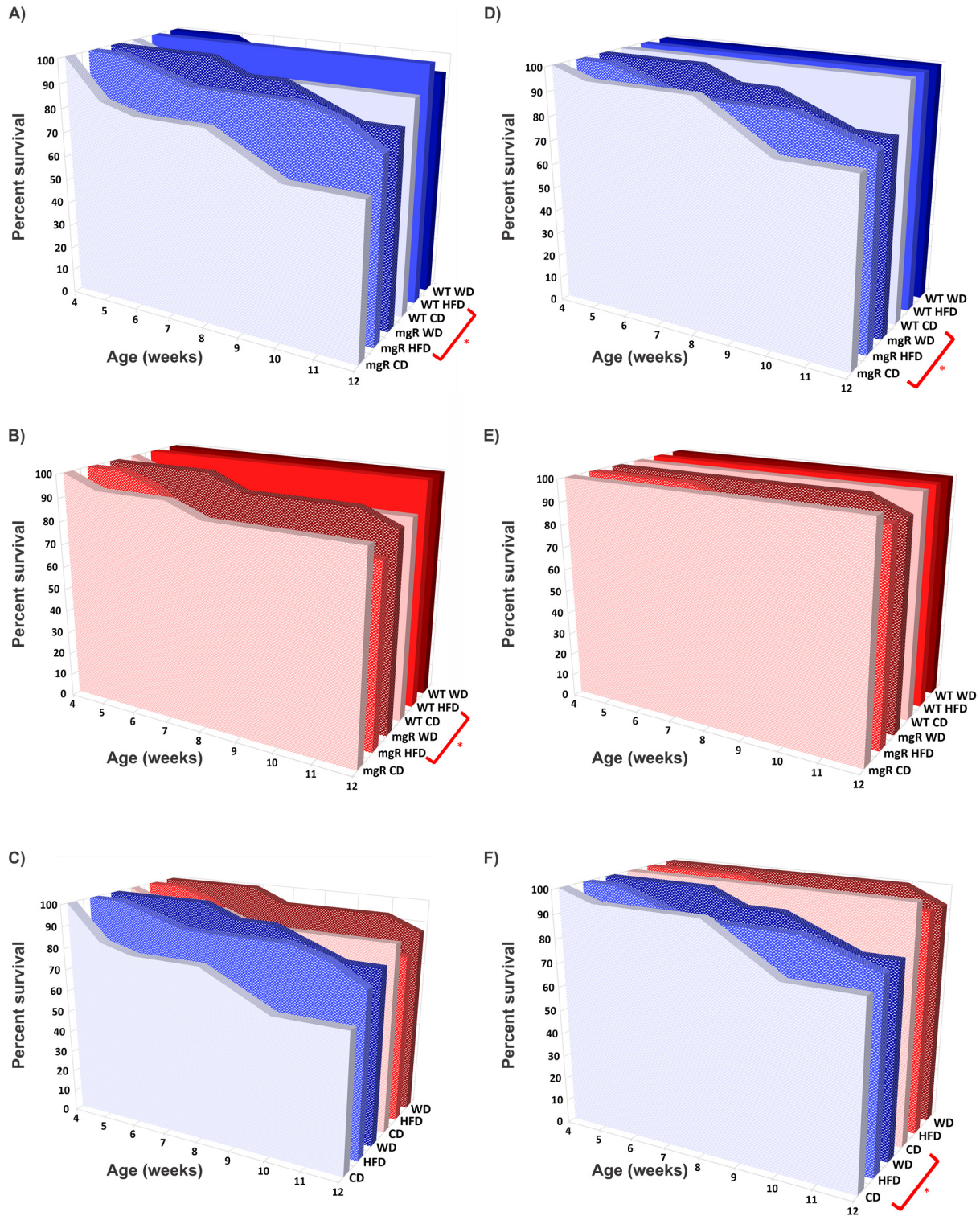


Figure 4.1: Survival of 4-12-week-old male and female WT and mgR mice fed with CD, HFD or WD. (Figure legend next page)

Figure 4.1: Survival of 4-12-week-old male and female WT and mgR mice fed with CD, HFD or WD. (Figure legend continued)

(A–C) Overall survival curves including all causes of death. (D–F) Aortic-rupture-specific survival curves. (A and D) Male WT and mgR mice fed with CD, HFD or WD. (B and E) Female WT and mgR mice fed with CD, HFD or WD. (C and F) Male (blue) and female (red) mgR mice fed with CD, HFD or WD. Survival curves are shown from 4-12 weeks of age, $n = 14-21$ mice per group. Significance was assessed by log-rank test and indicated as $*p < 0.05$.

Table 4.1: Survival of mice fed with CD, HFD or WD at the experimental endpoint of 12 weeks.

Sex	Genotype	Diet	Overall survival (all causes of death) in %	Aortic-rupture-specific survival in %
Male	WT	CD	90	100
		HFD	100	100
		WD	93	100
	mgR	CD	64	76
		HFD	76	80
		WD	81	81
Female	WT	CD	88	100
		HFD	100	100
		WD	100	100
	mgR	CD	88	100
		HFD	79	94
		WD	87	93

4.2 Analysis of aortae of male and female mgR mice fed with CD, HFD or WD (gross view)

Aneurysms which are known to increase the risk of aortic rupture were analyzed from the gross view of dissected aortae [Condeemi *et al.*, 2020]. Variations of aneurysm region (aortic root versus arch) and severity (less or more dilated) were observed in both male and female mgR mice (Figure 4.2A). We observed no signs of dilation in the descending aortae for both genotypes and sexes, under any of the dietary conditions. Therefore, the focus of the study was only ascending aorta. While measuring aneurysmal dilation, the aortic diameter was measured at the most dilated part

of the ascending aorta. Aortae from both male and female mgR mice dilated ≥ 2 -fold than male and female WT mice when they were fed with CD, HFD or WD, except female mgR mice fed with HFD. Diet alone did not contribute to the difference in aortic diameter, but biological sex did. Aortae from HFD-fed female mgR mice were less dilated than HFD-fed male mgR mice but not in CD or WD (**Figure 4.2A–D**). Since HFD reduced aortic aneurysm in female mgR mice, our studies focused on CD and HFD by analyzing various aneurysm phenotypes and its downstream effectors.

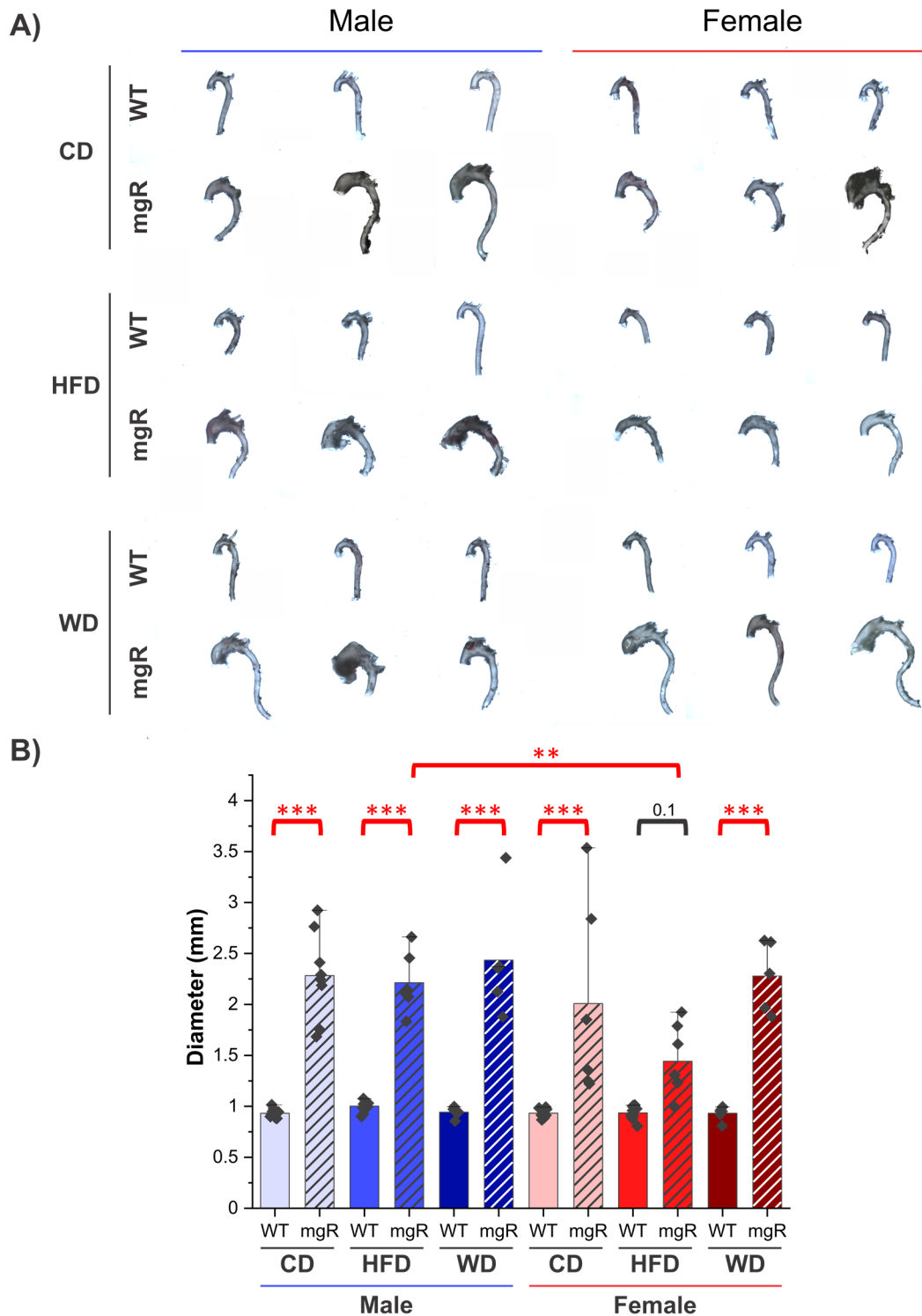


Figure 4.2: Analysis of thoracic aortae from male and female WT and mgR mice fed with CD, HFD or WD at 12 weeks. (A) Gross view of the entire thoracic aortae. **(B)** The most dilated region in each aorta shown in A was quantified and plotted according to the genotype, diets, and biological sex as indicated on the x-axis. Each data point represents an individual mouse and error bars represent \pm SEM, $n = 5-10$ mice per group. Significance was assessed by 3-way ANOVA and indicated as * $p < 0.05$, ** $p < 0.01$, and *** $p < 0.001$.

4.3 Analysis of aortae of male and female mgR mice fed with CD or HFD (cross section)

To further characterize ascending aortic aneurysms, the aortic lumen area and wall thickness were determined in male and female WT and mgR mice fed with CD or HFD using cross sections (**Figure 4.3**). The aortae from the male mgR mice showed a greater lumen area than male WT mice fed with CD (3.3-fold) or HFD (2.5-fold) (**Figure 4.3A and B**). The aortic wall was also thicker in male mgR than in WT mice fed with CD (1.7-fold) or HFD (1.6-fold) (**Figure 4.3A and C**). In females, the lumen area was greater in CD-fed mgR mice (3.9-fold) than in CD-fed WT mice, but the difference was lost when they were fed with HFD (**Figure 4.3A and B**). The aortic wall thickness was not different between female WT and mgR mice fed with CD or HFD, emphasizing that the aortic wall only thickened in male mgR mice over the course of the experiment (**Figure 4.3A and C**). Diet or sex alone did not contribute to changes in lumen area or thickness (**Figure 4.3A–C**). When analyzed through histology, the adipocytes in perivascular adipose tissues from both male and female mice under all dietary conditions did not exhibit any observable hypertrophy or hyperplasia. Therefore, analysis of perivascular fat depot was excluded from the study.

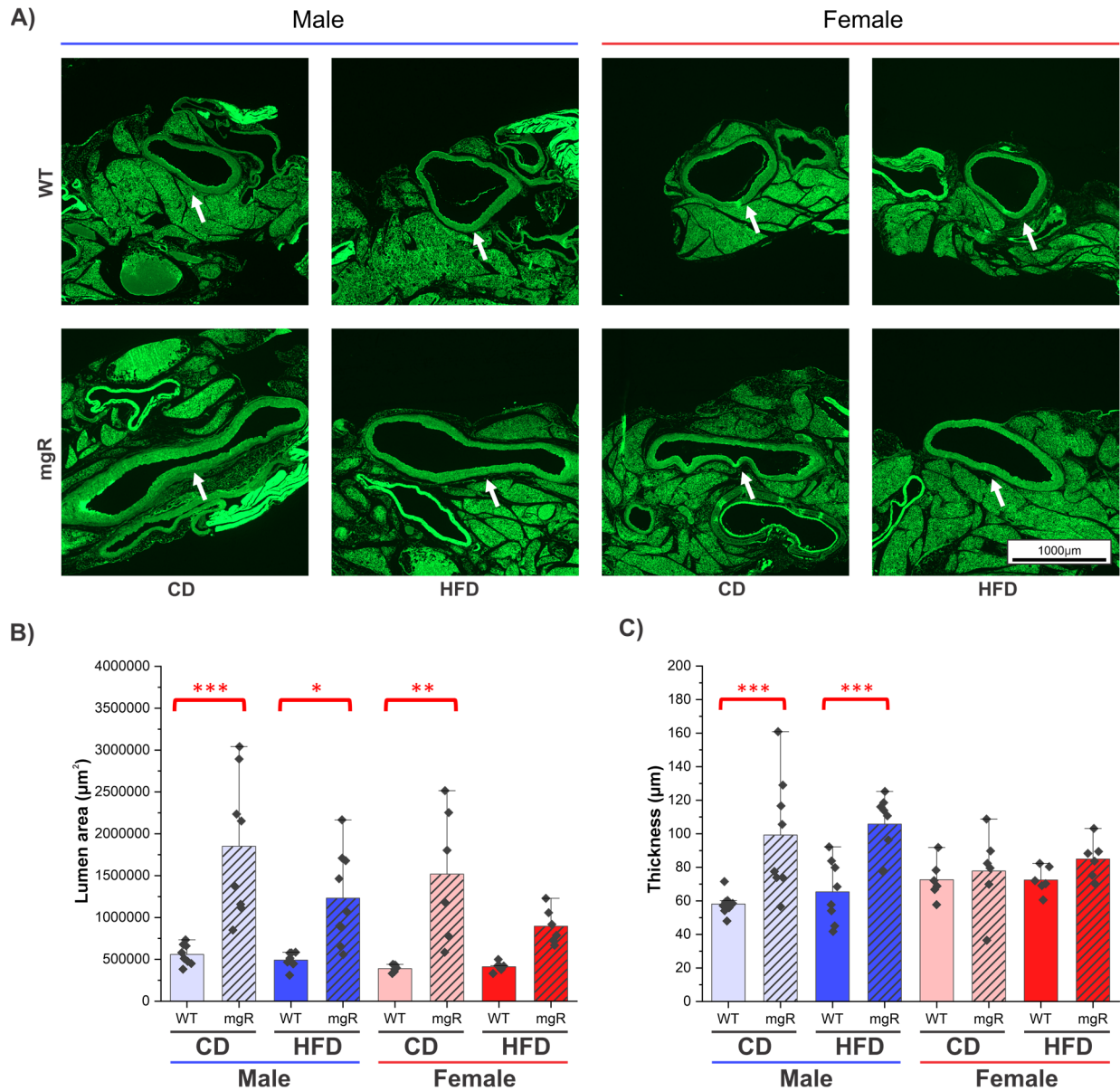


Figure 4.3: Ascending aortic lumen area and thickness of male and female WT and mgR mice fed with CD, HFD or WD at 12 weeks of age. (A) Autofluorescence images of aorta cross sections taken at 50× magnification. Arrows point to the ascending aorta. **(B)** Quantification of lumen area. Note that the procedure was independent of the tissue shape as explained in Material and Methods. **(C)** Quantification of aortic wall thickness. Each data point represents an individual mouse and error bars represent ± SEM, n = 6–9 mice per group. Significance was assessed by 3-way ANOVA and indicated as *p<0.05, **p<0.01, and ***p<0.001.

4.4 HFD-induced changes in FBN1 deposition, assembly and gene expression levels of male and female mgR mice

FBN1 plays an important role in elastogenesis and the aortic phenotype in MFS [*Pereira et al., 1999; Sabatier et al., 2009; Sabatier et al., 2014; Kumra et al., 2019; Zhang et al., 2022*]. Yet, the role of HFD and biological sex in FBN1 deposition and assembly was not studied. As expected, immunofluorescence staining revealed that both male and female WT mice had a higher FBN1 deposition in the ascending aorta than male and female mgR mice fed with CD or HFD (**Figure 4.4A and B**). FBN1 fibers in mgR ascending aortae appeared thinner and more fragmented than in WT aortae, but aortae from both WT and mgR mice deposited more FBN1 in the adventitia and the intimal endothelial layer under all these conditions. HFD alone did not contribute to the difference in FBN1 deposition or assembly in males or females. Unexpectedly, FBN1 was deposited more in male WT mice fed with HFD than in female WT mice fed with HFD but not in mgR mice whose FBN1 deposition was only genotype-dependent (**Figure 4.4A and B**). Surprisingly, the *Fbn1* gene expression was not different under all conditions (**Figure 4.4C**).

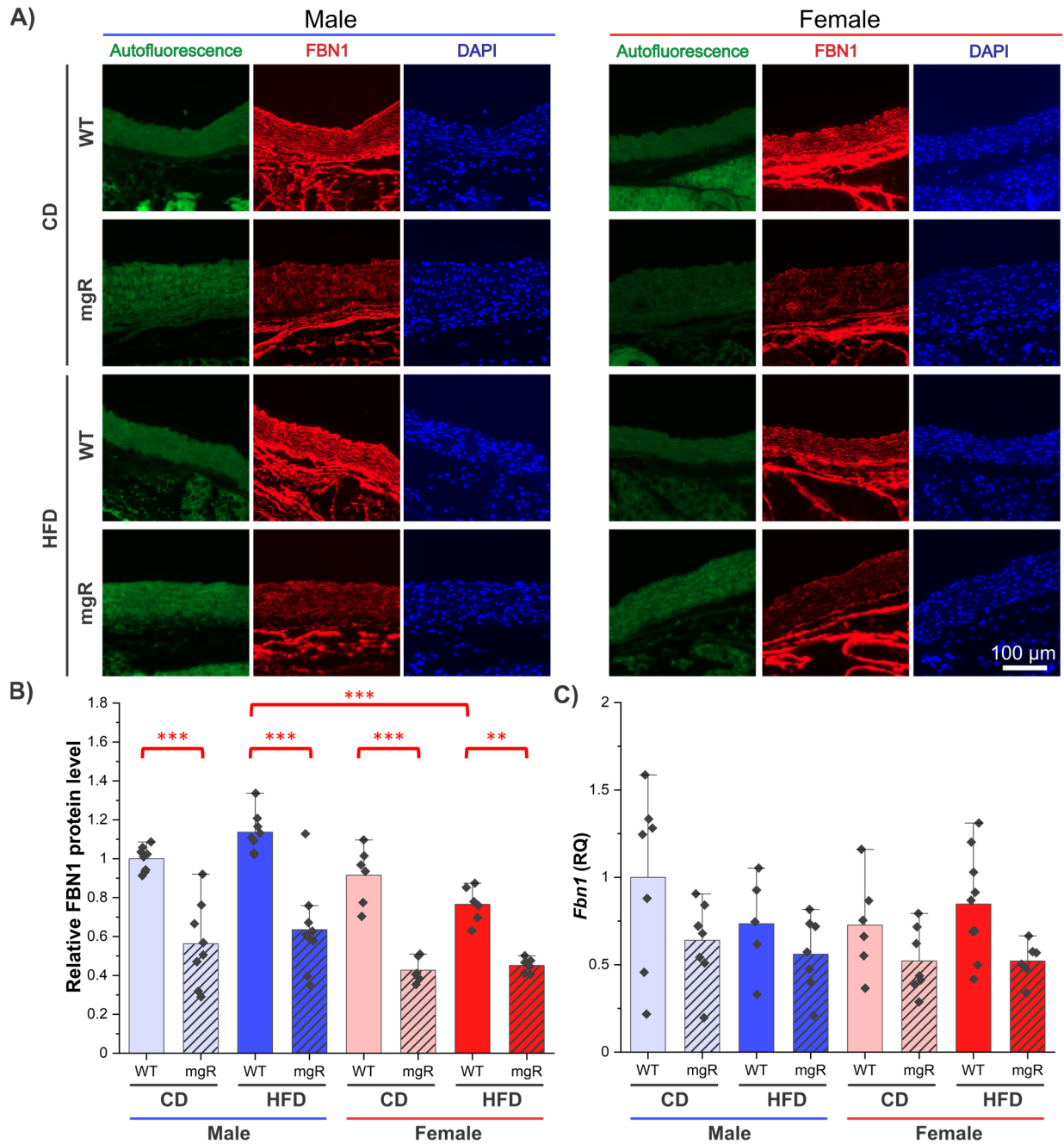


Figure 4.4: FBN1 deposition, assembly and *Fbn1* gene expression levels in ascending aortae from male and female WT and mgR mice fed with CD or HFD at 12 weeks of age. (A) Immunofluorescence analysis of FBN1. Autofluorescence of the aorta is shown in green, whereas nuclear counterstain with DAPI is shown in blue for all images. **(B)** Quantification of FBN1 protein levels quantified from images as shown in A. **(C)** Analysis of *Fbn1* gene expression levels by qPCR. Each data point represents an individual mouse and error bars represent \pm SEM, $n = 6-9$ mice per group. Significance was assessed by 3-way ANOVA and indicated as * $p < 0.05$, ** $p < 0.01$, and *** $p < 0.001$.

4.5 HFD-induced changes in HIF-1 α protein and gene expression levels of male and female mgR mice

HIF-1 α is a major modulator of hypoxia, which is a known characteristic of the MFS aorta [Oller *et al.*, 2021; Zhang *et al.*, 2022]. The role of HFD and sex in modulating HIF-1 α levels in the ascending aortae were analyzed through immunofluorescence (**Figure 4.5A and B**). Under all conditions, the HIF-1 α protein was only localized in the media layer but not in the adventitia or intima. Male mgR mice revealed higher HIF-1 α levels than male WT mice fed with CD or HFD. Female mgR mice also had a higher HIF-1 α level than female WT mice fed with HFD but not with CD. Both HFD and biological sex alone did not contribute to the HIF-1 α levels. Overall, the elevated HIF-1 α levels in female mgR mice was HFD-dependent but not in male mgR mice. Unlike protein levels, the *Hif1a* gene expression was not different with different genotype, diet and biological sex in these mice (**Figure 4.5C**).

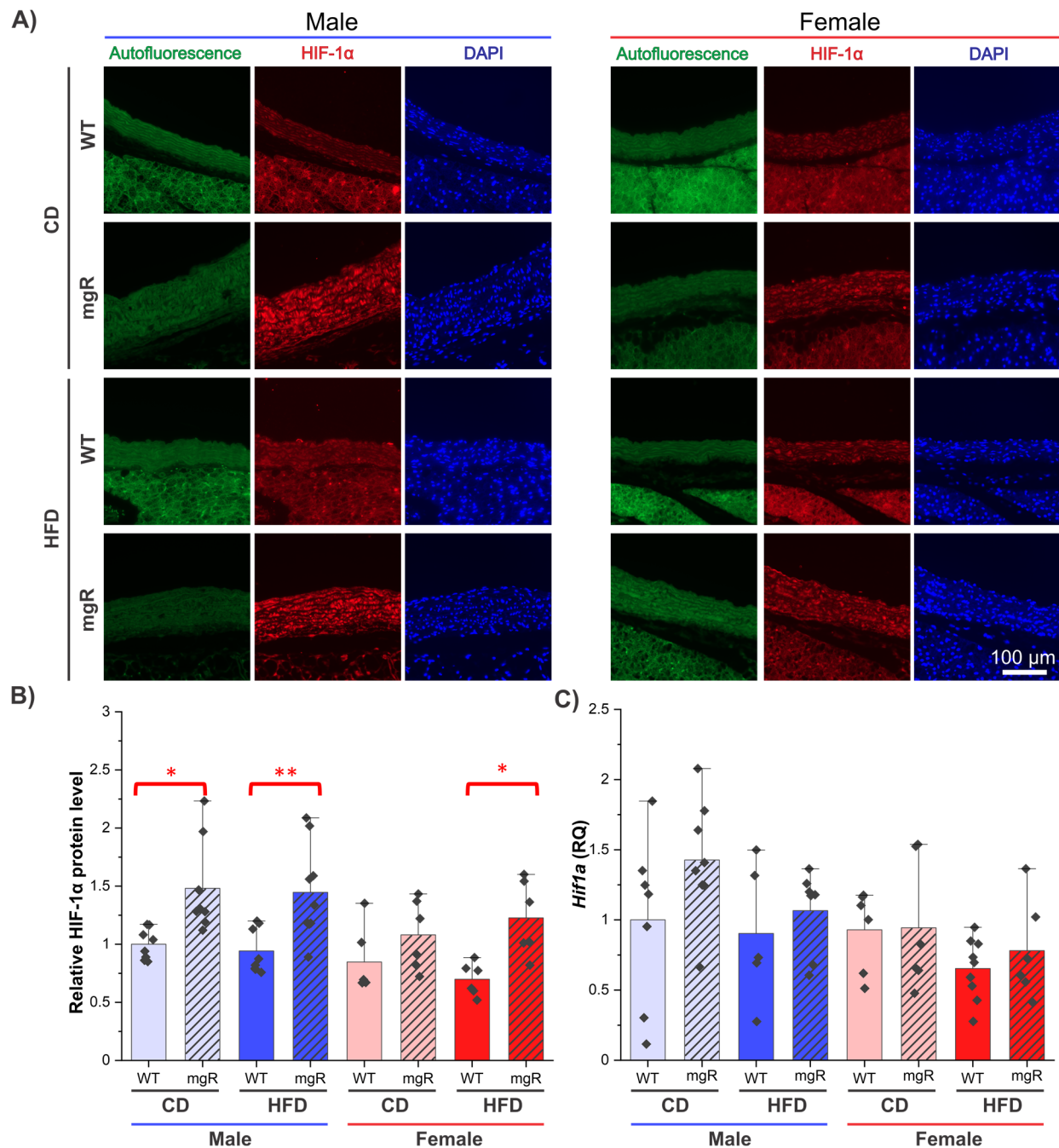


Figure 4.5: HIF-1 α protein and *Hif1a* gene expression levels in ascending aortae from male and female WT and mgR mice fed with CD or HFD at 12 weeks of age. (A) Immunofluorescence analysis of HIF-1 α on cross sections of ascending aortae. Autofluorescence of the aorta is shown in green, whereas nuclear counterstain with DAPI is shown in blue for all images. **(B)** Quantification of HIF-1 α protein levels as shown in A. **(C)** Analysis of *Hif1a* gene expression levels by qPCR. Each data point represents an individual mouse and error bars represent \pm SEM, $n = 6-9$ mice per group. Significance was assessed by 3-way ANOVA and indicated as * $p < 0.05$, ** $p < 0.01$, and *** $p < 0.001$.

4.6 HFD-induced changes in elastic fiber fragmentations, *Mmp2* and *Mmp9* gene expression levels of male and female mgR mice

Elastic fiber fragmentation was visualized by staining ascending aorta sections with the Hart's procedure, which provided the basis for the following quantification (**Figure 4.6A and B**). Male and female mgR mice showed a higher number of elastic fiber fragmentation than WT mice fed with CD or HFD. However, CD or HFD alone did not change the amount of elastic fiber fragmentation in male and female WT and mgR mice. Surprisingly, female mgR mice demonstrated a lower number of elastic fragmentation than male mgR mice fed with HFD but not with CD, correlating with the aortic diameter. However, *Mmp2* and *Mmp9* gene expression which were known to contribute to elastic fiber fragmentations were not different under all conditions (**Figure 4.6C**) [*Klein & Bischoff, 2011; Lu & Aikawa, 2015*].

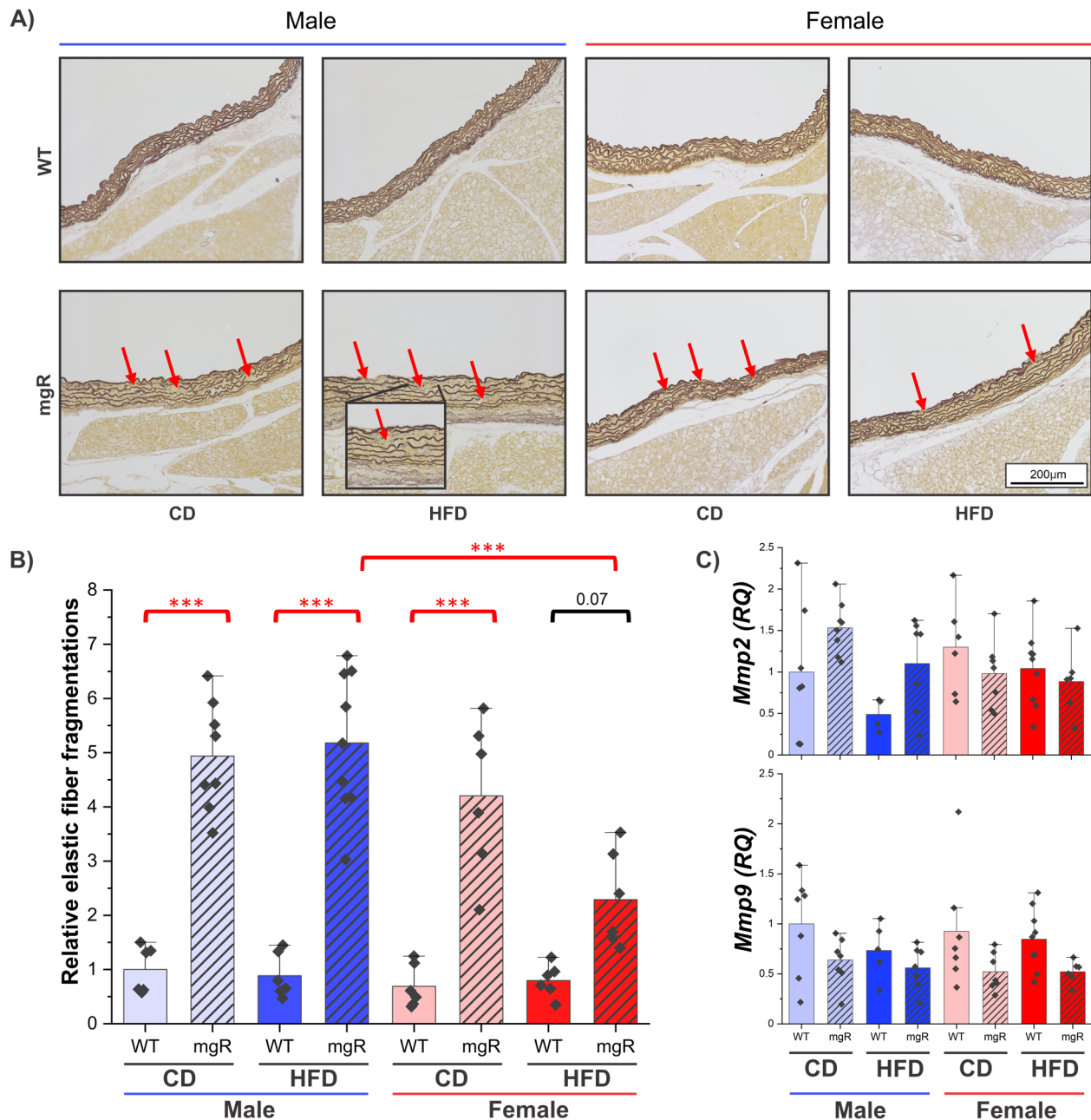


Figure 4.6: Elastic fiber fragmentation and *Mmp2* and *Mmp9* gene expression levels in ascending aortae from male and female WT and mgR mice fed with CD or HFD at 12 weeks of age. (A) Hart's staining of the ascending aortae cross sections to visualize the integrity of the elastic lamellae. Arrows point to examples of elastic fiber fragmentation. The inset shows an example of elastic fiber fragmentation for clarity. (B) Quantification of elastic fiber fragmentation (see Materials and Methods). (C) Analysis of *Mmp2* and *Mmp9* gene expression levels by qPCR. Each data point represents an individual mouse and error bars represent \pm SEM, $n = 6-9$ mice per group. Significance was assessed by 3-way ANOVA and indicated as * $p < 0.05$, ** $p < 0.01$, and *** $p < 0.001$.

4.7 HFD-induced changes in MMP-12 protein and gene expression of male and female mgR mice

MMP-12 was recently discovered to be upregulated in MFS through reduction of miR-122 [Zhang *et al.*, 2022]. Through immunofluorescence staining and quantification, MMP-12 protein levels which were known to be regulated by HIF-1 α in the aortic wall were not different under all conditions (**Figure 4.7A and B**). However, the *Mmp12* gene expression was higher in male mgR mice than male WT mice fed with CD but not with HFD, which showed only an increasing trend (**Figure 4.7C**). The male mgR mice fed with CD showed an increased trend of *Mmp12* gene expression compared to the male mgR mice fed with HFD. These differences and trends were not observed between female mgR and WT mice that expressed relative low levels of *Mmp12*. Thus, male mgR mice had higher *Mmp12* expression than female mgR mice when they were fed with CD but not with HFD.

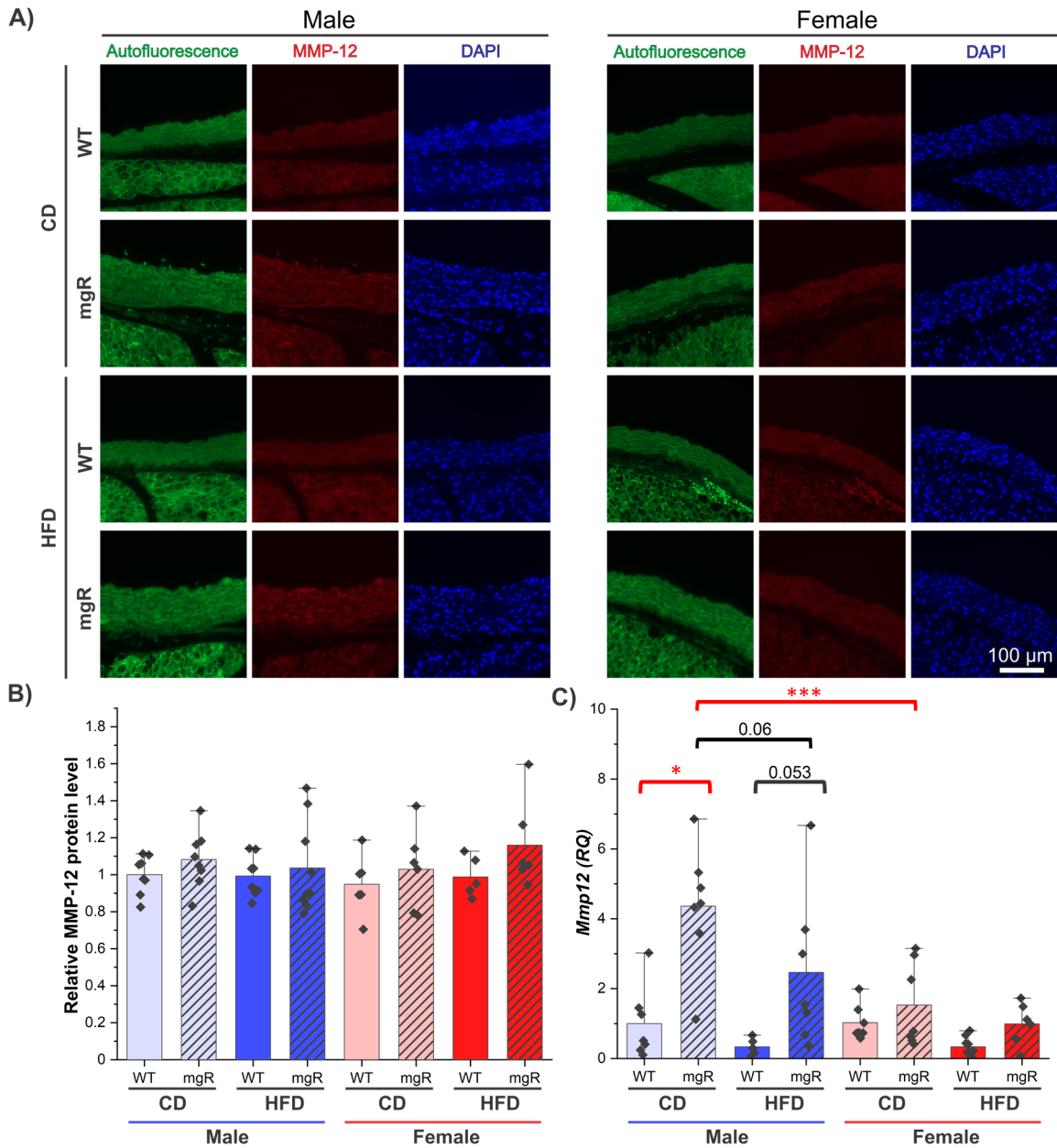


Figure 4.7: MMP-12 protein and gene expression in ascending aortae from male and female WT and mgR mice fed with CD or HFD at 12 weeks of age. (A) Immunofluorescence analysis of MMP-12 on cross sections of ascending aortae. Autofluorescence of the aorta is shown in green, whereas nuclear counterstain with DAPI is shown in blue for all images. **(B)** Quantification of MMP-12 protein level as shown in A. **(C)** Analysis of *Mmp12* gene expression levels by qPCR. Each data point represents an individual mouse and error bars represent \pm SEM, $n = 6-9$ mice per group. Significance was assessed by 3-way ANOVA and indicated as * $p < 0.05$, ** $p < 0.01$, and *** $p < 0.001$.

4.8 HFD-induced changes in proteoglycan deposition and *Acan* and *Vcan* gene expression levels of male and female mgR mice

Proteoglycans, and specifically aggrecan and versican, are known to be deposited higher in MFS and regulated by HIF-1 α [Cikach *et al.*, 2018; Shimomura *et al.*, 2021]. Alcian blue staining of proteoglycans confirmed that male and female mgR mice deposited higher proteoglycan levels than male and female WT mice, respectively (**Figure 4.8A and B**). HFD alone did not change the proteoglycan deposition in the ascending aortae. However, male mgR mice fed with HFD had a higher proteoglycan deposition than female mgR mice fed with HFD but not with CD. To determine whether aggrecan or versican are differentially regulated in these mice, both *Acan* and *Vcan* gene expression levels were evaluated (**Figure 4.8C**). However, there was no difference under all conditions.

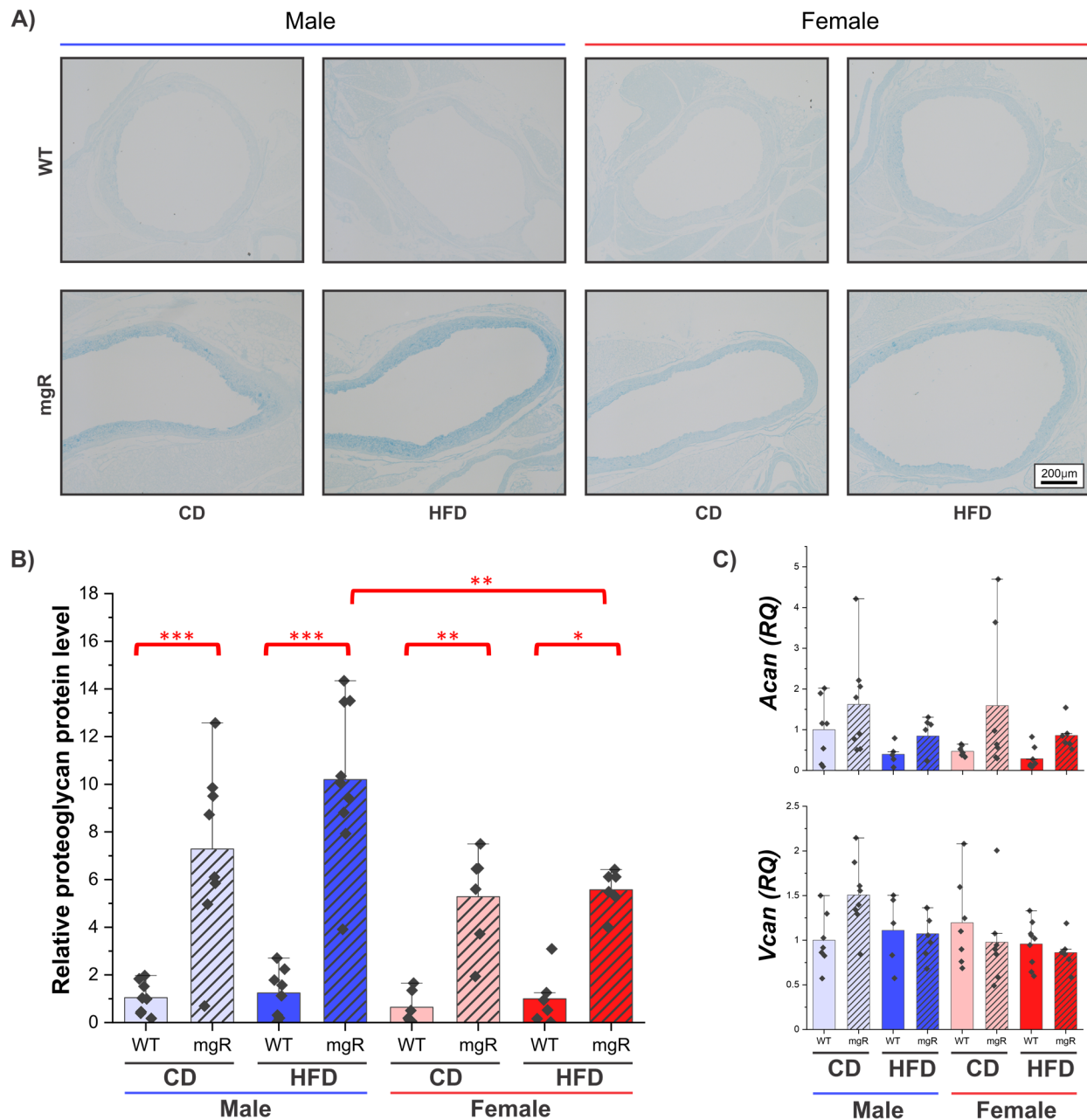


Figure 4.8: Proteoglycan deposition, *Acan* and *Vcan* gene expression levels in ascending aortae from male and female WT and mgR mice fed with CD or HFD at 12 weeks of age. (A) Proteoglycan staining of cross sections of ascending aortae was performed by alcian blue. **(B)** Quantification of proteoglycan protein levels as shown in A. **(C)** Analysis of *Acan* and *Vcan* gene expression levels through qPCR. Each data point represents an individual mouse and error bars represent \pm SEM, $n = 6-9$ mice per group. Significance was assessed by 3-way ANOVA and indicated as $*p < 0.05$, $**p < 0.01$, and $***p < 0.001$.

4.9 HFD-induced changes in collagen deposition and *Colla1* and *Col3a1* gene expression levels of male and female mgR mice

Collagens are generally highly regulated ECM proteins in MFS aorta, fibrosis and hypoxia [Xiong & Liu, 2017; Perrucci et al., 2020; Nettersheim et al., 2021]. Picrosirius red staining revealed that male mgR mice showed a higher collagen deposition than male WT mice fed with CD or HFD level (**Figure 4.9A and B**). Female mgR mice demonstrated a higher collagen deposition than female WT mice fed with HFD but not with CD. There was an increased trend noticeable that female mgR mice fed with HFD deposited more collagen than female mgR mice fed with CD but not between the male mgR mice fed with HFD and CD. The difference of biological sex alone did not change the collagen deposition levels. Despite these findings, the type of collagen was not determined. Collagen I or collagen III are commonly regulated in fibrosis, so both *Colla1* and *Col3a1* gene expression levels were analyzed [Wulandari et al., 2016]. Male mgR mice expressed more *Colla1* and *Col3a1* than male WT mice fed with CD but not with HFD (**Figure 4.9C**). The difference was lost among the female mice fed with CD or HFD that were characterized by low *Colla1* and *Col3a1* expression. HFD alone did not contribute the changes of *Colla1* and *Col3a1* expression. However, male mgR mice fed with CD expressed more *Colla1* and *Col3a1* than female mgR mice fed with CD but not with HFD.

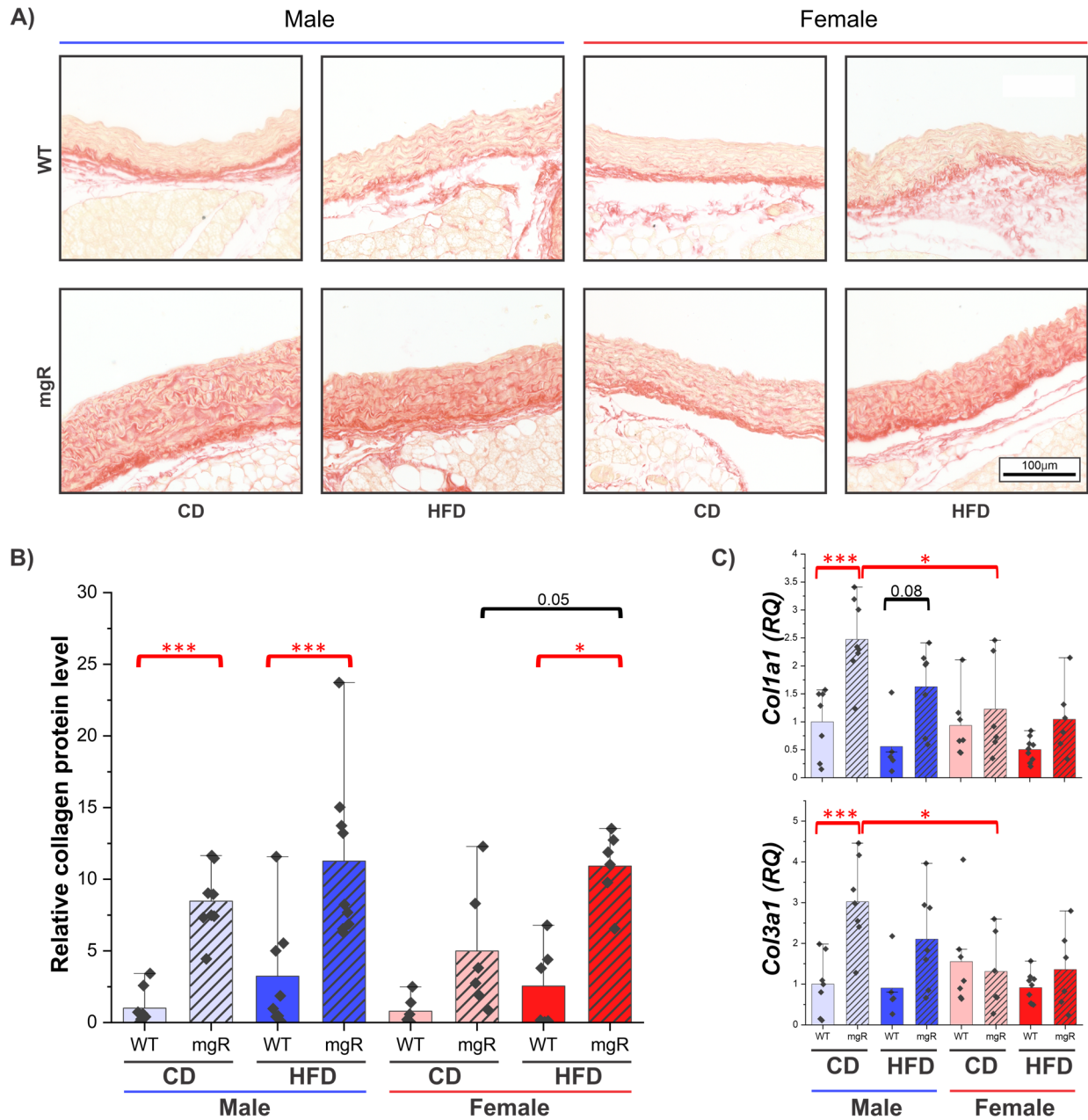


Figure 4.9: Collagen deposition and *Coll1a1* and *Col3a1* gene expression levels in ascending aortae from male and female WT and mgR mice fed with CD or HFD at 12 weeks of age. (A) Collagen staining of cross sections of ascending aortae was performed by picrosirius red. **(B)** Quantification of collagen protein levels as shown in A. **(C)** Analysis of *Coll1a1* and *Col3a1* gene expression levels through qPCR. Each data point represents an individual mouse and error bars represent \pm SEM, $n = 6-9$ mice per group. Significance was assessed by 3-way ANOVA and indicated as * $p < 0.05$, ** $p < 0.01$, and *** $p < 0.001$.

CHAPTER 5: DISCUSSION

5.1 Sexual dimorphism of mgR mice in metabolism

MFS individuals exhibit abnormal metabolism typically characterized by lipodystrophic phenotype with a significant subset of them being overweight or even obese [Erkula *et al.*, 2002; Graul-Neumann *et al.*, 2010; Yetman & McCrindle, 2010; Goldblatt *et al.*, 2011; Jacquinet *et al.*, 2014; Passarge *et al.*, 2016; von Kodolitsch *et al.*, 2019; Hansen *et al.*, 2020]. A recent study from the Reinhardt lab revealed that male mgR mice with fibrillin-1 deficiency had increased adipocyte size and elevated adipogenic markers in white adipose tissue, and furthermore, the recombinant C-terminal half of FBN1 reduced adipogenic differentiation particularly in the early commitment phase [Muthu *et al.*, 2022]. This study highlighted 2 key aspects in MFS metabolism: sexual dimorphism in MFS and inhibition of adipogenesis by fibrillin-1. The sex difference in MFS metabolism responding to multiple high-calorie diets was previously not studied. To investigate this, the growth curves in male and female WT and mgR mice were evaluated. Male and female WT mice had an increased body mass even after 1 week of HFD or WD confirming that these diets were valid for metabolic studies. HFD-fed or WD-fed female mgR mice were suppressed from weight gain but not male mgR mice. The resistance of gaining weight under HFD or WD in female mgR mice was confirmed by the ratio of body mass to tibia length. However, male mgR mice did not have a higher body mass to tibia length ratio when fed with WD, contradicting the growth curves. This revealed that male mgR mice were more prominent responding to HFD-induced weight gain. Comparing males to females, a study has shown that estrogen inhibits adipogenesis through Pref-1 which might explain why male mgR mice were heavier than female mgR mice when fed with HFD or WD [Wang *et al.*, 2010; Hudak & Sul, 2013].

Although different blood glucose levels were observed at various timepoints after insulin injection, there was no difference in insulin sensitivity based on AUC among the male and female WT and mgR mice fed with CD, HFD or WD except female WT mice fed with WD compared to CD. A study has shown that WD promoted local estrogen biosynthesis in adipose tissue [Goncalves *et al.*, 2021]. Therefore, female WT mice fed with WD had an improved insulin sensitivity compared to CD. However, this difference was lost between CD- and WD-fed mgR mice suggesting that deficiency of fibrillin-1 facilitates alterations in insulin sensitivity and glucose homeostasis in female mgR mice. It is known that estrogen promotes inhibition of adipogenesis, reduces adipose tissue oxidative stress and inflammation [Wang *et al.*, 2010; Stubbins *et al.*, 2012; Hudak & Sul, 2013]. Since the improved insulin sensitivity was only noted in female mgR mice and not in case of males, it is possible that deficiency of fibrillin-1 differentially regulates estrogen levels in female MFS mice under different dietary condition, thereby to improve glucose regulation. In a previous work from lab, a significant drop in the survival rate of mgR mice was observed after 12 weeks of age, when fed with HFD (unpublished data). In order to have increased number of viable mgR mice for analysis under the current study, ITT was performed at 10 weeks of age. This was an earlier timepoint compared to other metabolic studies [Macotela *et al.*, 2009] and at 10 weeks of age no sex-specific alterations in the insulin sensitivity was observed between the WT and mgR mice under any of the dietary conditions.

Glucose metabolism was evaluated by GTT in these mice at 11 weeks of age. Genotype and diet alone did not promote glucose intolerance in males or females. However, male WT mice were more glucose intolerant than female WT mice when fed with HFD but not CD or WD based on AUC. This once again reflected the role of estrogen in females rescuing abnormal metabolic phenotype [Hudak & Sul, 2013]. However, among the mgR mice, glucose intolerance of males

and females was the same. With these findings, we concluded that the metabolic phenotype was genotype and sex dependent, consequently leading to sexual dimorphism responding to HFD or WD. Despite these findings revealed different aspects in glucose metabolism, there were few limitations in this study. ITT and GTT were conducted at different ages of the mice (10 and 11 weeks, respectively) because it takes one week for the mice to recover metabolically from ITT or GTT before the next metabolic analysis can be performed. This is a likely cause for the observed variance between ITT and GTT results. Lastly, the diets were only fed to the mice up to 12-week of age because the mgR mice often die soon after this time period which makes a longer analysis complicated. Therefore, the longer-term consequences of diet and sex are yet to be investigated, possibly with a different MFS mouse model with longer life span.

5.2 Sexual dimorphism of mgR mice in aortic aneurysm

With excess adiposity, the aortic aneurysm progression and formation are often worsened in humans [Yetman & McCrindle, 2010]. Therefore, we investigated the survival rate and aortic aneurysm in male and female WT and mgR mice fed with CD, HFD or WD. Male and female mgR mice had a lower survival rate than WT mice fed with HFD. The survival rate was the same between WT and mgR mice fed with CD or WD because either WT mice had a reduced trend of survival rate or mgR mice still maintained a relatively high survival rate in males or females. The cause of death was determined through dissection whether it was aortic rupture or not. Male mgR mice had a lower aortic-specific survival rate than male WT mice fed with CD revealing that HFD or WD potentially rescued aortic complications. The aortic-rupture-specific survival rate of male mgR mice was less than the survival rate of female mgR mice when they were fed with CD but not HFD or WD showing more severe aneurysm phenotype in male mgR mice. However, the

difference between the overall survival and the aortic-rupture-specific survival among these mice needs to be determined. The deaths caused by non-aortic rupture could be due to reduced food intake, growth deficits and other cardiac complications [Bergner & Goldberger, 2010]. Nevertheless, these significant findings showed the role of aortic complications in survival rate of these mice and the sexual dimorphism responding to the CD, HFD and WD. To understand the reasons behind these findings, both characterizations of thoracic aortic aneurysm and diet-induced downstream mechanisms in these mice were investigated.

First, the in situ aortic diameter in the gross view was determined. There was heterogeneity in aneurysm region and severity among the male and female mgR mice. Heterogeneity was reported in mgR and *Fbn1*^{C1041G/+} mice, but the role of diets in heterogeneity of aortic aneurysm was undetermined [Chen et al., 2021; Zhang et al., 2022]. SMCs in different region of the thoracic aorta can behave differently due to the origin of SMCs. There was no dilation in descending aorta where SMCs were derived from somites [Pouget et al., 2006]. However, the dilation was observed from the root to aortic arch in male and female mgR mice fed with any diet. The SMCs at the root and outer media layer in ascending aorta were embryonically derived from second heart field (SHF), whereas the SMCs that were located distal away from the heart in ascending aorta and at the aortic arch were derived from cardiac neural crest cells (CNC) [Psaltis & Simari, 2015; Sawada et al., 2017]. In addition, a study showed that adventitial stem cells antigen-1 positive (Sca-1⁺) progenitor cells were more abundant in *Fbn1*^{C1041G/+} mice and could contribute to the heterogeneity of aortic aneurysm [Gharraee et al., 2022]. To investigate the role of diet and biological sex in SMC lineage in the future, the distribution of SHF- and CNC-derived cells in thoracic aortic aneurysm can be studied by breeding mgR mouse colonies with another mouse colonies that have *Mef2c-Cre* (promoter in SHF lineage) or *Wnt1-Cre* (promoter in CNC lineage)

mice with express *LacZ* in the ROSA26 locus. The β -galactosidase-positive areas will be evaluated. The amount of adventitial SMC progenitor cells, which are mesenchymal-like cells, can be determined by staining Sca-1 through immunofluorescence in mice fed with CD, HFD or WD in future studies as well. This will identify which SMC origin contributes to the aneurysm.

Through the analysis of aortic diameter in males, mgR was confirmed as a validated mouse model to study MFS aortic aneurysm, but the sexual dimorphism of aortic aneurysm responding to HFD or WD was not known [Schwill *et al.*, 2013; Chen *et al.*, 2019]. Male and female mgR mice had more dilated aortae than the respective WT mice but not female mgR mice fed with HFD. Aortae from male mgR mice were also more dilated than female mgR mice when fed with HFD which potentially targeted adventitial SMC progenitor cells, CNC- or SHF-derived SMCs. Since HFD rescued aortic aneurysm in female mgR mice, our study focused on CD and HFD but not WD. To further characterize aortic aneurysm and determine the mechanism behind it, lumen area and wall thickness of the aortae were evaluated through capturing the autofluorescence images of the cross-sectioned aortae. Female mgR mice not only had a thinner aortic wall but also had an advantage responding to HFD to reduce their lumen area compared to male mgR mice. The results were different between diameter from the gross view and lumen area from the cross sections because of the limitation in embedding. In gross view, aortic diameter was measured at the most aneurysm region perpendicular to the inner wall of the aorta, whereas in the cross sections, aortic wall thickness and lumen area could only be measured at a horizontal plane due to the embedding process from the root to the arch (**Figure 5.1**). The other reason was that the mice from the gross view were not the same mice from the cross sections. The heterogeneity could create the difference between these two analyses. Despite the technical and heterogeneity limitations, female mgR mice

had a positive response to HFD reducing their aortic phenotype in both gross view and cross sections.

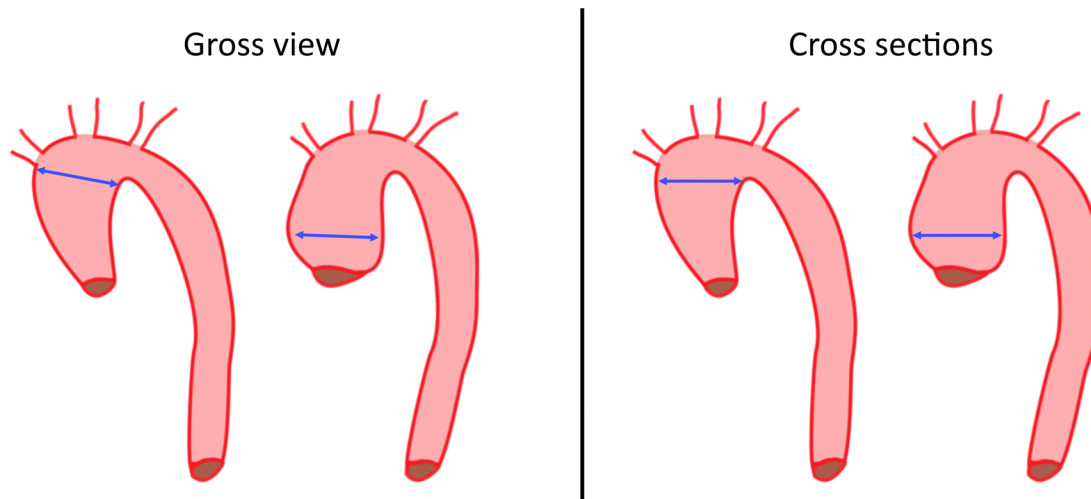


Figure 5.1: Comparison between gross view and cross sections. The ascending aortic diameter was measured at the most dilated region perpendicular to the inner wall of the aorta in gross view. Aortic wall thickness and lumen area could only be measured at one horizontal plane depending on the orientation of the specimen in the paraffin block.

FBN1 regulation is important for elastogenesis and in relation to aneurysm phenotype [Pereira et al., 1999; Sabatier et al., 2009; Sabatier et al., 2014; Kumra et al., 2019; Zhang et al., 2022]. FBN1 deposition was reduced and the assembled FBN1 fibers were thinner and more fragmented in the mgR mice than WT mice. This indicated that FBN1 deposition and assembly were genotype-dependent but not diet-dependent. Surprisingly, FBN1 deposited more in male WT mice than female WT mice fed with HFD potentially due to the elevation of epigenetic modification through histone H3 acetylation in male WT mice, but the epigenetic modification of *Fbn1* gene in female mice was not confirmed [Gaikwad et al., 2010]. Our data might suggest that female WT mice had a different epigenetic modification of *Fbn1* responding to HFD. Unexpectedly, there was no difference of the *Fbn1* gene expression in all these conditions. We propose that FBN1 could be

deposited more in the aorta in an early stage of life, but FBN1 was not regulated as the mice aged similar to elastin turnover [Burnett *et al.*, 1982; Davidson *et al.*, 1982]. In addition, there were more SMC nuclei in the media layer orientated radially instead of orientated parallel with the FBN1 fibers. This result supported previous research in *Eln*^{-/-} mice that the loss of ECM integrity promoted the SMC phenotypic switching from contractile to synthetic which was observed in other aneurysm studies as well [Misra *et al.*, 2016; Pedroza *et al.*, 2020].

HIF-1 α is an important transcription factor regulating hypoxia in MFS due to mitochondrial dysfunction and thickening of aortic wall [Oller *et al.*, 2021; Zhang *et al.*, 2022]. As expected, male mgR mice had an elevation of HIF-1 α protein levels compared to male WT mice, whereas female mgR mice had an elevated HIF-1 α protein levels compared to female WT mice when fed with HFD but not CD. Estrogen is known to promote mitochondrial efficiency potentially reducing HIF-1 α level and explaining why the same HIF-1 α level was observed between female mgR and WT mice fed with CD [Duckles *et al.*, 2006; Yang *et al.*, 2015]. However, HFD might have a stronger role promoting HIF-1 α levels in the media layer of the aorta. This result correlated with multiple metabolic and cardiovascular studies that HFD elevates HIF-1 α protein levels [Sun *et al.*, 2013; Semenza, 2014; Han *et al.*, 2019]. Although *Hif1a* gene expression did not correlate the protein level, *Hif1a* expression is shown to be reduced by Repressor Element 1-Silencing Transcription Factor in prolonged hypoxia. While the *Hif1a* gene expression is suppressed, the HIF-1 α protein is still stable before turnover which explains the difference between HIF-1 α protein and gene expression level [Cavadas *et al.*, 2015].

Since deficiency of FBN1 provides less scaffold for elastogenesis and HIF-1 α promotes various MMPs remodeling ECM in MFS, elastic fiber fragmentation was expected to have a reverse correlation with FBN1 deposition and similar correlation with HIF-1 α [Zhang *et al.*, 2022]. As

predicted, elastic fibers were more fragmented in male mgR mice than in male WT mice fed with CD or HFD. Female mgR mice fed with HFD had similar elastic fiber fragmentation compared to female WT mice fed with HFD but not CD revealing that HFD specifically rescued female aortic aneurysm phenotype. Although the sexual dimorphism of elastic fiber fragmentation did not show in FBN1 deposition and assembly, from previous knowledge of hierarchical multistep molecular processes in elastogenesis, it is possible that other important accessory proteins such as FBLN4, FBLN5 and LTBP4 are modulated by diet and sex instead [El-Hallous *et al.*, 2007; Kumra *et al.*, 2018; Kumra *et al.*, 2019]. The other possible mechanism in regulating elastic fibers is MMPs. Both *Mmp2* and *Mmp9* gene expression levels which are known to promote elastic fiber fragmentation were analyzed, but there was no difference under all conditions, suggesting that the elastic fiber fragmentation was caused by other ECM remodeling mechanism [Klein & Bischoff, 2011; Lu & Aikawa, 2015]. MMP-12 protein levels, which are known to be elevated by reduced levels of miR-122 and increased levels of HIF-1 α in MFS to promote elastic fiber fragmentation, did not change under all conditions [Zhang *et al.*, 2022]. Interestingly, the *Mmp12* gene expression was higher in male mgR mice than male WT and female mgR mice fed with CD. This difference was lost when the mice were fed with HFD. The contradiction between MMP-12 protein turnover and elevated *Mmp12* gene expression levels could be due to post-translational modification. Tyrosine⁴¹⁴ (Tyr⁴¹⁴) in MMP-12 is known to be phosphorylated, but its functional role still requires more research [Bordoli *et al.*, 2014; Madzharova *et al.*, 2019]. Possibly, MMP-12 degrades the elastic fibers at an earlier timepoint than 12 weeks of age and subsequently get degraded due to post-translation modification. In transcription regulation, despite multiple transcription factors were recognized to regulate *Mmp2*, *Mmp9* and *Mmp12*, a unique transcription factor targeting *Mmp12* is currently unknown, but it might explain why *Mmp12* was regulated but not *Mmp2* or

Mmp9 [Robert et al., 2009; Li et al., 2013; Hiden et al., 2018]. The transcription regulation of *Mmp12* can be possibly analyzed by Assay for Transposase-Accessible Chromatin Sequencing to predict open regions of chromatin for specific transcription factors to bind or by chromatin immunoprecipitation to investigate the interaction between transcription factors and DNA.

Proteoglycan, which is known to be accumulated abnormally in MFS and upregulated by HIF-1 α , was evaluated as observed through alcian blue staining [Cikach et al., 2018; Shimomura et al., 2021]. The results of elastic fiber fragmentation and proteoglycan correlated with each other [Cikach et al., 2018]. Suggested by multiple studies, the build-up of proteoglycan promotes intralamellar swelling pressure, ultimately causing fragmentation of elastic lamellae [Humphrey, 2013; Roccabianca et al., 2014a; Roccabianca et al., 2014b; Cikach et al., 2018; Shen et al., 2019]. Studies showed that HFD promotes the estrogen level which might rescue aortic aneurysm; therefore, we propose that HFD rescued the aortic aneurysm in female mgR mice by elevating estrogen level [Wu et al., 2007; Tripathi et al., 2017; Qi et al., 2020; Goncalves et al., 2021]. With these interesting findings, both the gene expression of *Acan* and *Vcan*, encoding aggrecan and versican which are common proteoglycans regulated in MFS, were determined. Both *Acan* and *Vcan* gene expression levels were not different potentially due to turnover of proteoglycan as mice aged [Cikach et al., 2018].

Collagen is a key marker of fibrosis and is regulated by HIF-1 α [Xiong & Liu, 2017]. Recent studies suggested that aortae undergo fibrosis in MFS, and express and deposit higher levels of collagen [Perrucci et al., 2020; Nettersheim et al., 2021]. Our data of collagen deposition confirmed these findings and correlated with HIF-1 α protein levels. On a contrary, *Coll1a1* and *Col3a1* expression did not correlate the collagen deposition. HFD reduced both *Coll1a1* and *Col3a1* expression in male mgR mice. Although numerous studies showed that HFD promoted

Coll1a1 and *Col3a1* expression levels in the aorta [Halberg et al., 2009; Martinez-Martinez et al., 2013; Singh et al., 2021], heart and white adipose tissue, another study actually showed that HFD reduced *Col3a1* in the heart through epigenetic regulation of by histone H3 [Gaikwad et al., 2010]. We suspect that turnover of *Coll1a1* and *Col3a1* expression was involved with HFD, but the exact mechanisms are not known with contradictions of fibrotic studies. Unlike males, female mgR mice expressed low levels of *Coll1a1* and *Col3a1* like the WT mice fed with CD or HFD potentially by estrogen receptors acting as a corepressor leading to the turnover of *Coll1a1* and *Col3a1* expression [Dworatzek et al., 2019]. Even though it is known that HFD could potentially induce atherosclerosis or vascular calcification [Choudhary et al., 2017; Son et al., 2020; Wan et al., 2020], surprisingly, in the current study we did not observe any atherosclerotic plaque deposition or vascular calcification (analyzed through von Kossa staining, data not shown) in aortae of mgR mice in HFD or other dietary conditions. A possible explanation for which could be the experimental time frame of 12 weeks employed in this study, as opposed to the longer time frames of 16 weeks or longer used in other published work. We also did not observe any inflammatory cells (CD68 and CD3) in the aortae from male mgR mice fed with CD, HFD or WD (data not shown), which are more prone to have aneurysm. Since we did not observe any signs of inflammation in the aortae of mgR mice, we did not further analyze any inflammatory factors (TNF- α , IL-6 and PPAR- γ) secreted by white adipose tissue in the current study.

Overall, an intriguing and novel finding from our study is the rescue effect mediated by HFD in female mgR mice, in the pathogenesis of TAA. Based on the substantial literature evidence on the role of estrogen and sexual dimorphism in TAA [Wu et al., 2007; Tripathi et al., 2017; Qi et al., 2020; Goncalves et al., 2021], it is possible that differential regulation of estrogen is the responsible cause for the protective phenotype observed in our study in the MFS female mice.

Surgical procedures such as ovariectomy could be further employed in MFS mice from young and older age groups to analyze the role of sex hormones in regulating the syndromic TAA in different dietary conditions. These experimental approaches may enable better understanding of sex-specific metabolic regulation and its consequence on TAA initiation and progression.

CHAPTER 6: CONCLUSION AND KEY FINDINGS

In conclusion, HFD promoted weight gain in male mgR mice, but female mgR mice were resistant (Figure 6.1). In ITT and GTT analysis, mgR mice and female mice showed an improved metabolic phenotype. Furthermore, HFD rescued the aortic aneurysm in female mgR mice. Even though HFD was not able to reduce all aortic aneurysm markers in female mgR mice (thicker aortic wall, FBN1 deficiency, elevated HIF-1 α and collagen levels), HFD was sufficient to attenuate certain key aortic aneurysm markers (reduced aortic diameter, elastic fiber fragmentation and proteoglycan levels). HFD also minimized aortic rupture occurrence, *Mmp12*, *Colla1* and *Col3a1* gene expression levels in male mgR mice (Figure 6.2). A personalized dietary adjustment with high fat content might be beneficial and improve MFS patients' aneurysm progression, especially in females.

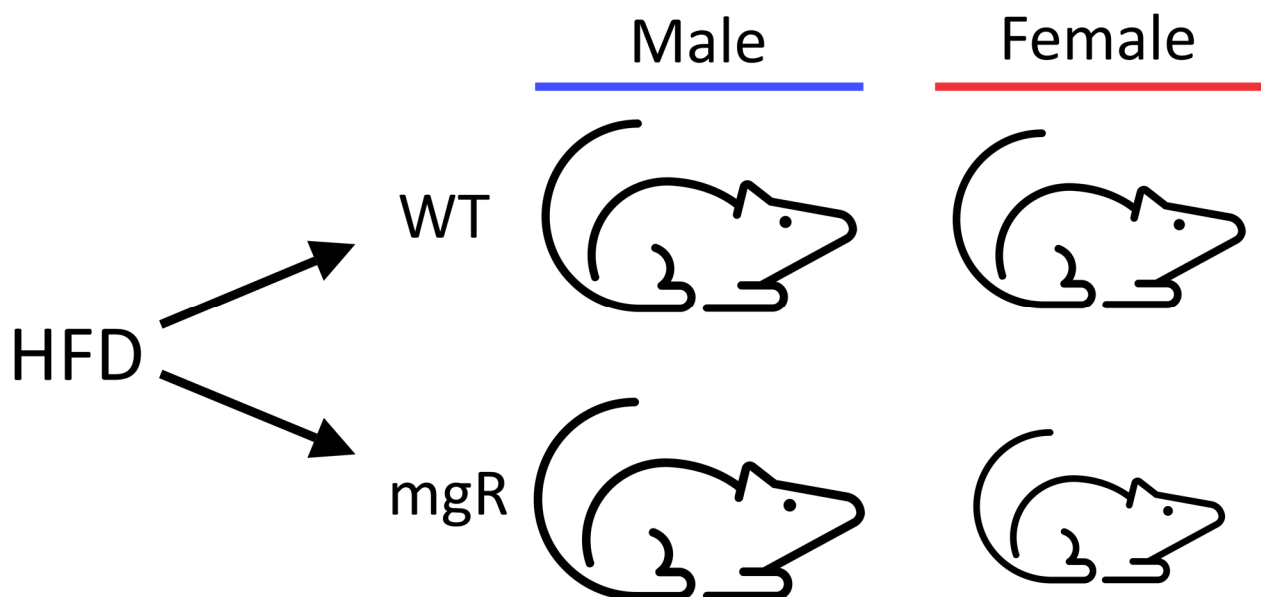


Figure 6.1: Schematic of metabolic phenotype in 12-week-old male and female WT and mgR mice fed with HFD. Female mgR mice were resistant to HFD-induced weight gain but not male mgR mice. The size of the mouse schematics is meant to represent the relative weight.

	WT		mgR		
	Male/Female	Male		Female	
	CD/HFD	CD	HFD	CD	HFD
Survival (reduced by aortic rupture)	=	↓	=	=	=
Aneurysm development					
FBN1	=	↓	↓	↓	↓
HIF-1α	=	↑	↑	=	↑
Elastic fiber fragmentation	=	↑	↑	↑	↑
<i>Mmp12</i>	=	↑	=	=	=
Proteoglycan	=	↑	↑	↑	↑
Collagen	=	↑	↑	=	↑

Figure 6.2: Schematic of aortic aneurysm phenotype in 12-week-old male and female WT and mgR mice fed with CD or HFD. = signs indicate no changes, upwards arrows indicate increased level, downwards arrows indicate decreased level. Thin arrows indicate a trend.

REFERENCES

- Aguirre KM, McCormick RJ, Schwarzbauer JE. (1994). Fibronectin self-association is mediated by complementary sites within the amino-terminal one-third of the molecule. *J Biol Chem* **269**, 27863-27868
- Alhuzaimi AN, Aldawsari KA, AlAhmadi M. (2021). Isolated left subclavian artery with right aortic arch: case report and literature review of 50 cases. *Gen Thorac Cardiovasc Surg* **69**, 885-889
- Allan JA, Docherty AJ, Barker PJ, Huskisson NS, Reynolds JJ, Murphy G. (1995). Binding of gelatinases A and B to type-I collagen and other matrix components. *Biochem J* **309** (Pt 1), 299-306
- Ampofo E, Kietzmann T, Zimmer A, Jakupovic M, Montenarh M, Gotz C. (2010). Phosphorylation of the von Hippel-Lindau protein (VHL) by protein kinase CK2 reduces its protein stability and affects p53 and HIF-1alpha mediated transcription. *Int J Biochem Cell Biol* **42**, 1729-1735
- Aspberg A, Adam S, Kostka G, Timpl R, Heinegard D. (1999). Fibulin-1 is a ligand for the C-type lectin domains of aggrecan and versican. *J Biol Chem* **274**, 20444-20449
- Aspberg A. (2012). The different roles of aggrecan interaction domains. *J Histochem Cytochem* **60**, 987-996
- Azeloglu EU, Albro MB, Thimmappa VA, Ateshian GA, Costa KD. (2008). Heterogeneous transmural proteoglycan distribution provides a mechanism for regulating residual stresses in the aorta. *Am J Physiol Heart Circ Physiol* **294**, H1197-H1205
- Bastien M, Dagenais F, Dumont E, Vadeboncoeur N, Dion B, Royer M, Gaudet-Savard T, Poirier P. (2012). Assessment of management of cardiovascular risk factors in patients with thoracic aortic disease. *Blood Press Monit* **17**, 235-242
- Beck K, Chan VC, Shenoy N, Kirkpatrick A, Ramshaw JA, Brodsky B. (2000). Destabilization of osteogenesis imperfecta collagen-like model peptides correlates with the identity of the residue replacing glycine. *Proc Natl Acad Sci USA* **97**, 4273-4278
- Bella J, Berman HM. (1996). Crystallographic evidence for C alpha-H...O=C hydrogen bonds in a collagen triple helix. *J Mol Biol* **264**, 734-742
- Benede-Ubieto R, Estevez-Vazquez O, Ramadori P, Cubero FJ, Nevzorova YA. (2020). Guidelines and considerations for metabolic tolerance tests in mice. *Diabetes Metab Syndr Obes* **13**, 439-450
- Bergner DW, Goldberger JJ. (2010). Diabetes mellitus and sudden cardiac death: what are the data? *Cardiol J* **17**, 117-129
- Bordoli MR, Yum J, Breitkopf SB, Thon JN, Italiano JE, Jr., Xiao J, Worby C, Wong SK, Lin G, Edenius M, Keller TL, Asara JM, Dixon JE, Yeo CY, Whitman M. (2014). A secreted tyrosine kinase acts in the extracellular environment. *Cell* **158**, 1033-1044
- Bultmann-Mellin I, Conradi A, Maul AC, Dinger K, Wempe F, Wohl AP, Imhof T, Wunderlich FT, Bunck AC, Nakamura T, Koli K, Bloch W, Ghanem A, Heinz A, von Melchner H, Sengle G, Sterner-Kock A. (2015). Modeling autosomal recessive cutis laxa type 1C in mice reveals distinct functions for Ltbp-4 isoforms. *Dis Model Mech* **8**, 403-415
- Bultmann H, Santas AJ, Peters DM. (1998). Fibronectin fibrillogenesis involves the heparin II binding domain of fibronectin. *J Biol Chem* **273**, 2601-2609

- Burnett W, Finnigan-Bunick A, Yoon K, Rosenbloom J. (1982). Analysis of elastin gene expression in the developing chick aorta using cloned elastin cDNA. *J Biol Chem* **257**, 1569-1572
- Cai CL, Liang X, Shi Y, Chu PH, Pfaff SL, Chen J, Evans S. (2003). Isl1 identifies a cardiac progenitor population that proliferates prior to differentiation and contributes a majority of cells to the heart. *Dev Cell* **5**, 877-889
- Cakirer S, Karaarslan E, Kayabali M, Rozanes I. (2002). Separate origins of the left internal and external carotid arteries from the aortic arch: MR angiographic findings. *AJNR Am J Neuroradiol* **23**, 1600-1602
- Canadas V, Vilacosta I, Bruna I, Fuster V. (2010). Marfan syndrome. Part 1: pathophysiology and diagnosis. *Nat Rev Cardiol* **7**, 256-265
- Cavadas MA, Mesnieres M, Crifo B, Manresa MC, Selfridge AC, Scholz CC, Cummins EP, Cheong A, Taylor CT. (2015). REST mediates resolution of HIF-dependent gene expression in prolonged hypoxia. *Sci Rep* **5**, 17851
- Chen JZ, Sawada H, Moorleggen JJ, Weiland M, Daugherty A, Sheppard MB. (2019). Aortic strain correlates with elastin fragmentation in fibrillin-1 hypomorphic mice. *Circ Rep* **1**, 199-205
- Chen JZ, Sawada H, Ye D, Katsumata Y, Kukida M, Ohno-Urabe S, Moorleggen JJ, Franklin MK, Howatt DA, Sheppard MB, Mullick AE, Lu HS, Daugherty A. (2021). Deletion of AT1a (angiotensin II type 1a) receptor or inhibition of angiotensinogen synthesis attenuates thoracic aortopathies in fibrillin1(C1041G/+) mice. *Arterioscler Thromb Vasc Biol* **41**, 2538-2550
- Chen Y, Ali T, Todorovic V, O'Leary JM, Kristina DA, Rifkin DB. (2005). Amino acid requirements for formation of the TGF-beta-latent TGF-beta binding protein complexes. *J Mol Biol* **345**, 175-186
- Cheung K, Boodhwani M, Chan KL, Beauchesne L, Dick A, Coutinho T. (2017). Thoracic aortic aneurysm growth: role of sex and aneurysm etiology. *J Am Heart Assoc* **6**
- Choi J, Bergdahl A, Zheng Q, Starcher B, Yanagisawa H, Davis EC. (2009). Analysis of dermal elastic fibers in the absence of fibulin-5 reveals potential roles for fibulin-5 in elastic fiber assembly. *Matrix Biol* **28**, 211-220
- Choudhary D, Adhikary S, Gautam J, Maurya P, Ahmad N, Kushwaha P, Khan MP, Kumar A, Barthwal M, Maurya R, Trivedi R. (2017). Detrimental effects of atherogenic and high fat diet on bone and aortic calcification rescued by an isoflavonoid Caviunin beta-D-glucopyranoside. *Biomedicine & pharmacotherapy = Biomedecine & pharmacotherapie* **92**, 757-771
- Choudhury R, McGovern A, Ridley C, Cain SA, Baldwin A, Wang MC, Guo C, Mironov AJ, Drymoussi Z, Trump D, Shuttleworth A, Baldock C, Kielty CM. (2009). Differential regulation of elastic fiber formation by fibulins -4 and -5. *J Biol Chem* **284**, 24553-24567
- Chung J, Coutinho T, Chu MWA, Ouzounian M. (2020). Sex differences in thoracic aortic disease: A review of the literature and a call to action. *J Thorac Cardiovasc Surg* **160**, 656-660
- Cikach FS, Koch CD, Mead TJ, Galatioto J, Willard BB, Emerton KB, Eagleton MJ, Blackstone EH, Ramirez F, Roselli EE, Apte SS. (2018). Massive aggrecan and versican accumulation in thoracic aortic aneurysm and dissection. *JCI Insight* **3**
- Cocciolone AJ, Hawes JZ, Staiculescu MC, Johnson EO, Murshed M, Wagenseil JE. (2018). Elastin, arterial mechanics, and cardiovascular disease. *Am J Physiol Heart Circ Physiol* **315**, H189-H205

- Collod-Beroud G, Le Bourdelles S, Ades L, Ala-Kokko L, Booms P, Boxer M, Child A, Comeglio P, De Paepe A, Hyland JC, Holman K, Kaitila I, Loeys B, Matyas G, Nuytinck L, Peltonen L, Rantamaki T, Robinson P, Steinmann B, Junien C, Beroud C, Boileau C. (2003). Update of the UMD-FBN1 mutation database and creation of an FBN1 polymorphism database. *Hum Mutat* **22**, 199-208
- Condemi F, Campisi S, Viallon M, Croisille P, Avril S. (2020). Relationship between ascending thoracic aortic aneurysms hemodynamics and biomechanical properties. *IEEE Trans Biomed Eng* **67**, 949-956
- Corson GM, Charbonneau NL, Keene DR, Sakai LY. (2004). Differential expression of fibrillin-3 adds to microfibril variety in human and avian, but not rodent, connective tissues. *Genomics* **83**, 461-472
- da Rocha-Azevedo B, Grinnell F. (2013). Fibroblast morphogenesis on 3D collagen matrices: the balance between cell clustering and cell migration. *Exp Cell Res* **319**, 2440-2446
- Dagenais F. (2011). Anatomy of the thoracic aorta and of its branches. *Thorac Surg Clin* **21**, 219-227, viii
- Davidson JM, Smith K, Shibahara S, Tolstoshev P, Crystal RG. (1982). Regulation of elastin synthesis in developing sheep nuchal ligament by elastin mRNA levels. *J Biol Chem* **257**, 747-754
- Davies RR, Goldstein LJ, Coady MA, Tittle SL, Rizzo JA, Kopf GS, Elefteriades JA. (2002). Yearly rupture or dissection rates for thoracic aortic aneurysms: simple prediction based on size. *Ann Thorac Surg* **73**, 17-27
- Davis EC, Li L. (2017). Histological and electron microscope staining for the identification of elastic fiber networks. *Methods Mol Biol* **1627**, 385-393
- Debelle L, Tamburro AM. (1999). Elastin: molecular description and function. *Int J Biochem Cell Biol* **31**, 261-272
- Detaint D, Faivre L, Collod-Beroud G, Child AH, Loeys BL, Binquet C, Gautier E, Arbustini E, Mayer K, Arslan-Kirchner M, Stheneur C, Halliday D, Beroud C, Bonithon-Kopp C, Claustres M, Plauchu H, Robinson PN, Kiotsekoglou A, De Backer J, Ades L, Francke U, De Paepe A, Boileau C, Jondeau G. (2010). Cardiovascular manifestations in men and women carrying a FBN1 mutation. *Eur Heart J* **31**, 2223-2229
- Di Conza G, Trusso Cafarello S, Lorocho S, Mennerich D, Deschoemaeker S, Di Matteo M, Ehling M, Gevaert K, Prenen H, Zahedi RP, Sickmann A, Kietzmann T, Moretti F, Mazzone M. (2017). The mTOR and PP2A pathways regulate PHD2 phosphorylation to fine-tune HIF1alpha levels and colorectal cancer cell survival under hypoxia. *Cell Rep* **18**, 1699-1712
- Di Lullo GA, Sweeney SM, Korkko J, Ala-Kokko L, San Antonio JD. (2002). Mapping the ligand-binding sites and disease-associated mutations on the most abundant protein in the human, type I collagen. *J Biol Chem* **277**, 4223-4231
- Dietz HC, Cutting GR, Pyeritz RE, Maslen CL, Sakai LY, Corson GM, Puffenberger EG, Hamosh A, Nanthakumar EJ, Curristin SM, Stetten G, Meyers DA, Francomano CA. (1991). Marfan syndrome caused by a recurrent de novo missense mutation in the fibrillin gene. *Nature* **352**, 337-339
- Djokic J, Fagotto-Kaufmann C, Bartels R, Nelea V, Reinhardt DP. (2013). Fibulin-3, -4, and -5 are highly susceptible to proteolysis, interact with cells and heparin, and form multimers. *J Biol Chem* **288**, 22821-22835
- Dobrin PB. (1978). Mechanical properties of arteries. *Physiol Rev* **58**, 397-460

- Duckles SP, Krause DN, Stirone C, Procaccio V. (2006). Estrogen and mitochondria: a new paradigm for vascular protection? *Mol Interv* **6**, 26-35
- Duckworth D. (1869). Case of aneurism of the descending thoracic aorta, which burst into the pericardium and left bronchus. *Edinb Med J* **14**, 1075-1084
- Durigova M, Nagase H, Mort JS, Roughley PJ. (2011). MMPs are less efficient than ADAMTS5 in cleaving aggrecan core protein. *Matrix Biol* **30**, 145-153
- Dworatzek E, Mahmoodzadeh S, Schriever C, Kusumoto K, Kramer L, Santos G, Fliegner D, Leung YK, Ho SM, Zimmermann WH, Lutz S, Regitz-Zagrosek V. (2019). Sex-specific regulation of collagen I and III expression by 17beta-Estradiol in cardiac fibroblasts: role of estrogen receptors. *Cardiovasc Res* **115**, 315-327
- Dyksterhuis LB, Baldock C, Lammie D, Wess TJ, Weiss AS. (2007). Domains 17-27 of tropoelastin contain key regions of contact for coacervation and contain an unusual turn-containing crosslinking domain. *Matrix Biol* **26**, 125-135
- El-Hallous E, Sasaki T, Hubmacher D, Getie M, Tiedemann K, Brinckmann J, Bätge B, Davis EC, Reinhardt DP. (2007). Fibrillin-1 interactions with fibulins depend on the first hybrid domain and provide an adapter function to tropoelastin. *J Biol Chem* **282**, 8935-8946
- Ely JJ, Bishop MA, Lammey ML, Sleeper MM, Steiner JM, Lee DR. (2010). Use of biomarkers of collagen types I and III fibrosis metabolism to detect cardiovascular and renal disease in chimpanzees (*Pan troglodytes*). *Comp Med* **60**, 154-158
- Ensenberger MG, Annis DS, Mosher DF. (2004). Actions of the functional upstream domain of protein F1 of *Streptococcus pyogenes* on the conformation of fibronectin. *Biophys Chem* **112**, 201-207
- Erkula G, Jones KB, Sponseller PD, Dietz HC, Pyeritz RE. (2002). Growth and maturation in Marfan syndrome. *Am J Med Genet* **109**, 100-115
- Evanko SP, Angello JC, Wight TN. (1999). Formation of hyaluronan- and versican-rich pericellular matrix is required for proliferation and migration of vascular smooth muscle cells. *Arterioscler Thromb Vasc Biol* **19**, 1004-1013
- Eyre DR, Paz MA, Gallop PM. (1984). Cross-linking in collagen and elastin. *Ann Rev Biochem* **53**, 717-748
- Faivre L, Gorlin RJ, Wirtz MK, Godfrey M, Dagonneau N, Samples JR, Le Merrer M, Collod-Beroud G, Boileau C, Munnich A, Cormier-Daire V. (2003). In frame fibrillin-1 gene deletion in autosomal dominant Weill-Marchesani syndrome. *J Med Genet* **40**, 34-36
- Fanjul-Fernandez M, Folgueras AR, Cabrera S, Lopez-Otin C. (2010). Matrix metalloproteinases: evolution, gene regulation and functional analysis in mouse models. *Biochim Biophys Acta* **1803**, 3-19
- Freeman LJ, Lomas A, Hodson N, Sherratt MJ, Mellody KT, Weiss AS, Shuttleworth A, Kiely CM. (2005). Fibulin-5 interacts with fibrillin-1 molecules and microfibrils. *Biochem J* **388**, 1-5
- Fukuda Y, Ferrans VJ, Crystal RG. (1984). Development of elastic fibers of nuchal ligament, aorta, and lung of fetal and postnatal sheep: an ultrastructural and electron microscopic immunohistochemical study. *Am J Anat* **170**, 597-629
- Gaikwad AB, Gupta J, Tikoo K. (2010). Epigenetic changes and alteration of Fbn1 and Col3A1 gene expression under hyperglycaemic and hyperinsulinaemic conditions. *Biochem J* **432**, 333-341
- Gelse K, Poschl E, Aigner T. (2003). Collagens-structure, function, and biosynthesis. *Adv Drug Deliv Rev* **55**, 1531-1546

- Gharraee N, Sun Y, Swisher JA, Lessner SM. (2022). Age and sex dependency of thoracic aortopathy in a mouse model of Marfan syndrome. *Am J Physiol Heart Circ Physiol* **322**, 44-56
- Goldblatt J, Hyatt J, Edwards C, Walpole I. (2011). Further evidence for a marfanoid syndrome with neonatal progeroid features and severe generalized lipodystrophy due to frameshift mutations near the 3' end of the FBN1 gene. *Am J Med Genet A* **155A**, 717-720
- Goncalves RM, Delgobo M, Agnes JP, Das Neves RN, Falchetti M, Casagrande T, Garcia APV, Vieira TC, Somensi N, Bruxel MA, Mendes D, Rafacho A, Bafica A, Gelain DP, Moreira JCF, Cassali GD, Bishop AJR, Zanotto-Filho A. (2021). COX-2 promotes mammary adipose tissue inflammation, local estrogen biosynthesis, and carcinogenesis in high-sugar/fat diet treated mice. *Cancer Lett* **502**, 44-57
- Graul-Neumann LM, Kienitz T, Robinson PN, Baasanjav S, Karow B, Gillessen-Kaesbach G, Fahsold R, Schmidt H, Hoffmann K, Passarge E. (2010). Marfan syndrome with neonatal progeroid syndrome-like lipodystrophy associated with a novel frameshift mutation at the 3' terminus of the FBN1-gene. *Am J Med Genet A* **152A**, 2749-2755
- Groth KA, Hove H, Kyhl K, Folkestad L, Gaustadnes M, Vejlstrup N, Stochholm K, Ostergaard JR, Andersen NH, Gravholt CH. (2015). Prevalence, incidence, and age at diagnosis in Marfan syndrome. *Orphanet J Rare Dis* **10**, 153
- Halberg N, Khan T, Trujillo ME, Wernstedt-Asterholm I, Attie AD, Sherwani S, Wang ZV, Landskroner-Eiger S, Dineen S, Magalang UJ, Brekken RA, Scherer PE. (2009). Hypoxia-inducible factor 1alpha induces fibrosis and insulin resistance in white adipose tissue. *Mol Cell Biol* **29**, 4467-4483
- Han J, He Y, Zhao H, Xu X. (2019). Hypoxia inducible factor-1 promotes liver fibrosis in nonalcoholic fatty liver disease by activating PTEN/p65 signaling pathway. *J Cell Biochem* **120**, 14735-14744
- Handford PA, Mayhew M, Brownlee GG. (1991). Calcium binding to fibrillin? *Nature* **353**, 395
- Hanneman K, Newman B, Chan F. (2017). Congenital variants and anomalies of the aortic arch. *Radiographics* **37**, 32-51
- Hansen LB, von Kodolitsch Y, Schroeder F, Benninghoven D. (2020). Body image in patients with Marfan syndrome. *J Clin Med* **9**
- Hedtke T, Schrader CU, Heinz A, Hoehenwarter W, Brinckmann J, Groth T, Schmelzer CEH. (2019). A comprehensive map of human elastin cross-linking during elastogenesis. *FEBS J* **286**, 3594-3610
- Hidden U, Eyth CP, Majali-Martinez A, Desoye G, Tam-Amersdorfer C, Huppertz B, Ghaffari Tabrizi-Wizsy N. (2018). Expression of matrix metalloproteinase 12 is highly specific for non-proliferating invasive trophoblasts in the first trimester and temporally regulated by oxygen-dependent mechanisms including HIF-1A. *Histochem Cell Biol* **149**, 31-42
- Horiguchi M, Inoue T, Ohbayashi T, Hirai M, Noda K, Marmorstein LY, Yabe D, Takagi K, Akama TO, Kita T, Kimura T, Nakamura T. (2009). Fibulin-4 conducts proper elastogenesis via interaction with cross-linking enzyme lysyl oxidase. *Proc Natl Acad Sci USA* **106**, 19029-19034
- Hubmacher D, El-Hallous E, Nelea V, Kaartinen MT, Lee ER, Reinhardt DP. (2008). Biogenesis of extracellular microfibrils: Multimerization of the fibrillin-1 C-terminus into bead-like structures enables self-assembly. *Proc Natl Acad Sci USA* **105**, 6548-6553

- Hubmacher D, Bergeron E, Fagotto-Kaufmann C, Sakai LY, Reinhardt DP. (2014). Early fibrillin-1 assembly monitored through a modifiable recombinant cell approach. *Biomacromolecules* **15**, 1456-1468
- Hudak CS, Sul HS. (2013). Pref-1, a gatekeeper of adipogenesis. *Front Endocrinol (Lausanne)* **4**, 79
- Humphrey JD. (2013). Possible mechanical roles of glycosaminoglycans in thoracic aortic dissection and associations with dysregulated transforming growth factor-beta. *J Vasc Res* **50**, 1-10
- Ishimoto T, Lanaspa MA, Rivard CJ, Roncal-Jimenez CA, Orlicky DJ, Cicerchi C, McMahan RH, Abdelmalek MF, Rosen HR, Jackman MR, MacLean PS, Diggle CP, Asipu A, Inaba S, Kosugi T, Sato W, Maruyama S, Sanchez-Lozada LG, Sautin YY, Hill JO, Bonthron DT, Johnson RJ. (2013). High-fat and high-sucrose (western) diet induces steatohepatitis that is dependent on fructokinase. *Hepatology* **58**, 1632-1643
- Isogai Z, Aspberg A, Keene DR, Ono RN, Reinhardt DP, Sakai LY. (2002). Versican interacts with fibrillin-1 and links extracellular microfibrils to other connective tissue networks. *J Biol Chem* **277**, 4565-4572
- Jacquinet A, Verloes A, Callewaert B, Coremans C, Coucke P, de Paepe A, Kornak U, Lebrun F, Lomet J, Pierard GE, Robinson PN, Symoens S, Van Maldergem L, Debray FG. (2014). Neonatal progeroid variant of Marfan syndrome with congenital lipodystrophy results from mutations at the 3' end of FBN1 gene. *Eur J Med Genet* **57**, 230-234
- Jadidi M, Razian SA, Habibnezhad M, Anttila E, Kamenskiy A. (2021). Mechanical, structural, and physiologic differences in human elastic and muscular arteries of different ages: comparison of the descending thoracic aorta to the superficial femoral artery. *Acta Biomater* **119**, 268-283
- Judge DP, Dietz HC. (2005). Marfan's syndrome. *Lancet* **366**, 1965-1976
- Juvonen T, Ergin MA, Galla JD, Lansman SL, Nguyen KH, McCullough JN, Levy D, de Asla RA, Bodian CA, Griep RB. (1997). Prospective study of the natural history of thoracic aortic aneurysms. *Ann Thorac Surg* **63**, 1533-1545
- Kadoglou NP, Liapis CD. (2004). Matrix metalloproteinases: contribution to pathogenesis, diagnosis, surveillance and treatment of abdominal aortic aneurysms. *Curr Med Res Opin* **20**, 419-432
- Kandemirli SG. (2020). Intrathoracic bifurcation of the left common carotid artery associated with rib fusion and Klippel-Feil syndrome. *Surg Radiol Anat* **42**, 411-415
- Karimi A, Milewicz DM. (2016). Structure of the Elastin-Contractile Units in the Thoracic Aorta and How Genes That Cause Thoracic Aortic Aneurysms and Dissections Disrupt This Structure. *Can J Cardiol* **32**, 26-34
- Kiani C, Lee V, Cao L, Chen L, Wu Y, Zhang Y, Adams ME, Yang BB. (2001). Roles of aggrecan domains in biosynthesis, modification by glycosaminoglycans and product secretion. *Biochem J* **354**, 199-207
- Kiani C, Chen L, Wu YJ, Yee AJ, Yang BB. (2002). Structure and function of aggrecan. *Cell Res* **12**, 19-32
- Kim YS, Joh TH. (2012). Matrix metalloproteinases, new insights into the understanding of neurodegenerative disorders. *Biomol Ther (Seoul)* **20**, 133-143
- Kinori M, Wehrli S, Kassem IS, Azar NF, Maumenee IH, Mets MB. (2017). Biometry Characteristics in Adults and Children With Marfan Syndrome: From the Marfan Eye Consortium of Chicago. *Am J Ophthalmol* **177**, 144-149

- Klein T, Bischoff R. (2011). Physiology and pathophysiology of matrix metalloproteases. *Amino Acids* **41**, 271-290
- Kobayashi N, Kostka G, Garbe JH, Keene DR, Bachinger HP, Hanisch FG, Markova D, Tsuda T, Timpl R, Chu ML, Sasaki T. (2007). A comparative analysis of the fibulin protein family. Biochemical characterization, binding interactions, and tissue localization. *J Biol Chem* **282**, 11805-11816
- Kramann R, Goettsch C, Wongboonsin J, Iwata H, Schneider RK, Kuppe C, Kaesler N, Chang-Panesso M, Machado FG, Gratwohl S, Madhurima K, Hutcheson JD, Jain S, Aikawa E, Humphreys BD. (2016). Adventitial MSC-like cells are progenitors of vascular smooth muscle cells and drive vascular calcification in chronic kidney disease. *Cell Stem Cell* **19**, 628-642
- Kumra H, Sabatier L, Hassan A, Sakai T, Mosher DF, Brinckmann J, Reinhardt DP. (2018). Roles of fibronectin isoforms in neonatal vascular development and matrix integrity. *PLoS Biol* **16**, e2004812
- Kumra H, Nelea V, Hakami H, Pagliuzza A, Djokic J, Xu J, Yanagisawa H, Reinhardt DP. (2019). Fibulin-4 exerts a dual role in LTBP-4L-mediated matrix assembly and function. *Proc Natl Acad Sci USA* **116**, 20428-20437
- Kuusela P, Ruoslahti E, Vaheri A. (1975). Polypeptides of a glycoprotein antigen (SF) present in serum and surface of normal but not of transformed chicken fibroblasts. *Biochim Biophys Acta* **379**, 295-303
- Lackey DE, Lazaro RG, Li P, Johnson A, Hernandez-Carretero A, Weber N, Vorobyova I, Tsukamoto H, Osborn O. (2016). The role of dietary fat in obesity-induced insulin resistance. *Am J Physiol* **311**, E989-E997
- Le Goff C, Mahaut C, Wang LW, Allali S, Abhyankar A, Jensen S, Zylberberg L, Collod-Beroud G, Bonnet D, Alanay Y, Brady AF, Cordier MP, Devriendt K, Genevieve D, Kiper PO, Kitoh H, Krakow D, Lynch SA, Le Merrer M, Megarbane A, Mortier G, Odent S, Polak M, Rohrbach M, Sillence D, Stolte-Dijkstra I, Superti-Furga A, Rimoin DL, Topouchian V, Unger S, Zabel B, Bole-Feysot C, Nitschke P, Handford P, Casanova JL, Boileau C, Apte SS, Munnich A, Cormier-Daire V. (2011). Mutations in the TGF β binding-protein-like domain 5 of FBN1 are responsible for acromicric and geleophysic dysplasias. *Am J Hum Genet* **89**, 7-14
- LeBaron RG, Zimmermann DR, Ruoslahti E. (1992). Hyaluronate binding properties of versican. *J Biol Chem* **267**, 10003-10010
- Lech C, Swaminathan A. (2017). Abdominal aortic emergencies. *Emerg Med Clin North Am* **35**, 847-867
- Leroux-Berger M, Queguiner I, Maciel TT, Ho A, Relaix F, Kempf H. (2011). Pathologic calcification of adult vascular smooth muscle cells differs on their crest or mesodermal embryonic origin. *J Bone Miner Res* **26**, 1543-1453
- Li G, Zhang Y, Qian Y, Zhang H, Guo S, Sunagawa M, Hisamitsu T, Liu Y. (2013). Interleukin-17A promotes rheumatoid arthritis synoviocytes migration and invasion under hypoxia by increasing MMP2 and MMP9 expression through NF-kappaB/HIF-1alpha pathway. *Mol Immunol* **53**, 227-236
- Li W, Chi N, Rathnayake RAC, Wang R. (2021). Distinctive roles of fibrillar collagen I and collagen III in mediating fibroblast-matrix interaction: A nanoscopic study. *Biochem Biophys Res Commun* **560**, 66-71

- Li Y, Yang N, Zhou X, Bian X, Qiu G, Zhang M, Lin H, Li D. (2018). LncRNA and mRNA interaction study based on transcriptome profiles reveals potential core genes in the pathogenesis of human thoracic aortic dissection. *Mol Med Report* **18**, 3167-3176
- Liang L, Ye S, Jiang R, Zhou X, Zhou J, Meng S. (2022). Liensinine alleviates high fat diet (HFD)-induced non-alcoholic fatty liver disease (NAFLD) through suppressing oxidative stress and inflammation via regulating TAK1/AMPK signaling. *Int Immunopharmacol* **104**, 108306
- Lin G, Tiedemann K, Vollbrandt T, Peters H, Bätge B, Brinckmann J, Reinhardt DP. (2002). Homo- and heterotypic fibrillin-1 and -2 interactions constitute the basis for the assembly of microfibrils. *J Biol Chem* **277**, 50795-50804
- Lin PH, Chaikof EL. (2000). Embryology, anatomy, and surgical exposure of the great abdominal vessels. *Surg Clin North Am* **80**, 417-433, xiv
- Little CB, Flannery CR, Hughes CE, Mort JS, Roughley PJ, Dent C, Caterson B. (1999). Aggrecanase versus matrix metalloproteinases in the catabolism of the interglobular domain of aggrecan in vitro. *Biochem J* **344 Pt 1**, 61-68
- Liu K, Fang C, Shen Y, Liu Z, Zhang M, Ma B, Pang X. (2017). Hypoxia-inducible factor 1a induces phenotype switch of human aortic vascular smooth muscle cell through PI3K/AKT/AEG-1 signaling. *Oncotarget* **8**, 33343-33352
- Liu X, Zhao Y, Gao J, Pawlyk B, Starcher B, Spencer JA, Yanagisawa H, Zuo J, Li T. (2004). Elastic fiber homeostasis requires lysyl oxidase-like 1 protein. *Nat Genet* **36**, 178-182
- Loeys BL, Gerber EE, Riegert-Johnson D, Iqbal S, Whiteman P, McConnell V, Chillakuri CR, Macaya D, Coucke PJ, De Paepe A, Judge DP, Wigley F, Davis EC, Mardon HJ, Handford P, Keene DR, Sakai LY, Dietz HC. (2010). Mutations in fibrillin-1 cause congenital scleroderma: stiff skin syndrome. *Sci Transl Med* **2**, 23ra20-23ra20
- Lönnqvist L, Reinhardt DP, Sakai LY, Peltonen L. (1998). Evidence for furin-type activity-mediated C-terminal processing of profibrillin-1 and interference in the processing by certain mutations. *Hum Mol Genet* **7**, 2039-2044
- Lu H, Aikawa M. (2015). Many faces of matrix metalloproteinases in aortic aneurysms. *Arterioscler Thromb Vasc Biol* **35**, 752-754
- Lundbaek K. (1962). Intravenous glucose tolerance as a tool in definition and diagnosis of diabetes mellitus. *Br Med J* **1**, 1507-1513
- MacFarlane EG, Parker SJ, Shin JY, Kang BE, Ziegler SG, Creamer TJ, Bagirzadeh R, Bedja D, Chen Y, Calderon JF, Weissler K, Frischmeyer-Guerrero PA, Lindsay ME, Habashi JP, Dietz HC. (2019). Lineage-specific events underlie aortic root aneurysm pathogenesis in Loeys-Dietz syndrome. *J Clin Invest* **129**, 659-675
- Macotela Y, Boucher J, Tran TT, Kahn CR. (2009). Sex and depot differences in adipocyte insulin sensitivity and glucose metabolism. *Diabetes* **58**, 803-812
- Madzharova E, Kastl P, Sabino F, Auf dem Keller U. (2019). Post-translational modification-dependent activity of matrix metalloproteinases. *Int J Mol Sci* **20**
- Mallinger R, Kulnig W, Bock P. (1992). Symmetrically banded collagen fibrils: observations on a new cross striation pattern in vivo. *Anat Rec* **232**, 45-51
- Mao Y, Schwarzbauer JE. (2005). Fibronectin fibrillogenesis, a cell-mediated matrix assembly process. *Matrix Biol* **24**, 389-399
- Maqueda A, Moyano JV, Hernandez Del Cerro M, Peters DM, Garcia-Pardo A. (2007). The heparin III-binding domain of fibronectin (III4-5 repeats) binds to fibronectin and inhibits fibronectin matrix assembly. *Matrix Biol* **26**, 642-651

- Martinez-Martinez E, Miana M, Jurado-Lopez R, Rousseau E, Rossignol P, Zannad F, Cachofeiro V, Lopez-Andres N. (2013). A role for soluble ST2 in vascular remodeling associated with obesity in rats. *PLoS One* **8**, e79176
- McGee M, Wagner WD. (2003). Chondroitin sulfate anticoagulant activity is linked to water transfer: relevance to proteoglycan structure in atherosclerosis. *Arterioscler Thromb Vasc Biol* **23**, 1921-1927
- McKenzie ED, Roeser ME, Thompson JL, De Leon LE, Adachi I, Heinle JS, Mery CM, Fraser CD, Jr. (2016). Descending aortic translocation for relief of distal tracheal and proximal bronchial compression. *Ann Thorac Surg* **102**, 859-862
- Meijboom LJ, Timmermans J, Zwinderman AH, Engelfriet PM, Mulder BJ. (2005). Aortic root growth in men and women with the Marfan's syndrome. *Am J Cardiol* **96**, 1441-1444
- Merrilees MJ, Lemire JM, Fischer JW, Kinsella MG, Braun KR, Clowes AW, Wight TN. (2002). Retrovirally mediated overexpression of versican v3 by arterial smooth muscle cells induces tropoelastin synthesis and elastic fiber formation in vitro and in neointima after vascular injury. *Circ Res* **90**, 481-487
- Milewicz D, Pyeritz RE, Crawford ES, Byers PH. (1992). Marfan syndrome: defective synthesis, secretion, and extracellular matrix formation of fibrillin by cultured dermal fibroblasts. *J Clin Invest* **89**, 79-86
- Milewicz DM, Grossfield J, Cao SN, Kielty C, Covitz W, Jewett T. (1995). A mutation in FBN1 disrupts profibrillin processing and results in isolated skeletal features of the Marfan syndrome. *J Clin Invest* **95**, 2373-2378
- Milewicz DM, Braverman AC, De Backer J, Morris SA, Boileau C, Maumenee IH, Jondeau G, Evangelista A, Pyeritz RE, European Reference Network for Rare Multisystemic Vascular Disease HRDWG. (2021). Marfan syndrome. *Nat Rev Dis Primers* **7**, 64
- Misra A, Sheikh AQ, Kumar A, Luo J, Zhang J, Hinton RB, Smoot L, Kaplan P, Urban Z, Qyang Y, Tellides G, Greif DM. (2016). Integrin beta3 inhibition is a therapeutic strategy for supra-aortic stenosis. *J Exp Med* **213**, 451-463
- Miyamoto C, Kugo H, Hashimoto K, Sawaragi A, Zaima N, Moriyama T. (2018). Effect of a high-sucrose diet on abdominal aortic aneurysm development in a hypoperfusion-induced animal model. *J Oleo Sci* **67**, 589-597
- Morrison PR, Edsall JT, Miller SG. (1948). Preparation and properties of serum and plasma proteins; the separation of purified fibrinogen from fraction I of human plasma. *J Am Chem Soc* **70**, 3103-3108
- Murillo H, Lane MJ, Punn R, Fleischmann D, Restrepo CS. (2012). Imaging of the aorta: embryology and anatomy. *Semin Ultrasound CT MR* **33**, 169-190
- Muthu ML, Tiedemann K, Fradette J, Komarova S, Reinhardt DP. (2022). Fibrillin-1 regulates white adipose tissue development, homeostasis, and function. *Matrix Biol* **110**, 106-128
- Nagase H, Visse R, Murphy G. (2006). Structure and function of matrix metalloproteinases and TIMPs. *Cardiovasc Res* **69**, 562-573
- Nam JK, Kim AR, Choi SH, Kim JH, Han SC, Park S, Lee YJ, Kim J, Cho J, Lee HJ, Lee YJ. (2021). Pharmacologic Inhibition of HIF-1alpha Attenuates Radiation-Induced Pulmonary Fibrosis in a Preclinical Image Guided Radiation Therapy. *Int J Radiat Oncol Biol Phys* **109**, 553-566
- Nettersheim FS, Lemties J, Braumann S, Geissen S, Bokredenghel S, Nies R, Hof A, Winkels H, Freeman BA, Klinke A, Rudolph V, Baldus S, Mehrkens D, Mollenhauer M, Adam M.

- (2021). Nitro-oleic acid (NO₂-OA) reduces thoracic aortic aneurysm progression in a mouse model of Marfan syndrome. *Cardiovasc Res*
- Nienaber CA, Fattori R, Mehta RH, Richartz BM, Evangelista A, Petzsch M, Cooper JV, Januzzi JL, Ince H, Sechtem U, Bossone E, Fang J, Smith DE, Isselbacher EM, Pape LA, Eagle KA, International Registry of Acute Aortic D. (2004). Gender-related differences in acute aortic dissection. *Circulation* **109**, 3014-3021
- Noda K, Dabovic B, Takagi K, Inoue T, Horiguchi M, Hirai M, Fujikawa Y, Akama TO, Kusumoto K, Zilberberg L, Sakai LY, Koli K, Naitoh M, von Melchner H, Suzuki S, Rifkin DB, Nakamura T. (2013). Latent TGF-beta binding protein 4 promotes elastic fiber assembly by interacting with fibulin-5. *Proc Natl Acad Sci USA* **110**, 2852-2857
- Noda K, Kitagawa K, Miki T, Horiguchi M, Akama TO, Taniguchi T, Taniguchi H, Takahashi K, Ogra Y, Mecham RP, Terajima M, Yamauchi M, Nakamura T. (2020). A matricellular protein fibulin-4 is essential for the activation of lysyl oxidase. *Sci Adv* **6**
- Nonaka R, Sato F, Wachi H. (2014). Domain 36 of tropoelastin in elastic fiber formation. *Biol Pharm Bull* **37**, 698-702
- Norton PA, Hynes RO. (1990). In vitro splicing of fibronectin pre-mRNAs. *Nucleic Acids Res* **18**, 4089-4097
- Ogobuiro I, Wehrle CJ, Tuma F. (2022) *Anatomy, thorax, heart coronary arteries*,
- Okita K, Iwahashi H, Kozawa J, Okauchi Y, Funahashi T, Imagawa A, Shimomura I. (2014). Usefulness of the insulin tolerance test in patients with type 2 diabetes receiving insulin therapy. *J Diabetes Investig* **5**, 305-312
- Olin AI, Morgelin M, Sasaki T, Timpl R, Heinegard D, Aspberg A. (2001). The proteoglycans aggrecan and Versican form networks with fibulin-2 through their lectin domain binding. *J Biol Chem* **276**, 1253-1261
- Oller J, Gabande-Rodriguez E, Ruiz-Rodriguez MJ, Desdin-Mico G, Aranda JF, Rodrigues-Diez R, Ballesteros-Martinez C, Blanco EM, Roldan-Montero R, Acuna P, Forteza Gil A, Martin-Lopez CE, Nistal JF, Lino Cardenas CL, Lindsay ME, Martin-Ventura JL, Briones AM, Redondo JM, Mittelbrunn M. (2021). Extracellular tuning of mitochondrial respiration leads to aortic aneurysm. *Circulation* **143**, 2091-2109
- Orgel JP, Wess TJ, Miller A. (2000). The in situ conformation and axial location of the intermolecular cross-linked non-helical telopeptides of type I collagen. *Structure* **8**, 137-142
- Orio F, Jr., Palomba S, Cascella T, Savastano S, Lombardi G, Colao A. (2007). Cardiovascular complications of obesity in adolescents. *J Endocrinol Invest* **30**, 70-80
- Ozsvar J, Yang C, Cain SA, Baldock C, Tarakanova A, Weiss AS. (2021). Tropoelastin and elastin assembly. *Front Bioeng Biotechnol* **9**, 643110
- Paiocchi VL, Faletta FF, Ferrari E, Schlossbauer SA, Leo LA, Maisano F. (2021). Multimodality imaging of the anatomy of the aortic root. *J Cardiovasc Dev Dis* **8**
- Pankov R, Cukierman E, Katz BZ, Matsumoto K, Lin DC, Lin S, Hahn C, Yamada KM. (2000). Integrin dynamics and matrix assembly: tensin-dependent translocation of alpha(5)beta(1) integrins promotes early fibronectin fibrillogenesis. *J Cell Biol* **148**, 1075-1090
- Pape LA, Tsai TT, Isselbacher EM, Oh JK, O'Gara P T, Evangelista A, Fattori R, Meinhardt G, Trimarchi S, Bossone E, Suzuki T, Cooper JV, Froehlich JB, Nienaber CA, Eagle KA, International Registry of Acute Aortic Dissection I. (2007). Aortic diameter \geq 5.5 cm is not a good predictor of type A aortic dissection: observations from the International Registry of Acute Aortic Dissection (IRAD). *Circulation* **116**, 1120-1127

- Papke CL, Yanagisawa H. (2014). Fibulin-4 and fibulin-5 in elastogenesis and beyond: Insights from mouse and human studies. *Matrix Biol* **37**, 142-149
- Passarge E, Robinson PN, Graul-Neumann LM. (2016). Marfanoid-progeroid-lipodystrophy syndrome: a newly recognized fibrillinopathy. *Eur J Hum Genet* **24**, 1244-1247
- Pedroza AJ, Tashima Y, Shad R, Cheng P, Wirka R, Churovich S, Nakamura K, Yokoyama N, Cui JZ, Iosef C, Hiesinger W, Quertermous T, Fischbein MP. (2020). Single-cell transcriptomic profiling of vascular smooth muscle cell phenotype modulation in Marfan syndrome aortic aneurysm. *Arterioscler Thromb Vasc Biol* **40**, 2195-2211
- Pereira L, Lee SY, Gayraud B, Andrikopoulos K, Shapiro SD, Bunton T, Biery NJ, Dietz HC, Sakai LY, Ramirez F. (1999). Pathogenetic sequence for aneurysm revealed in mice underexpressing fibrillin-1. *Proc Natl Acad Sci USA* **96**, 3819-3823
- Perrucci GL, Rurali E, Corliano M, Balzo M, Piccoli M, Moschetta D, Pini A, Gaetano R, Antona C, Egea G, Fischer G, Malesevic M, Alamanni F, Cogliati E, Paolin A, Pompilio G, Nigro P. (2020). Cyclophilin A/EMMPRIN Axis Is Involved in Pro-Fibrotic Processes Associated with Thoracic Aortic Aneurysm of Marfan Syndrome Patients. *Cells* **9**
- Petersen MC, Shulman GI. (2018). Mechanisms of insulin action and insulin resistance. *Physiol Rev* **98**, 2133-2223
- Piha-Gossack A, Sossin WS, Reinhardt DP. (2012). The evolution of extracellular fibrillins and their functional domains. *PLoS One* **7**, e33560
- Pouget C, Gautier R, Teillet MA, Jaffredo T. (2006). Somite-derived cells replace ventral aortic hemangioblasts and provide aortic smooth muscle cells of the trunk. *Development* **133**, 1013-1022
- Psaltis PJ, Simari RD. (2015). Vascular wall progenitor cells in health and disease. *Circ Res* **116**, 1392-1412
- Pyeritz RE. (2000). The Marfan syndrome. *Annu Rev Med* **51**, 481-510
- Qi X, Wang F, Chun C, Saldarriaga L, Jiang Z, Pruitt EY, Arnaoutakis GJ, Upchurch GR, Jr., Jiang Z. (2020). A validated mouse model capable of recapitulating the protective effects of female sex hormones on ascending aortic aneurysms and dissections (AADs). *Physiol Rep* **8**, e14631
- Rabkin SW. (2014). Differential expression of MMP-2, MMP-9 and TIMP proteins in thoracic aortic aneurysm - comparison with and without bicuspid aortic valve: a meta-analysis. *Vasa* **43**, 433-442
- Rabkin SW. (2017). The role matrix metalloproteinases in the production of aortic aneurysm. *Prog Mol Biol Transl Sci* **147**, 239-265
- Randell A, Daneshtalab N. (2017). Elastin microfibril interface-located protein 1, transforming growth factor beta, and implications on cardiovascular complications. *J Am Soc Hypertens* **11**, 437-448
- Rappu P, Salo AM, Myllyharju J, Heino J. (2019). Role of prolyl hydroxylation in the molecular interactions of collagens. *Essays Biochem* **63**, 325-335
- Reinhardt DP, Keene DR, Corson GM, Pöschl E, Bächinger HP, Gambée JE, Sakai LY. (1996a). Fibrillin 1: Organization in microfibrils and structural properties. *J Mol Biol* **258**, 104-116
- Reinhardt DP, Sasaki T, Dzamba BJ, Keene DR, Chu ML, Göhring W, Timpl R, Sakai LY. (1996b). Fibrillin-1 and fibulin-2 interact and are colocalized in some tissues. *J Biol Chem* **271**, 19489-19496
- Riambau V, Bockler D, Brunkwall J, Cao P, Chiesa R, Coppi G, Czerny M, Fraedrich G, Haulon S, Jacobs MJ, Lachat ML, Moll FL, Setacci C, Taylor PR, Thompson M, Trimarchi S,

- Verhagen HJ, Verhoeven EL, Esvs Guidelines C, Kolh P, de Borst GJ, Chakfe N, Debus ES, Hinchliffe RJ, Kakkos S, Koncar I, Lindholt JS, Vega de Ceniga M, Vermassen F, Verzini F, Document R, Kolh P, Black JH, 3rd, Busund R, Bjorck M, Dake M, Dick F, Eggebrecht H, Evangelista A, Grabenwoger M, Milner R, Naylor AR, Ricco JB, Rousseau H, Schmidli J. (2017). Editor's choice - management of descending thoracic aorta diseases: clinical practice guidelines of the European Society for Vascular Surgery (ESVS). *Eur J Vasc Endovasc Surg* **53**, 4-52
- Robert I, Aussems M, Keutgens A, Zhang X, Hennuy B, Viatour P, Vanstraelen G, Merville MP, Chapelle JP, de Leval L, Lambert F, Dejardin E, Gothot A, Chariot A. (2009). Matrix metalloproteinase-9 gene induction by a truncated oncogenic NF-kappaB2 protein involves the recruitment of MLL1 and MLL2 H3K4 histone methyltransferase complexes. *Oncogene* **28**, 1626-1638
- Robertson IB, Horiguchi M, Zilberberg L, Dabovic B, Hadjiolova K, Rifkin DB. (2015). Latent TGF-beta-binding proteins. *Matrix Biol* **47**, 44-53
- Roccabianca S, Ateshian GA, Humphrey JD. (2014a). Biomechanical roles of medial pooling of glycosaminoglycans in thoracic aortic dissection. *Biomech Model Mechanobiol* **13**, 13-25
- Roccabianca S, Bellini C, Humphrey JD. (2014b). Computational modelling suggests good, bad and ugly roles of glycosaminoglycans in arterial wall mechanics and mechanobiology. *J R Soc Interface* **11**, 20140397
- Roman MJ, Devereux RB, Preiss LR, Asch FM, Eagle KA, Holmes KW, LeMaire SA, Maslen CL, Milewicz DM, Morris SA, Prakash SK, Pyeritz RE, Ravekes WJ, Shohet RV, Song HK, Weinsaft JW, Gen TACI. (2017). Associations of age and sex with marfan phenotype: The National Heart, Lung, and Blood Institute GenTAC (Genetically Triggered Thoracic Aortic Aneurysms and Cardiovascular Conditions) Registry. *Circ Cardiovasc Genet* **10**
- Romere C, Duerschmid C, Bournat J, Constable P, Jain M, Xia F, Saha PK, Del Solar M, Zhu B, York B, Sarkar P, Rendon DA, Gaber MW, LeMaire SA, Coselli JS, Milewicz DM, Sutton VR, Butte NF, Moore DD, Chopra AR. (2016). Asprosin, a fasting-induced glucogenic protein hormone. *Cell* **165**, 566-579
- Sabatier L, Chen D, Fagotto-Kaufmann C, Hubmacher D, McKee MD, Annis DS, Mosher DF, Reinhardt DP. (2009). Fibrillin assembly requires fibronectin. *Mol Biol Cell* **20**, 846-858
- Sabatier L, Miosge N, Hubmacher D, Lin G, Davis EC, Reinhardt DP. (2011). Fibrillin-3 expression in human development. *Matrix Biol* **30**, 43-52
- Sabatier L, Djokic J, Fagotto-Kaufmann C, Chen M, Annis DS, Mosher DF, Reinhardt DP. (2013). Complex contributions of fibronectin to initiation and maturation of microfibrils. *Biochem J* **456**, 283-295
- Sabatier L, Djokic J, Hubmacher D, Dzafik D, Nelea V, Reinhardt DP. (2014). Heparin/heparan sulfate controls fibrillin-1, -2 and -3 self-interactions in microfibril assembly. *FEBS Lett* **588**, 2890-2897
- Safar ME, Levy BI, Struijker-Boudier H. (2003). Current perspectives on arterial stiffness and pulse pressure in hypertension and cardiovascular diseases. *Circulation* **107**, 2864-2869
- Saharinen J, Taipale J, Monni O, Keski-Oja J. (1998). Identification and characterization of a new latent transforming growth factor-beta-binding protein, LTBP-4. *J Biol Chem* **273**, 18459-18469
- Saharinen J, Keski-Oja J. (2000). Specific sequence motif of 8-Cys repeats of TGF-beta binding proteins, LTBPs, creates a hydrophobic interaction surface for binding of small latent TGF-beta. *Mol Biol Cell* **11**, 2691-2704

- Sakai LY, Keene DR, Engvall E. (1986). Fibrillin, a new 350-kD glycoprotein, is a component of extracellular microfibrils. *J Cell Biol* **103**, 2499-2509
- Sawada H, Rateri DL, Moorleggen JJ, Majesky MW, Daugherty A. (2017). Smooth muscle cells derived from second heart field and cardiac neural crest reside in spatially distinct domains in the media of the ascending aorta-brief report. *Arterioscler Thromb Vasc Biol* **37**, 1722-1726
- Sawicki GS, Lewis CL, Ferris DP. (2009). It pays to have a spring in your step. *Exerc Sport Sci Rev* **37**, 130-138
- Schmelzer CEH, Heinz A, Troilo H, Lockhart-Cairns MP, Jowitt TA, Marchand MF, Bidault L, Bignon M, Hedtke T, Barret A, McConnell JC, Sherratt MJ, Germain S, Hulmes DJS, Baldock C, Muller L. (2019). Lysyl oxidase-like 2 (LOXL2)-mediated cross-linking of tropoelastin. *FASEB J* **33**, 5468-5481
- Schneider CA, Rasband WS, Eliceiri KW. (2012). NIH Image to ImageJ: 25 years of image analysis. *Nat Methods* **9**, 671-675
- Schuh C, Leiva-Sabadini C, Huang S, Barrera NP, Bozec L, Aguayo S. (2022). Nanomechanical and molecular characterization of aging in dentinal collagen. *J Dent Res*, 220345211072484
- Schwill S, Seppelt P, Grunhagen J, Ott CE, Jugold M, Ruhparwar A, Robinson PN, Karck M, Kallenbach K. (2013). The fibrillin-1 hypomorphic mgR/mgR murine model of Marfan syndrome shows severe elastolysis in all segments of the aorta. *J Vasc Surg* **57**, 1628-1636, 1636 e1621-1623
- Scuderi GJ, Woolf N, Dent K, Golish SR, Cuellar JM, Cuellar VG, Yeomans DC, Carragee EJ, Angst MS, Bowser R, Hanna LS. (2010). Identification of a complex between fibronectin and aggrecan G3 domain in synovial fluid of patients with painful meniscal pathology. *Clin Biochem* **43**, 808-814
- Semenza GL. (2014). Hypoxia-inducible factor 1 and cardiovascular disease. *Annu Rev Physiol* **76**, 39-56
- Shapiro SD, Endicott SK, Province MA, Pierce JA, Campbell EJ. (1991). Marked longevity of human lung parenchymal elastic fibers deduced from prevalence of D-aspartate and nuclear weapons-related radiocarbon. *J Clin Invest* **87**, 1828-1834
- Shen YH, Lu HS, LeMaire SA, Daugherty A. (2019). Unfolding the story of proteoglycan accumulation in thoracic aortic aneurysm and dissection. *Arterioscler Thromb Vasc Biol* **39**, 1899-1901
- Shimizu K, Miyata H, Abekura Y, Oka M, Kushamae M, Kawamata T, Mizutani T, Kataoka H, Nozaki K, Miyamoto S, Aoki T. (2019). High-fat diet intake promotes the enlargement and degenerative changes in the media of intracranial aneurysms in rats. *J Neuropathol Exp Neurol* **78**, 798-807
- Shimomura S, Inoue H, Arai Y, Nakagawa S, Fujii Y, Kishida T, Shin-Ya M, Ichimaru S, Tsuchida S, Mazda O, Takahashi K. (2021). Mechanical stimulation of chondrocytes regulates HIF-1 α under hypoxic conditions. *Tissue Cell* **71**, 101574
- Shin SJ, Yanagisawa H. (2019). Recent updates on the molecular network of elastic fiber formation. *Essays Biochem* **63**, 365-376
- Shu J, Dolman GE, Duan J, Qiu G, Ilyas M. (2016). Statistical colour models: an automated digital image analysis method for quantification of histological biomarkers. *Biomed Eng Online* **15**, 46

- Singh P, Carraher C, Schwarzbauer JE. (2010). Assembly of fibronectin extracellular matrix. *Annu Rev Cell Dev Biol* **26**, 397-419
- Singh R, Kaundal RK, Zhao B, Bouchareb R, Lebeche D. (2021). Resistin induces cardiac fibroblast-myofibroblast differentiation through JAK/STAT3 and JNK/c-Jun signaling. *Pharmacol Res* **167**, 105414
- Sipila KH, Drushinin K, Rappu P, Jokinen J, Salminen TA, Salo AM, Kapyla J, Myllyharju J, Heino J. (2018). Proline hydroxylation in collagen supports integrin binding by two distinct mechanisms. *J Biol Chem* **293**, 7645-7658
- Son M, Oh S, Jang JT, Park CH, Son KH, Byun K. (2020). Attenuating effects of pyrogallol-phloroglucinol-6,6-bieckol on vascular smooth muscle cell phenotype changes to osteoblastic cells and vascular calcification induced by high fat diet. *Nutrients* **12**
- Song Y, Xie Y, Liu F, Zhao C, Yu R, Ban S, Ye Q, Wen J, Wan H, Li X, Ma R, Meng Z. (2013). Expression of matrix metalloproteinase-12 in aortic dissection. *BMC Cardiovasc Disord* **13**, 34
- Sottile J, Hocking DC, Langenbach KJ. (2000). Fibronectin polymerization stimulates cell growth by RGD-dependent and -independent mechanisms. *J Cell Sci* **113 Pt 23**, 4287-4299
- Stanhope KL. (2016). Sugar consumption, metabolic disease and obesity: the state of the controversy. *Crit Rev Clin Lab Sci* **53**, 52-67
- Steed MM, Tyagi N, Sen U, Schuschke DA, Joshua IG, Tyagi SC. (2010). Functional consequences of the collagen/elastin switch in vascular remodeling in hyperhomocysteinemic wild-type, eNOS^{-/-}, and iNOS^{-/-} mice. *Am J Physiol* **299**, L301-L311
- Stefanovic B. (2013). RNA protein interactions governing expression of the most abundant protein in human body, type I collagen. *Wiley Interdiscip Rev RNA* **4**, 535-545
- Steffensen B, Wallon UM, Overall CM. (1995). Extracellular matrix binding properties of recombinant fibronectin type II-like modules of human 72-kDa gelatinase/type IV collagenase. High affinity binding to native type I collagen but not native type IV collagen. *J Biol Chem* **270**, 11555-11566
- Stubbins RE, Najjar K, Holcomb VB, Hong J, Nunez NP. (2012). Oestrogen alters adipocyte biology and protects female mice from adipocyte inflammation and insulin resistance. *Diabetes Obes Metab* **14**, 58-66
- Sun K, Halberg N, Khan M, Magalang UJ, Scherer PE. (2013). Selective inhibition of hypoxia-inducible factor 1 α ameliorates adipose tissue dysfunction. *Mol Cell Biol* **33**, 904-917
- Sun Y, Liang X, Najafi N, Cass M, Lin L, Cai CL, Chen J, Evans SM. (2007). Islet 1 is expressed in distinct cardiovascular lineages, including pacemaker and coronary vascular cells. *Dev Biol* **304**, 286-296
- Szpinda M. (2005). A new variant of aberrant left brachiocephalic trunk in mam: case report and literature review. *Folia Morphol (Praha)* **64**, 47-50
- Takahara Y, Tokunou T, Ichiki T. (2018). Suppression of abdominal aortic aneurysm formation in mice by teneligliptin, a dipeptidyl peptidase-4 inhibitor. *J Atheroscler Thromb* **25**, 698-708
- Taskinen MR, Packard CJ, Boren J. (2019). Dietary fructose and the metabolic syndrome. *Nutrients* **11**
- Tiedemann K, Bätge B, Müller PK, Reinhardt DP. (2001). Interactions of fibrillin-1 with heparin/heparan sulfate: Implications for microfibrillar assembly. *J Biol Chem* **276**, 36035-36042

- Tobey DJ, Reynolds TS, Kopchok GE, Donayre CE, Khoynezhad A, White RA. (2019). In vivo assessment of ascending and arch aortic compliance. *Ann Vasc Surg* **57**, 22-28
- Tomasini-Johansson BR, Annis DS, Mosher DF. (2006). The N-terminal 70-kDa fragment of fibronectin binds to cell surface fibronectin assembly sites in the absence of intact fibronectin. *Matrix Biol* **25**, 282-293
- Toonkool P, Jensen SA, Maxwell AL, Weiss AS. (2001). Hydrophobic domains of human tropoelastin interact in a context-dependent manner. *J Biol Chem* **276**, 44575-44580
- Tripathi R, Sainathan S, Ziganshin BA, Elefteriades JA. (2017). Thoracic aortic aneurysm from chronic antiestrogen therapy. *Int J Angiol* **26**, 60-63
- Tscheuschler A, Meffert P, Beyersdorf F, Heilmann C, Kocher N, Uffelmann X, Discher P, Siepe M, Kari FA. (2016). MMP-2 isoforms in aortic tissue and serum of patients with ascending aortic aneurysms and aortic root aneurysms. *PLoS One* **11**, e0164308
- Tsipouras P, Del Mastro R, Sarfarazi M, Lee B, Vitale E, Child AH, Godfrey M, Devereux RB, Hewett D, Steinmann B, Viljoen D, Sykes BC, Kilpatrick M, Ramirez F, The International Marfan Syndrome Collaborative S. (1992). Genetic linkage of the Marfan syndrome, ectopia lentis, and congenital contractural arachnodactyly to the fibrillin genes on chromosomes 15 and 5. *N Engl J Med* **326**, 905-909
- Tucker WD, Arora Y, Mahajan K. (2022) *Anatomy, blood vessels*,
- Ugarova TP, Zamarron C, Veklich Y, Bowditch RD, Ginsberg MH, Weisel JW, Plow EF. (1995). Conformational transitions in the cell binding domain of fibronectin. *Biochemistry* **34**, 4457-4466
- Urban JP, Maroudas A, Bayliss MT, Dillon J. (1979). Swelling pressures of proteoglycans at the concentrations found in cartilaginous tissues. *Biorheology* **16**, 447-464
- Vinue A, Gonzalez-Navarro H. (2015). Glucose and insulin tolerance tests in the mouse. *Methods Mol Biol* **1339**, 247-254
- von Kodolitsch Y, Demolder A, Girdauskas E, Kaemmerer H, Kornhuber K, Muino Mosquera L, Morris S, Neptune E, Pyeritz R, Rand-Hendriksen S, Rahman A, Riise N, Robert L, Staufenbiel I, Szocs K, Vanem TT, Linke SJ, Vogler M, Yetman A, De Backer J. (2019). Features of Marfan syndrome not listed in the Ghent nosology - the dark side of the disease. *Expert Rev Cardiovasc Ther* **17**, 883-915
- Vrhovski B, Jensen S, Weiss AS. (1997). Coacervation characteristics of recombinant human tropoelastin. *Eur J Biochem* **250**, 92-98
- Vuorio E, de Crombrughe B. (1990). The family of collagen genes. *Ann Rev Biochem* **59**, 837-872
- Wagenseil JE, Mecham RP. (2007). New insights into elastic fiber assembly. *Birth Defects Res C Embryo Today* **81**, 229-240
- Wagenseil JE, Ciliberto CH, Knutsen RH, Levy MA, Kovacs A, Mecham RP. (2010). The importance of elastin to aortic development in mice. *Am J Physiol Heart Circ Physiol* **299**, H257-H264
- Wallis DD, Putnam EA, Cretoiu JS, Carmical SG, Cao SN, Thomas G, Milewicz DM. (2003). Profibrillin-1 maturation by human dermal fibroblasts: proteolytic processing and molecular chaperones. *J Cell Biochem* **90**, 641-652
- Wan J, Feng Y, Du L, Veeraraghavan VP, Mohan SK, Guo S. (2020). Antiatherosclerotic activity of eriocitrin in high-fat-diet-induced atherosclerosis model rats. *J Environ Pathol Toxicol Oncol* **39**, 61-75

- Wang GL, Semenza GL. (1995). Purification and characterization of hypoxia-inducible factor 1. *J Biol Chem* **270**, 1230-1237
- Wang Y, Zhao L, Smas C, Sul HS. (2010). Pref-1 interacts with fibronectin to inhibit adipocyte differentiation. *Mol Cell Biol* **30**, 3480-3492
- Wasteson P, Johansson BR, Jukkola T, Breuer S, Akyurek LM, Partanen J, Lindahl P. (2008). Developmental origin of smooth muscle cells in the descending aorta in mice. *Development* **135**, 1823-1832
- Watanabe H, Yamada Y, Kimata K. (1998). Roles of aggrecan, a large chondroitin sulfate proteoglycan, in cartilage structure and function. *J Biochem* **124**, 687-693
- White HJ, Bordes S, Borger J. (2022) *Anatomy, abdomen and pelvis, aorta*,
- Wilhelm SM, Collier IE, Marmer BL, Eisen AZ, Grant GA, Goldberg GI. (1989). SV40-transformed human lung fibroblasts secrete a 92-kDa type IV collagenase which is identical to that secreted by normal human macrophages. *J Biol Chem* **264**, 17213-17221
- Wolinsky H. (1970). Comparison of medial growth of human thoracic and abdominal aortas. *Circ Res* **27**, 531-538
- Wu XF, Zhang J, Xin SJ, Duan ZQ, Zhang G. (2007). The role of estrogen in the formation and development of abdominal aortic aneurysm: experiment with rats. *Am J Surg* **87**, 471-474
- Wulandari E, Jusman SW, Moenadajat Y, Jusuf AA, Sadikin M. (2016). Expressions of collagen I and III in hypoxic keloid tissue. *Kobe J Med Sci* **62**, E58-E69
- Xiong A, Liu Y. (2017). Targeting hypoxia inducible factors-1alpha as a novel therapy in fibrosis. *Front Pharmacol* **8**, 326
- Xiong W, Meisinger T, Knispel R, Worth JM, Baxter BT. (2012). MMP-2 regulates Erk1/2 phosphorylation and aortic dilatation in Marfan syndrome. *Circ Res* **110**, e92-e101
- Xu X, Zhang F, Lu Y, Yu S, Sun W, Sun S, Cheng J, Ma J, Zhang M, Zhang C, Zhang Y, Zhang K. (2019). Silencing of NONO inhibits abdominal aortic aneurysm in apolipoprotein E-knockout mice via collagen deposition and inflammatory inhibition. *J Cell Mol Med* **23**, 7449-7461
- Yadin DA, Robertson IB, McNaught-Davis J, Evans P, Stoddart D, Handford PA, Jensen SA, Redfield C. (2013). Structure of the fibrillin-1 N-terminal domains suggests that heparan sulfate regulates the early stages of microfibril assembly. *Structure* **21**, 1743-1756
- Yamauchi M, Shiiba M. (2008). Lysine hydroxylation and cross-linking of collagen. *Methods Mol Biol* **446**, 95-108
- Yanagisawa H, Schluterman MK, Brekken RA. (2009). Fibulin-5, an integrin-binding matricellular protein: its function in development and disease. *J Cell Commun Signal* **3**, 337-347
- Yanagisawa H, Davis EC. (2010). Unraveling the mechanism of elastic fiber assembly: The roles of short fibulins. *Int J Biochem Cell Biol* **42**, 1084-1093
- Yang J, AlTahan A, Jones DT, Buffa FM, Bridges E, Interiano RB, Qu C, Vogt N, Li JL, Baban D, Ragoussis J, Nicholson R, Davidoff AM, Harris AL. (2015). Estrogen receptor-alpha directly regulates the hypoxia-inducible factor 1 pathway associated with antiestrogen response in breast cancer. *Proc Natl Acad Sci USA* **112**, 15172-15177
- Yetman AT, McCrindle BW. (2010). The prevalence and clinical impact of obesity in adults with Marfan syndrome. *Can J Cardiol* **26**, 137-139
- Yin X, Wanga S, Fellows AL, Barallobre-Barreiro J, Lu R, Davaapil H, Franken R, Fava M, Baig F, Skroblin P, Xing Q, Koolbergen DR, Groenink M, Zwinderman AH, Balm R, de Vries CJM, Mulder BJM, Viner R, Jahangiri M, Reinhardt DP, Sinha S, de Waard V, Mayr M.

- (2019). Glycoproteomic analysis of the aortic extracellular matrix in Marfan patients. *Arterioscler Thromb Vasc Biol* **39**, 1859-1873
- Zhang H, Hu W, Ramirez F. (1995). Developmental expression of fibrillin genes suggests heterogeneity of extracellular microfibrils. *J Cell Biol* **129**, 1165-1176
- Zhang L, Issa Bhaloo S, Chen T, Zhou B, Xu Q. (2018). Role of resident stem cells in vessel formation and arteriosclerosis. *Circ Res* **122**, 1608-1624
- Zhang Q, Checovich WJ, Peters DM, Albrecht RM, Mosher DF. (1994). Modulation of cell surface fibronectin assembly sites by lysophosphatidic acid. *J Cell Biol* **127**, 1447-1459
- Zhang R, Kumra H, Reinhardt DP. (2020). Quantification of extracellular matrix fiber systems related to ADAMTS proteins. *Methods Mol Biol* **2043**, 237-250
- Zhang RM, Tiedemann K, Muthu ML, Dinesh NEH, Komarova S, Ramkhelawon B, Reinhardt DP. (2022). Fibrillin-1-regulated miR-122 has a critical role in thoracic aortic aneurysm formation. *Cell Mol Life Sci* **79**, 314
- Zheng H, Qiu Z, Chai T, He J, Zhang Y, Wang C, Ye J, Wu X, Li Y, Zhang L, Chen L. (2021). Insulin resistance promotes the formation of aortic dissection by inducing the phenotypic switch of vascular smooth muscle cells. *Front Cardiovasc Med* **8**, 732122
- Zheng Q, Davis EC, Richardson JA, Starcher BC, Li T, Gerard RD, Yanagisawa H. (2006). Molecular analysis of fibulin-5 function during de novo synthesis of elastic fibers. *Mol Cell Biol* **27**, 1083-1095
- Zhou B, Pu WT. (2008). More than a cover: epicardium as a novel source of cardiac progenitor cells. *Regen Med* **3**, 633-635
- Zhou B, Li W, Zhao G, Yu B, Ma B, Liu Z, Xie N, Fu Y, Gong Z, Dai R, Zhang X, Kong W. (2018). Rapamycin prevents thoracic aortic aneurysm and dissection in mice. *J Vasc Surg*
- Zhu L, Vranckx R, Khau Van Kien P, Lalande A, Boisset N, Mathieu F, Wegman M, Glancy L, Gasc JM, Brunotte F, Bruneval P, Wolf JE, Michel JB, Jeunemaitre X. (2006). Mutations in myosin heavy chain 11 cause a syndrome associating thoracic aortic aneurysm/aortic dissection and patent ductus arteriosus. *Nat Genet* **38**, 343-349